PHOTO-STIMULATED OXIDATION OF MAGNETITE, AND AN APPLICATION TO MARS

by

ROBERT LOUIS HUGUENIN

B.Sc. (University of Pittsburgh, Pennsylvania, USA, 1969)

A thesis submitted in partial fulfillment
of the requirements for the degree of
Doctor of Science

Massachusetts Institute of Technology
Cambridge, Massachusetts
September, 1972

Signature of Author _____
Department of Earth and Planetary Sciences, September, 1972
Certified by _____
Thesis Supervisor
Accepted by _____
Chairman, Departmental Committee on Graduate Students

PHOTO-STIMULATED OXIDATION OF MAGNETITE, AND AN APPLICATION TO MARS

by

ROBERT LOUIS HUGUENIN

A thesis submitted to the Department of Earth and Planetary Sciences, September, 1972 in partial fulfillment of the requirements for the degree of Doctor of Science.

Abstract

It has been discovered that magnetite (Fe_3O_4) is rapidly oxidized to hematite (α-Fe_2O_3), upon illumination ($\lambda < .310\mu$) in an O_2-bearing atmosphere. A laboratory investigation has been carried out to determine the kinetics and mechanism of this rapid oxidation process. It has been found that the process consists of a series of constituent reactions which are common to most oxidation mechanisms: (1) atmospheric O_2 dissociates on the surface into two adsorbed atoms, upon colliding with a pair of adjacent vacant adsorption sites; (2) This step is followed by the oxidation of Fe(II) to Fe(III), simultaneous with electron attachment to the adsorbed O atoms, to form adsorbed O^-; (3) Step (2) is followed by the rapid attachment of a second electron to the adsorbed O^-, to form chemisorbed O^{2-}; (4) Finally, the chemisorbed O^{2-} ions are incorporated into the magnetite surface layer, forming hematite (α-Fe_2O_3) scales. The role of adsorbed H_2O in the formation of hematite nuclei, and the subsequent scale formation in the absence of H_2O by "nucleation disruption", is discussed. Although the principal oxidation product is hematite, the possibility of maghemite (γ-Fe_2O_3) formation, during nucleation, is discussed. The factor which allows this oxidation process to proceed in a low-temperature, low-O_2 partial pressure, water-free, otherwise nonoxidizing environment, is the presence of the ultraviolet light. The UV illumination gives rise to photoemission, which increases the rates of Fe(II) oxidation and the attachment of the electrons to the oxygen. The slowest step in the oxidation mechanism, and therefore the rate determining step, is the attachment of an electron to adsorbed O.

Finally, it is shown that the oxidation mechanism could occur in the present-day Martian surface environment. It would occur at a rate which is sufficiently fast to account for the extent of oxidation of the Martian surface that has been proposed in the oxidized basalt model of Adams and McCord (1969).

ACKNOWLEDGEMENTS

I would like to acknowledge the valuable discussions, guidance, and encouragement of Dr. Thomas B. McCord throughout this thesis. In addition, I wish to acknowledge Dr. Bruce Hapke for suggesting that UV illumination of the Martian surface may play a role in the formation of ferric oxides there. Dr. Hapke also introduced me to the techniques of the design and construction of vacuum systems. The discussions with Drs. John Adams, Roger Burns, John Lewis, Thomas McGetchin, Ronald Prinn, Carl Sagan, James Westphal, and John Wood were indispensable. Finally, I want to thank my wife, Nancy, for her direction and guidance throughout my educational pursuits, without which this thesis would not have been possible.

TABLE OF CONTENTS

TABLE OF CONTENTS (CONT'D)

TABLE OF CONTENTS (CONT'D)

TABLE OF CONTENTS (CONT'D)

LIST OF ILLUSTRATIONS

LIST OF ILLUSTRATIONS (CONT'D)

LIST OF ILLUSTRATIONS (CONT'D)

LIST OF ILLUSTRATIONS (CONT'D)

LIST OF ILLUSTRATIONS (CONT'D)

LIST OF ILLUSTRATIONS (CONT'D)

LIST OF ILLUSTRATIONS (CONT'D)

I. INTRODUCTION

RED PLANET MARS

One of the most controversial issues in planetary science today is also one of the oldest: the nature and origin of the red to ochre color of the Martian surface. In 1934 Wildt suggested that the color is due to the presence of iron oxides and hydroxides on the planet, based on the similarity of the color of the Martian surface to the color of ferric oxide- and hydroxide-bearing terrestrial rocks. Since, on the Earth, the ferric oxides and hydroxides in the rocks are known to have been formed principally as a result of the exposure of iron-bearing minerals to water, Wildt's proposal has resulted in controversies concerning the possibilities that at one time Mars has had an extensive hydrosphere.

There have since developed three principal theories on the nature and origin of the red to ochre color of the Martian surface. Two of these theories still attribute the color to the presence of ferric oxides, the limonite and the oxidized basalt models, while the third one attributes the color to the presence of polymers of carbon suboxide on the surface.

The Limonite Model.

One group of investigators (Dollfus, 1957, 1961; Sharonov, 1961; Moroz, 1964; Draper et al., 1964; Sagan et al., 1965; Sagan, 1966; Tull, 1966) suggests that the surface is composed of a thick layer of goethite (α-FeOOH) and limonite, a hydrous form of goethite. This model is based on the similarities of the polarimetric, colorimetric, and photometric properties of the Martian disk to those of powdered laboratory specimens of limonite, goethite, and several terrestrial rocks. Adamcik (1963) added further support to the limonite model when he calculated the H_2O equilibrium dissociation pressure of goethite, which was found to agree with the telescopic measurements of the Martian atmospheric water vapor pressure (Spinrad et al., 1963; Kaplan et al., 1964; Schorn et al., 1966). The origin of the thick limonite and goethite deposits on Mars has been attributed to subaqueous weathering (oxidation occuring in the presence of water) during an earlier epoch on Mars, when the environmental conditions were like the warm and humid tropical regions of the Earth (Sagan et al., 1965; Sagan, 1966).

The hydrosphere explanation has been attacked by O'Connor (1968b), however. He has demonstrated that the amount of water which would have been needed to oxidize such large amounts of iron and concentrate it on the surface would have been accompanied by a quantity of N_2 that disagrees with the presently observed amounts in the Martian atmosphere. Further, aqueous deposits of iron oxides would have been accompanied by large quantities of carbonates, the characteristic spectral features of which have not been detected in the telescopic Martian reflection spectra. The carbonates would be more stable than goethite or limonite in the Martian environment (O'Connor, 1968a).

The stability of a fossil deposit of limonite and goethite on Mars has been attacked by Schmalz (1959), Fish (1966), and O'Connor (1968a). They have shown that since $pH_2O \leq 3 \times 10^{-4}$ torr at the 13-torr elevation level, the goethite would be stable only for temperatures less than 200°K. On Mars, near the equator , temperatures below 200°K are generally reached after sunset (Morrison et. al., 1969; Sagan and Veverka, 1971). Above 200°K, goethite dissociates on Mars into hematite (α-Fe_2O_3) and H_2O.

The Oxidized Basalt Model

Binder and Cruikshank (1964, 1966) demonstrated that the reflectance spectrum of Mars between 1.05 μ and 2.1 μ is not compatible with the limonite model. They suggest, rather, that the surface is composed of igneous rocks with either a powdery coating or a surface stain of limonite. Younkin (1966) further demonstrated that the Martian reflectance spectrum, from .34 μ to 1.1 μ, shows no obvious similarity to any of the laboratory spectra of powdered limonite. Sinton (1967) showed that the strength of the characteristic ferric oxide .85 μ band, in the Martian reflectance spectra, is indicative of only 2% or 3% or less of goethite or ferric oxide on Mars. Van Tassel and Salisbury (1964), Salisbury (1966), Salisbury and Hunt (1968, 1969), Tombaugh (1968), and O'Leary and Rae (1968) have provided additional evidence that goethite and limonite are only minor constituents on the Martian surface, even though these ferric oxide-hydroxides are the principal species responsible for the red to ochre color of the surface. In a series of papers by Adams and McCord (Adams, 1968; Adams and McCord, 1969; McCord, 1969; McCord and Adams, 1969), it has been shown that the optical properties of the Martian surface

are best simulated in the laboratory by the properties of an olivine-bearing basalt, which has been oxidized to the extent that it contains between 1% and 5% ferric oxide. The brightest regions contain between 3% and 5% ferric oxide and have mean particle diameters less than .05 mm. The darkest regions contain between 1% and 3% ferric oxide and have mean particle diameters between .05 mm and .1 mm. All regions fall on a brightness and color continuum (McCord and Westphal, 1971; McCord et. al., 1971).

Carbon Suboxide

Another theory which has been proposed for the coloration of the Martian surface is that the surface is coated with a polymer of carbon suboxide (Plummer and Carson, 1969; Perls, 1971; Khare et al., 1972). The reflectance spectra (Plummer and Carson, 1969) of these polymers are not in good agreement with the spectra of Mars, however. Some arguments for and against the formation and stability of carbon suboxide on Mars are reviewed in Perls (1971).

PROBLEM AND APPROACH

The Oxidized Basalt Model satisfactorily accounts for all of the optical properties of the planet, and it involves geochemically common materials. However, no working mechanism has yet been proposed to account for the high oxidation state of the Martian surface.

Binder and Cruikshank (1964) and Salisbury (1966) suggest that, given a sufficiently long period of time to act, the tenuous Martian atmosphere could possibly chemically weather the surfaces of exposed mineral grains. O'Connor (1968a) has shown, however, that the water vapor pressure is too low and the CO_2 partial pressure is too high for the oxidation to occur. O'Connor (1968a) further points out that an abundance of water in the vicinity of volcanoes, if it exists, would not be a local source for the production of goethite or limonite, either. The water would be equilibrated to the strongly reducing magmatic and atmospheric conditions rather than being a well-circulated, highly-oxygenated system, as are the oxidizing ground waters of the Earth. Tombaugh (1968) suggests that possibly iron meteorites, upon impacting the surface, may expose permafrost. The ice would sublime and react with the meteoritic iron to form the

goethite and limonite. The arguments proposed by O'Connor (1968a) indicate that Tombaugh's model is also unlikely.

The arguments against the direct reaction of the Martian atmosphere with iron-bearing minerals on the surface have neglected an important parameter, however. In addition to the atmosphere and surface temperature, the Martian environment is characterized by the presence of ultraviolet radiation. It is well known that illumination can affect the rate of surface reactions, and even reverse their thermodynamically predicted directions (cf. Samorjai, 1964).

In 1969 the author and Dr. Bruce Hapke demonstrated that magnetite, an accessory iron-bearing mineral in some terrestrial basalts, could be rapidly altered to a bright red phase in air, upon illumination with a high intensity ultraviolet lamp. The nature of the alteration product or mechanism was not determined, but it was expected that the illumination in air resulted in the alteration of magnetite to a ferric oxide phase or phases. An attempt to determine whether the reaction could occur in a CO_2 atmosphere yielded uncertain results due to equipment limitations.

Problem

A subsequent experiment has been designed to determine the kinetics and mechanism of the magnetite alteration phenomenon observed in that 1969 study, and to identify the reaction products. The results of this investigation, and its application to the problem of forming ferric oxides on Mars, form the subject matter of this dissertation. It is not in the scope of this dissertation to discuss the genesis or geochemistry of the Martian surface materials, or to determine whether ferric oxides are the actual coloring agents of these materials.

Approach

In order to determine the alteration mechanism, the reactants, reaction product(s), and the kinetics of the alteration must be determined. By knowing the reactants and products, a single reaction can be written which describes the overall phase change. This reaction is stoichiometrically simple in the sense that its advancement is described by a single parameter: the extent of reaction. Instead of a single reaction taking place as written, however, such phase changes usually proceed through a network of reactions which

involve reactive intermediates that do not appear among the final reaction products. The identification of these intermediates, the definition of the proper sequence of constituent reactions, and the relative rates of the individual steps are determined through the use of the kinetic rate equation. The experimentally derived kinetic rate equation specifies the functional dependence of the reaction rate on the various parameters, which are found to affect the rate.

It was suspected, at the onset of this experiment, that the reaction product is composed principally of ferric oxide, and in fact it is (see section on alteration phase identification). In the following chapter magnetite and its oxidation products are described. Also described are the principal reactions, which result in the formation of these oxidation products. In the third chapter the experimental determination of the kinetic rate equation is described. Also in this chapter, the alteration phase identification is described. In the fourth chapter the mechanism is derived. In the fifth chapter, the rate of the reaction in a Mars-like environment, and some implications for the formation of ferric oxide, as well as ferric oxyhydroxide, on Mars are discussed.

II. MAGNETITE AND ITS ALTERATION PRODUCTS

MAGNETITE

The samples used in this experiment consist of a precipitated synthetic magnetite powder. The powder was sorted by the manufacturer (Fisher Scientific Co.) to have particle diameters of .04($\pm$.02) μ (1 μ = 10^{-4} cm.). The manufacturer determined (technique unknown) that the composition of the magnetite is represented by the formula $Fe^{2+}_{.762}Fe^{3+}_{2.24}O_4$. Impurities include < 2% by weight, indigenous H_2O, < 2 ppm As, and < 1 ppm Hg. Magnetite has the theoretical formula $Fe^{2+}Fe^{3+}_2O_4$, and, therefore, the samples possess an excess of cation vacancies, and they are more oxidized than the stoichiometric magnetite.

Structure

The magnetite structure is shown in figure 1a. It is an inverse iron spinel, which has a closest-packed cubic array of O^{2-} anions, that are accompanied by charge-compensating cations in interstitial positions. Each oxygen ion has 14 interstices surrounding it. Six of them are located in the cubic edge directions, each being surrounded by six oxygen ions. The remaining eight are oriented in the space-diagonal directions,

each being surrounded by four O^{2-} ions. The unit cell has 32 oxygen anions and 24 cations, and hence it is composed of four Fe_3O_4 formula units, shown in Figure 1b. In this unit cell there are sixty-four tetrahedral (A) sites, only eight of which are occupied by Fe^{3+}. The remaining tetrahedral sites are vacant. Eight Fe^{3+} and eight Fe^{2+} cations occupy sixteen of the thirty-two octahedral (B) sites (Verwey and Haayman, 1941; Miles et al., 1957).

The Electronic Properties of Magnetite

The properties of magnetite, which govern the nature of its oxidation, arise from its electronic characteristics. The ferric and ferrous cations are transition metal cations, so that their electronic characteristics are governed by the properties of their 3d electron configuration. The Fe^{3+} cations on both the A and B sites have 3d electrons which are in the high-spin configuration, i.e. each of the five cationic d orbitals is occupied by a single electron. The spins of these electrons are coupled parallel to one another in the α (spin-down) direction. The B-site Fe^{2+} cations have, in addition to the five α-spin electrons, an antiparallel β-spin electron paired with one of the α-spin electrons.

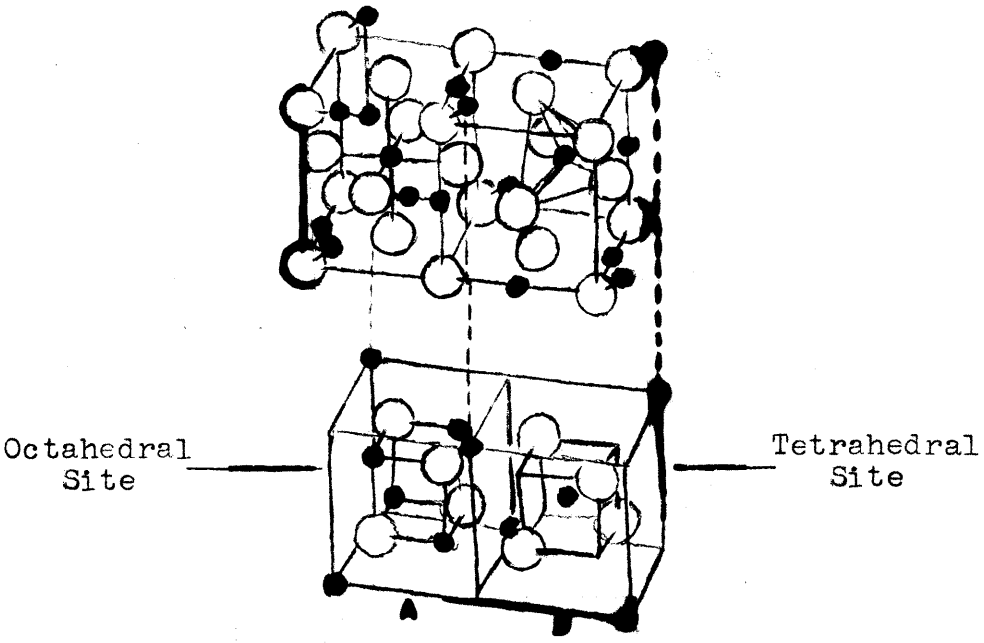

Figure 1a. The magnetite structure.

Magnetite

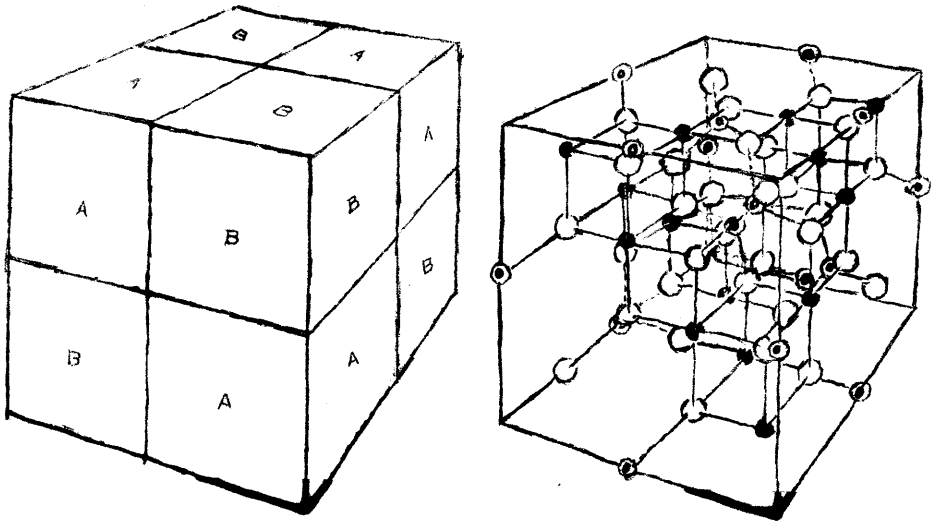

Packing Pattern of Repeating Units, A and B Being Shown in Figure 1b.

The Unit Lattice

⊙ - Tetrahedrally co-ordinated cation

● - Octahedrally co-ordinated cation

○ - Oxygen anion

Figure 1b. The unit cell.

Néel (1948) has shown that, below the Curie temperature (850°K), the α-spin electrons of all the Fe^{2+} and Fe^{3+} B-site cations are coupled parallel, and that the α-spins of the A-site d electrons are coupled anti-parallel to the α-spins of the unpaired electrons, on the B-sites. Above 120°K, the Verwey temperature, only two sets of lines are resolved in the Mössbauer spectra of magnetite (Bauminger et al., 1961; Ono et al., 1963), one set from the tetrahedral site cations and one from the octahedral site cations. From the Mössbauer data of Daniels and Rosencwaig (1969), it was found that the β-spin electrons of the Fe^{2+} cations hop to the nearest-neighbor Fe^{3+} cations, at a rate which is so high, that the Fe^{2+} and Fe^{3+} cations are indistinguishable. These β-spin electrons are not localized at discreet Fe^{2+} cations, but rather they are localized in Fe-Fe overlapping orbitals (Goodenough, 1971).

The charge transfer from Fe^{2+} to Fe^{3+} requires an activation energy of .04 eV (Miles et al., 1957). Heikes and Johnston (1957) have discussed the origin of this activation energy. If the β-spin electron is held at rest at one of the cation sites, for a long time relative to the vibrational period of the crystal

(10^{-12} - 10^{-13} sec.), then the site distorts and compensates for the additional charge. In order for the electron to move to an adjacent site, it is necessary that the surrounding anions be displaced so as to bring the Fe^{2+} cation back to the unstrained position (position occupied if the cation was Fe^{3+}). At this instant the potentials of the neighboring sites are degenerate, and the charge transfer can take place.

During electron hopping between cation sites, electron spin is conserved. The Pauli Exclusion Principle requires that two electrons, in the same orbital, have antiparallel spins. Therefore, since the spatial orbitals in the Fe^{2+} and Fe^{3+} cations are occupied by an α-spin electron, the β-spin electron transfer is constrained to occur from the Fe^{2+} cations to B-site Fe^{3+} cations. Charge transfer from the Fe^{2+} cations to A-site cations is spin-forbidden.

Since the room-temperature Mössbauer data show only two resolvable sets of lines, one from the A-site cations and one from the B-site cations, it is concluded that the time, t_{hop}, for a β-spin electron to hop from one B-site to another is too short for the resolution of the B-site Fe^{3+} and Fe^{2+} cations (Bauminger et al., 1961; Ono et. al., 1963; Daniels and Rosencwaig, 1969).

This finding requires that $t_{hop} < 10^{-8}$ sec. The condition for an electron to be localized is that $t_{hop} > 10^{-12}$ to 10^{-13} sec. Hence, the electron transfer time is within the interval $10^{-12} < t_{hop} < 10^{-8}$ sec.

In stoichiometric Magnetite, there is no natural way of grouping the B-site Fe^{2+} and Fe^{3+} cations into pairs, and therefore the β -spin electrons can migrate over the B-site sublattice. Hence, even though the polarons (β-spin electrons) are localized to overlapping Fe-Fe orbitals, stoichiometric magnetite has a very high static electrical conductivity ($\sigma \cong 10^{-2}$ ohm^{-1} cm^{-1}), under an applied electric field (Verwey and Haayman, 1941; Daniels and Rosencwaig, 1969).

The samples used in the experiment are non-stoichiometric, however, in that there is a deficit of Fe^{2+} cations, and a surplus of Fe^{3+} cations. Such magnetite contains both B-site vacancies and B-site Fe^{3+} cations in substitution for B-site Fe^{2+} cations (Verwey and Haayman, 1941). Nearly all of the available tetrahedral sites remain occupied by the Fe^{3+} ions, even in the most non-stoichiometric magnetite (Daniels and Rosencwaig, 1969).

Since the electrical conduction has an activation energy of .04 eV, incident photons with energies

greater than .04 eV, can be absorbed, leading to photo-conduction. The conduction in magnetite produces a continuum absorption which sweeps across the infrared and visible spectra, and which is so strong that the cationic electronic transition bands cannot be resolved. Waldron (1955) measured the infrared absorption spectrum of magnetite, for photon energies ranging between .04 eV ($\lambda = 30\mu$) and .19 eV ($\lambda = 6.7\mu$). His results are shown in figure 2a. In this figure the optical density, defined as $\log_{10}(I_o/I)$, is plotted as a function of the incident photon energy and wavelength (I_o is the incident radiation intensity and I is the transmitted intensity). It is expected that, if charge transfer is the only process responsible for photon absorption, in the range .04 eV to .19 eV, the optical density should be 0, at .04 eV, and it should increase smoothly with increased photon energy. In Figure 2a, it can be seen that the optical density is not 0 at .04 eV, and that there are two absorption bands, centered in the vacinity of .07 eV ($\lambda = 18\mu$) and .05 eV ($\lambda = 25\mu$). The band at .07 eV corresponds to the vibrations of the oxygen ions along the tetrahedral bond directions, viz. [111] . The band at .05 eV corresponds to the vibration of the oxygen ions in a

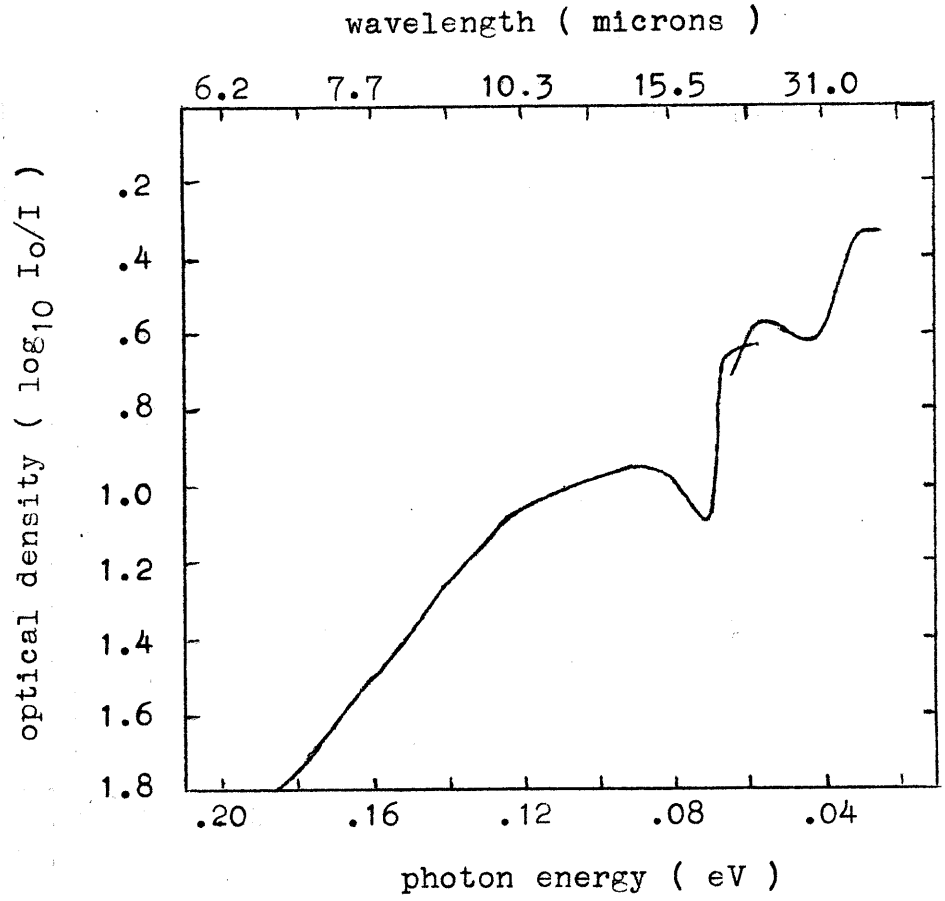

Figure 2a. The infrared absorption spectrum of magnetite, .04 eV to .19 eV (after Waldron, 1955)

direction nearly perpendicular to the first vibration mode. The non-zero optical density at .04 eV and lower energies is due to absorption from the long-wavelength leg of the .05 eV band, and the short-wavelength leg of a band centered at .03 eV ($\lambda = 41\mu$). The .03 eV band is attributed to the oscillations of the B-site cations, in their octahedral ligand environments (Waldron, 1955). From the short-wavelength end of the .07 eV band to .19 eV ($\lambda = 6.5\mu$), the absorption, by the β-spin conduction electrons, causes the continuous increase in optical density, with increasing photon energy, as expected (Waldron, 1955; Samokhvalov et al., 1969).

Balberg and Pankove (1971a) extended the transmission spectrum into the near-infrared wavelength region, from .15 eV ($\lambda = 8.3\mu$) to .75 eV ($\lambda = 1.65\mu$). Their results are shown in Figure 2b. As in Figure 2a, optical density is plotted as a function of incident photon energy and wavelength. The anomalous absorption features at .16 eV and .21 eV are attributed to Ti and Zn impurity bands (Balberg and Pankove, 1971a). The absorption by the conduction electrons displays a band edge at .3 eV ($\lambda = 4.1\mu$) in the curve. To interpret this band edge, the energy levels in which the

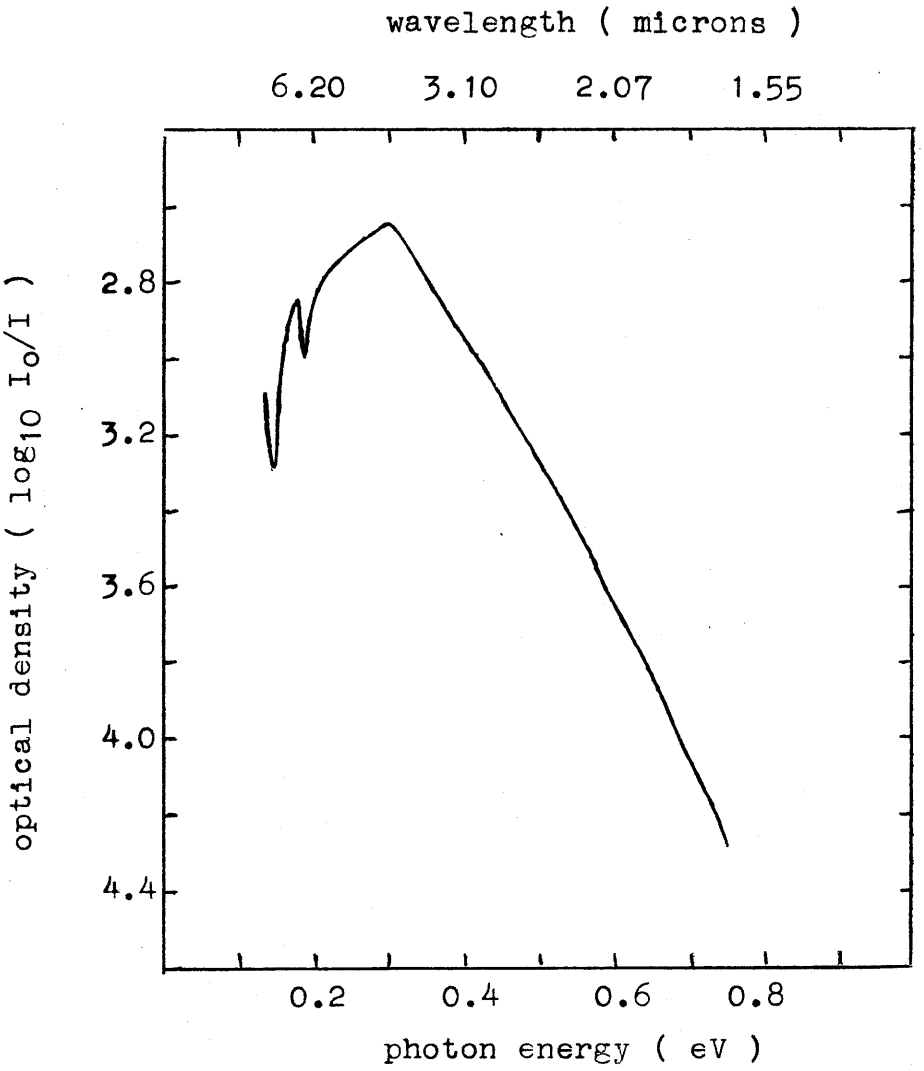

Figure 2b. The infrared absorption spectrum of magnetite, .15 eV to .75 eV (after Balberg and Pankove, 1971a).

β -electron can reside, are first described.

The degenerate 3d electron energy levels of the free Fe^{2+} ion are split, when placed in a regular octahedral site. Two of the cation orbitals, the d_{z2} and the d_{x2-y2} orbitals, have their lobes directed toward the six oxygen ligands . The other three d orbitals, the d_{xy}, d_{xz}, and d_{yz} orbitals, are directed between the ligands. The d_{xy}, d_{xz}, and d_{yz} orbitals are degenerate in a regular octahedral ligand field, and they are the ground state orbitals. The d_{z2} and d_{x2-y2} orbitals are degenerate, and they are the excited state orbitals. A trigonal distortion of the ligand field, resulting from the charge transfer between adjacent B-site cations, removes the degeneracy of the ground state orbitals. These three orbitals are split into a ground state singlet and two higher energy doublets (Yosida and Tachiki, 1957). The d_{z2} and d_{x2-y2} orbitals remain degenerate in the trigonal distortion.

The overlapping ground state singlet orbitals have a lower degeneracy than the overlapping higher-energy doublets, and, therefore, β -electron hopping, in the ground state, is more suppressed than hopping along the doublet orbitals, because of the stronger electron correlation in the singly degenerate ground

state (Bari et al., 1970). Therefore, the band edge in Figure 2b, at .3 eV, is attributed to the onset of conduction along the doublet orbitals (Balberg and Pankove, 1971a), i.e. the bottom of the doublet band lies .3 eV above the ground-state band. The cathodoluminescence studies of Balberg and Pankove (1971b) indicate that the width of the doublet band is .6 eV, and that the separation of the ground-state singlet band and the degenerate d_{z2} and d_{x2-y2} orbitals is 3.2 eV.

Miles et al. (1957) measured the optical density from 1.5 eV (λ = .83μ) to 6.2 eV (λ = .20μ). Their results are shown in Figure 2c. The onset of strong absorption at 1.8 eV (λ =.69μ) is assigned to charge transfer from the top of the O^{2-} 2p band to the ground state singlet orbital of the Fe^{3+} (Balberg and Pankove, 1971b). Wickersheim and Lefever (1962) indicate that such a band is characteristic of Fe^{3+} which is octahedrally coordinated by O^{2-} ions. The charge transfer band reaches its maximum intensity at around 3 eV. The absorption plateau, from 2.8 eV to 3.8 eV, probably corresponds to this charge transfer peak, and to the onset of conduction in the d_{z2} and d_{x2-y2} orbital bands. The width of this conduction band is

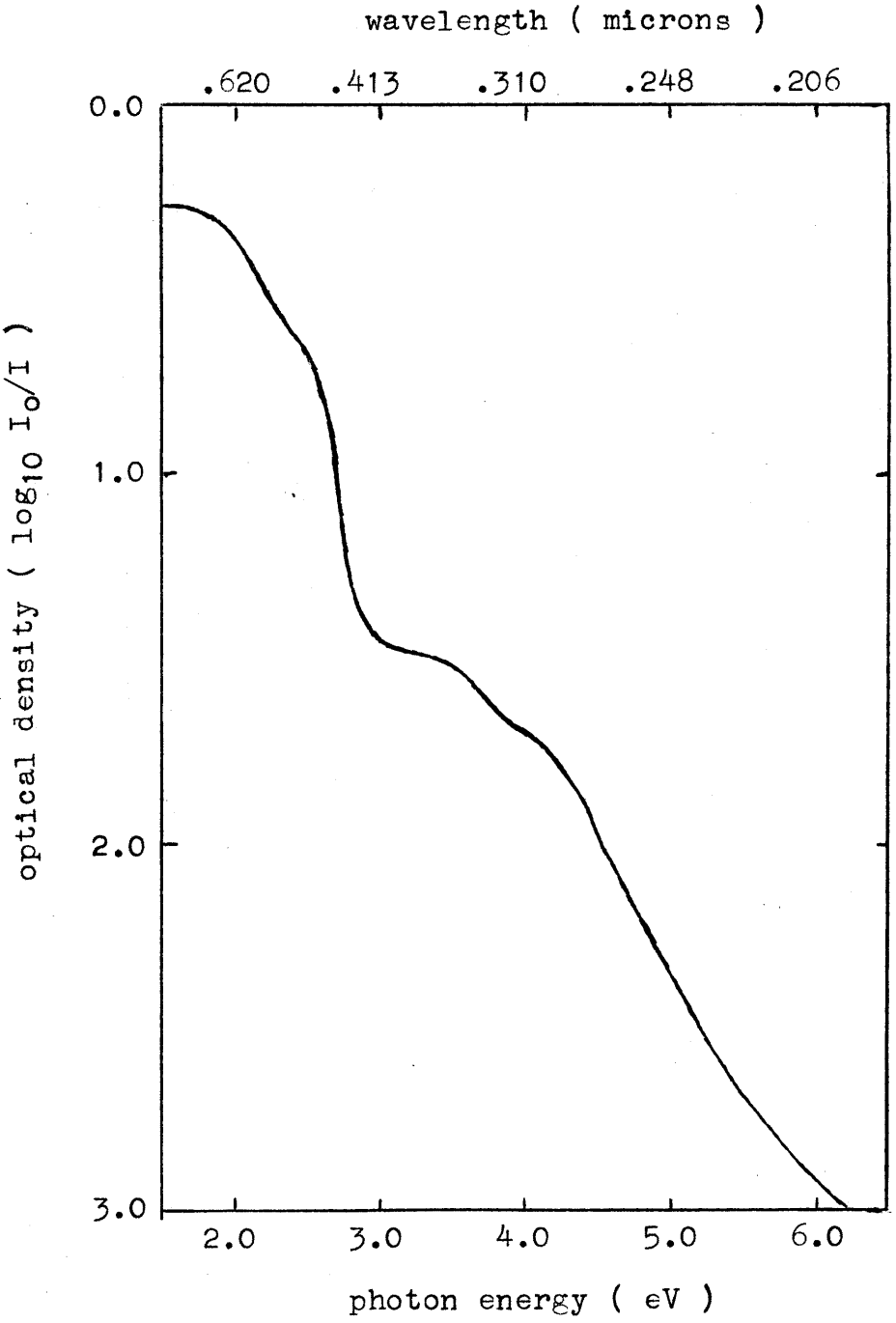

Figure 2c. The visible absorption spectrum of magnetite, 1.5 eV to 6.2 eV (after Miles et al., 1957).

probably .7 eV (Balberg and Pankove, 1971b).

Photoemission

The transmission characteristics of Figure 2c (Miles et al., 1957) was taken with a magnetite thin film, produced by the oxidation of an evaporated Fe film. The chemisorption of oxygen to Fe at temperatures between 100°C and ~300°C results in the formation of an amorphous Fe_3O_4 surface film, approximately 20 Å thick (Feitknecht, 1965). Heating to a temperature of 400°C, in a vacuum, produces crystalline Fe_3O_4. Some FeO is also probably present in the oxide film (Pignocco and Pellissier, 1967). Burshtein and Shurmovskaya (1964) measured the change in photoelectric work function of an Fe film, when oxidized. A maximum change of -.6 eV occurs for oxidized Fe, with oxygen adsorbed to it, and a change of -.2 eV occurs for the oxidized Fe layer without adsorbed oxygen on it. The photoelectric work function of Fe metal is $4.5 \pm .15$ eV (Eastman, 1970), so that the onset of photoemission from magnetite should occur for incident photon energies between 3.8 eV and 4.2 eV. The lower energy value is probably the more realistic value for magnetite in an O_2-bearing atmosphere. A photoelectric work function of 3.8 eV is in good agreement with the observed increase in absorption for photon

energies higher than 3.8 eV in Figure 2c.

Photoemission occurs when a ground state electron absorbs a photon, moves to the solid / atmosphere interface, and escapes the surface potential barrier. The photoelectric work function is the minimum photon energy which results in photoemission. This energy corresponds to the energy difference between the surface barrier and the singlet ground state electron orbital of the β-electron, shown in Figure 3. It will vary, depending upon the amount of adsorbed species on the surface, from a minimum of 3.8 eV in an O_2-bearing atmosphere, to about 4.2 eV in a vacuum.

Since the work function is large, compared with the conduction activation energy (.04 eV), there is a high probability of secondary electron excitation. In this case, an electron, which gains kinetic energy upon absorbing a photon, may collide with another electron, and partition the energy between the two electrons, cooling the first electron. This results in a decrease in the number of photoelectrons per incident photon. The number of emitted electrons per incident photon, the quantum yield, generally ranges from about 10^{-7} at the work function, 3.8 eV, to around 10^{-3} to 10^{-2} at 6 eV (Sommer and Spicer, 1965). The escape depth will be

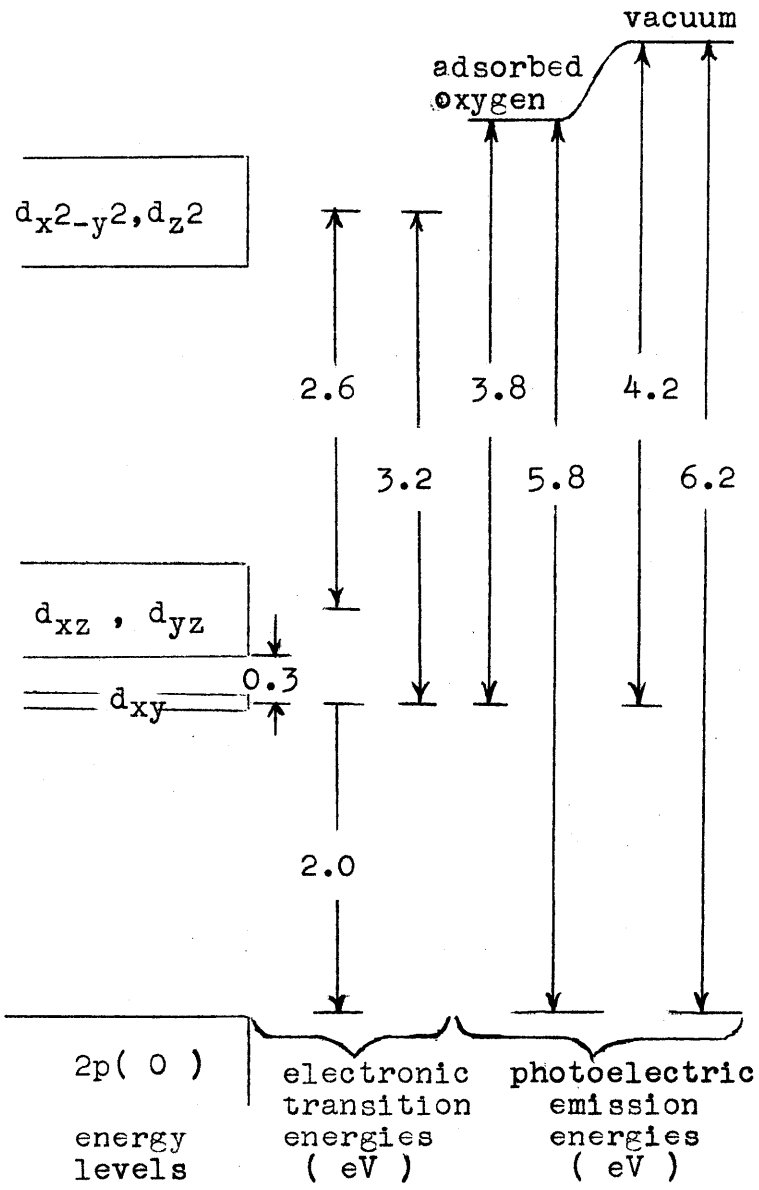

Figure 3. The energy level diagram of the β -electron of magnetite.

on the order of 15 Å to 100 Å (Sommer and Spicer, 1965).

Since the onset of strong absorption at 1.8 eV in Figure 2c is assigned to the onset of charge transfer from the top of the O^{2-} valence 2p band to the ground-state singlet orbital of the Fe^{3+} (Balberg and Pankove, 1971b), photoemission from the 2p valence band should occur for incident photon energies greater than about 5.6 to 5.8 eV. The electron energy level diagram of the β -electron of magnetite is presented in Figure 3.

THE OXIDATION PRODUCTS OF MAGNETITE

The oxidation products of magnetite include ferric oxides, as well as hydrous and anhydrous oxyhydroxides. The common feature of all of the oxidation products is that they are composed of stacks of close-packed oxygen/hydroxyl sheets, with various arrangements of ferric ions in the octahedral and tetrahedral interstices.

Hematite

Hematite (α -Fe_2O_3) is characterized by a hexagonal close-packed oxygen lattice, with ferric cations occupying octahedral interstices. It has the rhombohedral corundum structure, illustrated in Figure 4. The near-neighbor ferric ions along [111], the c-axis, are arranged such that the spins of the electrons are coupled antiparallel, while the spins of the electrons of the cations in the basal plane, (111), are coupled ferromagnetically. There is a strong antiferromagnetic cation-anion-cation coupling between the cations of neighboring basal planes, with the ratio of the strengths of the cation-anion-cation to cation-cation interactions being much greater than one (Goodenough, 1971). The Néel temperature is 963°K (Freier et al., 1962; Lielmezs and Chaklader, 1965). From the Néel

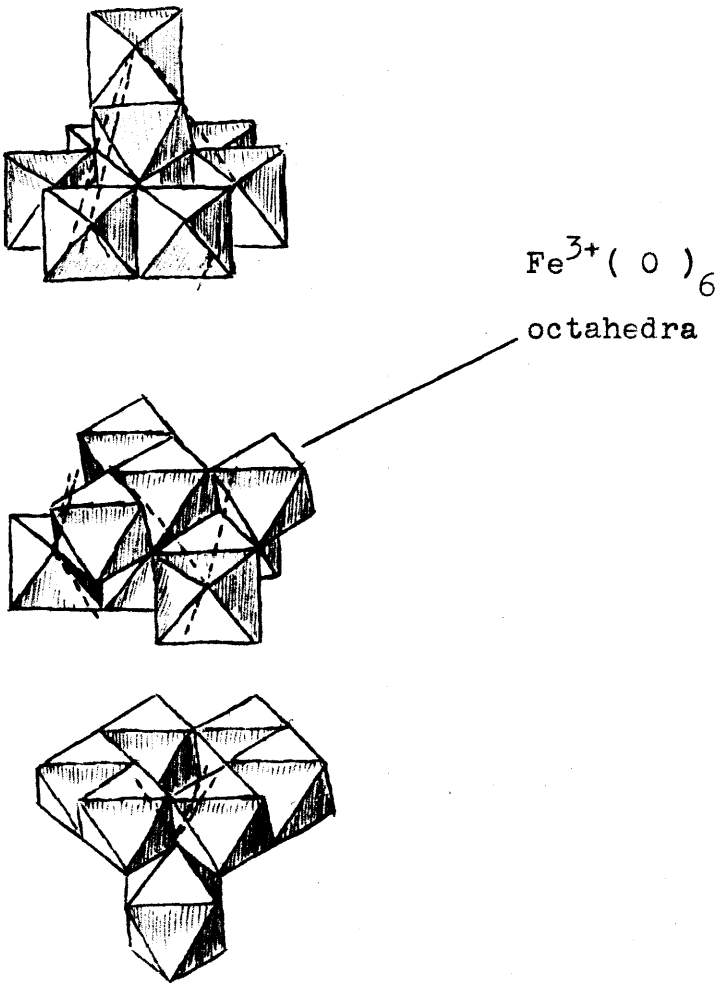

Figure 4. The hematite structure

temperature down to 250°K the spins lie in the basal planes, while below 250°K the spins flip to [111] with an entropy change of 600 erg/deg·g (Gallagher et al., 1964).

Optical transmission measurements were taken by Morin (1954), Baily (1960), and Gardner et al. (1963). Their results are shown in Figures 5a, 5b, and 5c, respectively. The absorption feature at .7 eV ($\lambda = 1.8\mu$), in Figure 5a, is associated with impurities (Morin, 1954). The absorption feature at 1.5 eV ($\lambda = .83\mu$) is due to the transition, $^6A_{1g}(^6S) \rightarrow {}^4T_{1g}(^4G)$, in Fe^{3+} (Wickersheim and Lefever, 1962). Morin (1954) attributes the stronger broad absorption feature, situated in the spectrum with its band edge at .95 eV ($\lambda = 1.3\mu$), and centered at 1.8 eV ($\lambda = .7\mu$), to conduction in the sp bands of oxygen. Morin (1954) and Wickersheim and Lefever (1962) attribute the other broad absorption feature, with its band edge at 1.9 eV ($\lambda = .7\ \mu$) and centered at 3.0 eV ($\lambda = .4\mu$), to charge transfer from the sp bands of oxygen to empty d levels of Fe^{3+}. Such charge transfer results in the temporary formation of Fe^{2+}. As a result, Fe^{2+} to Fe^{3+} charge transfer occurs via overlapping t_{2g} (d_{xy}, d_{xz}, and d_{yz}) orbitals,

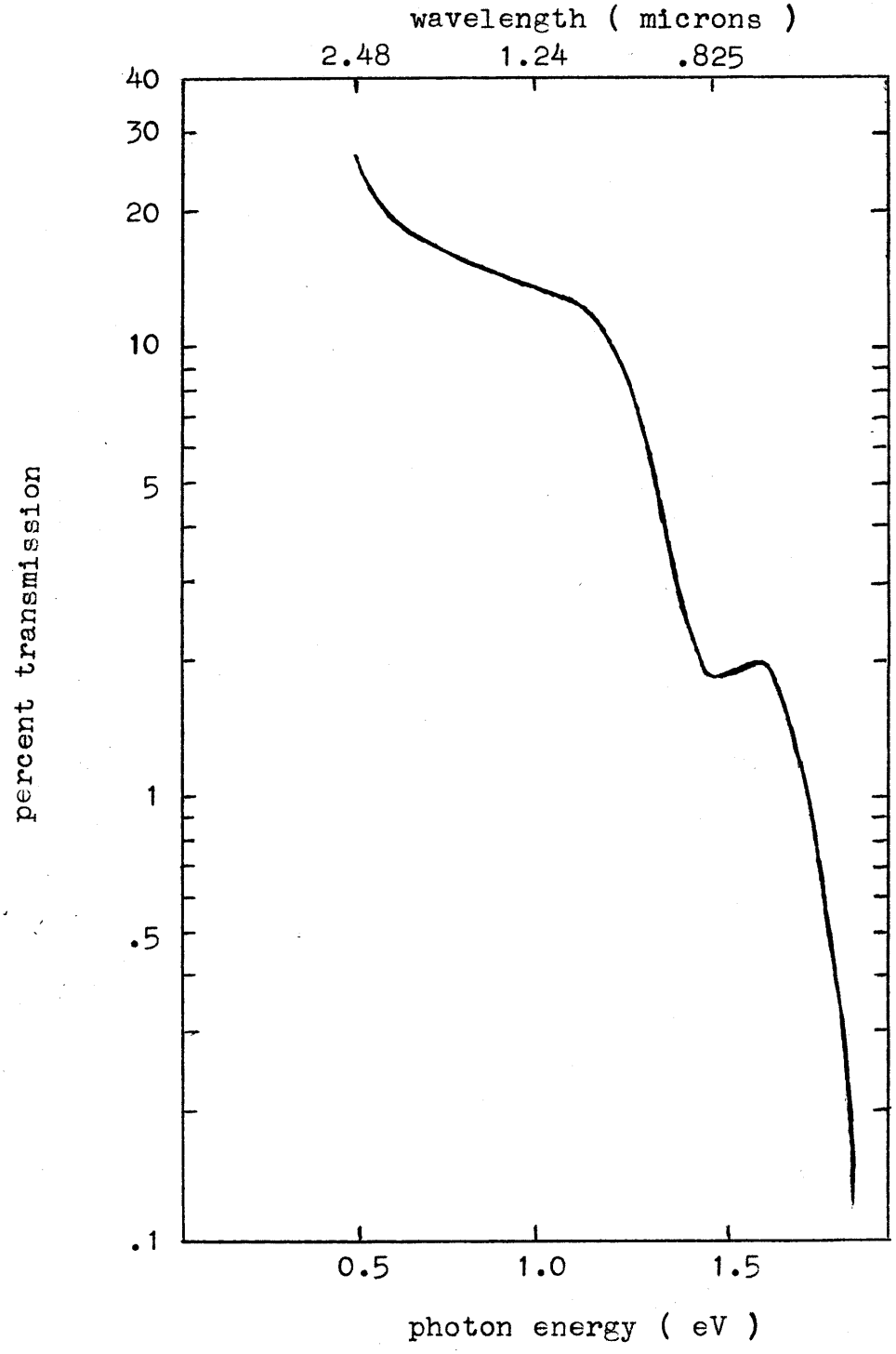

Figure 5a. The absorption spectrum of hematite, .5 eV to 2.0 eV (after Morin, 1954).

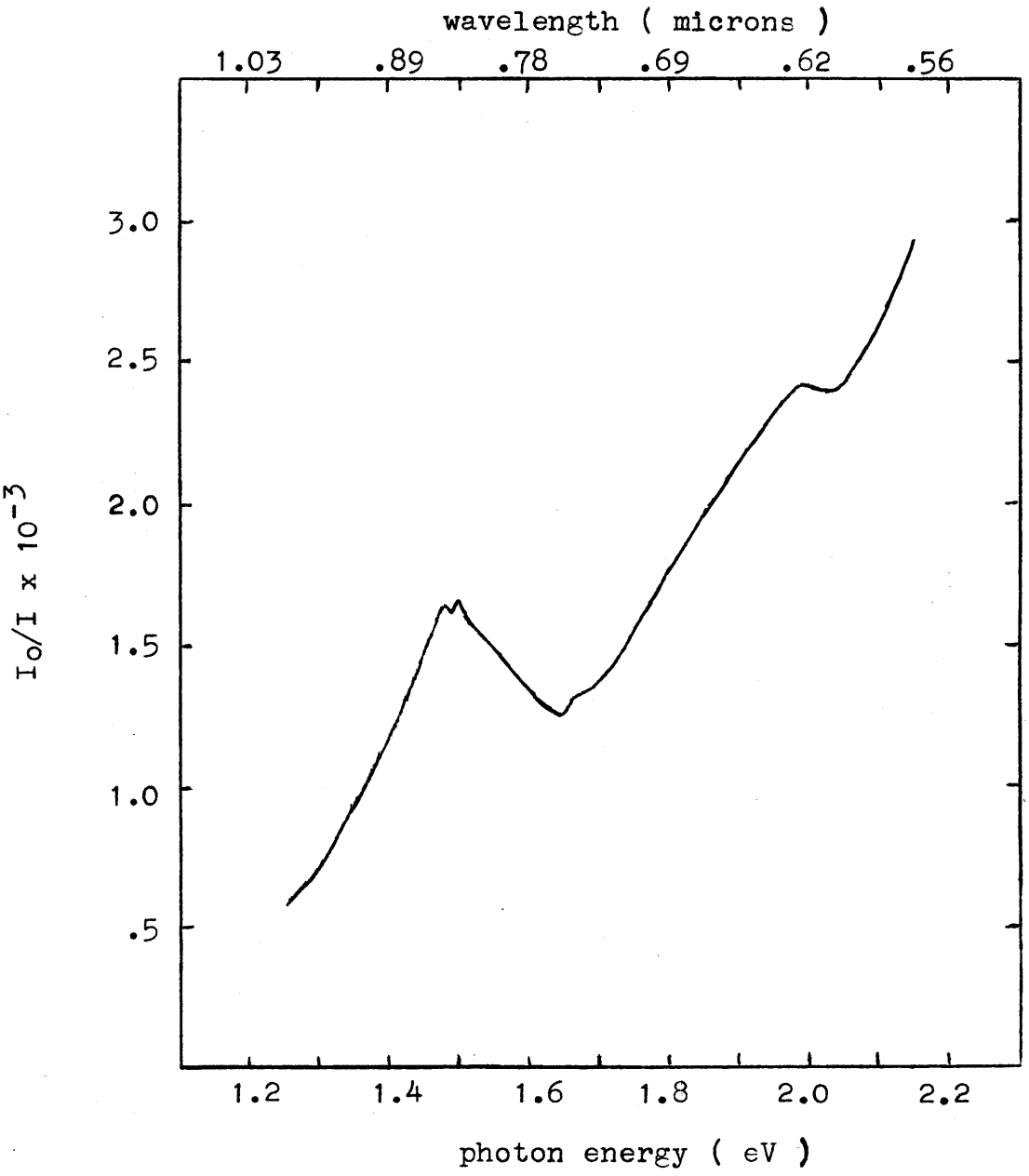

Figure 5b. The absorption spectrum of hematite, 1.2 eV to 2.1 eV (after Baily, 1960).

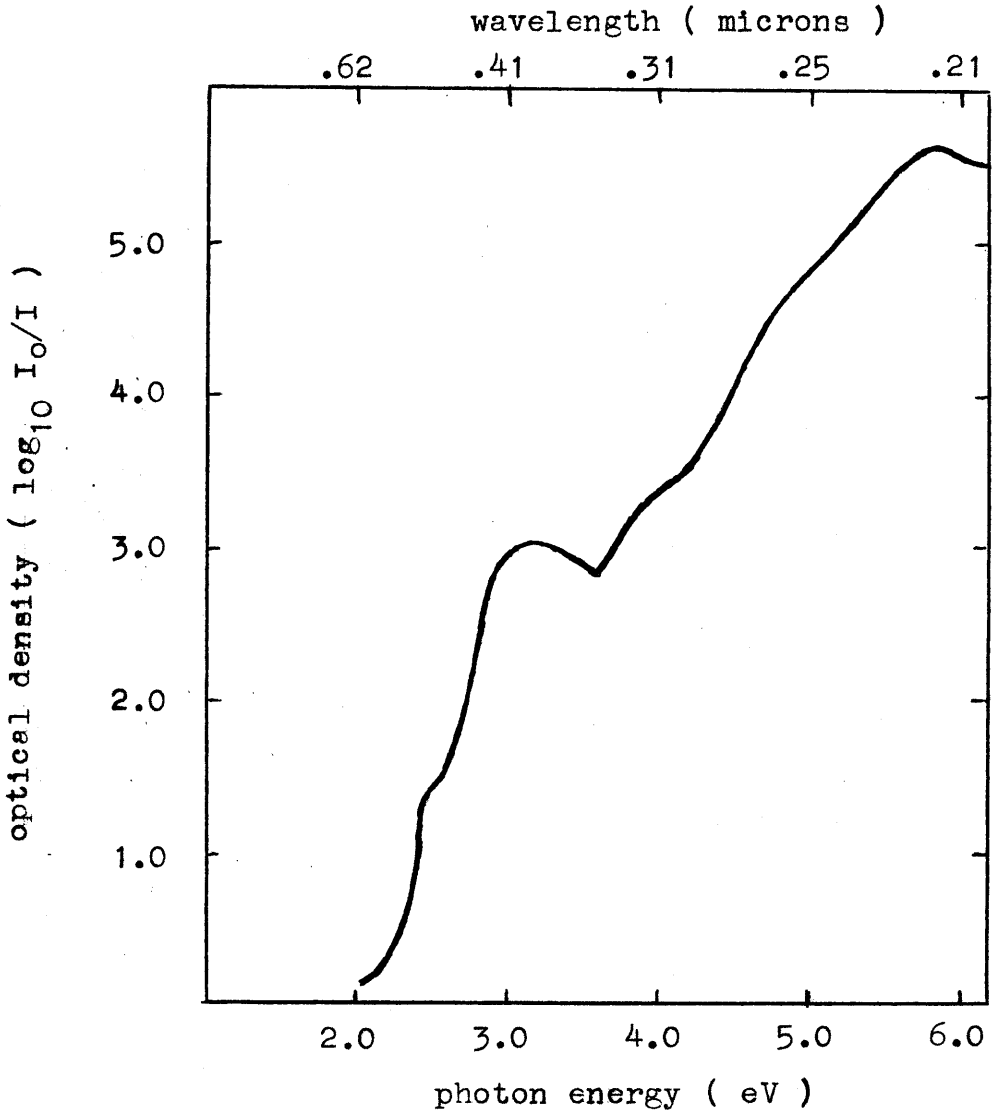

Figure 5c. The absorption spectrum of hematite, 2.0 eV to 6.2 eV (after Gardner et.al., 1963)

giving rise to additional absorption from 1.9 eV ($\lambda = .7\mu$) to 2.1 eV ($\lambda = .6\mu$). This charge transfer band is seen in the γ spectra of orthopyroxenes, containing significant amounts of Fe^{3+} (Burns, 1966). It is also seen in the spectra of amphiboles (Faye et al., 1968). In amphiboles the charge transfer occurs from Fe^{2+}, in M_1 sites (coordinated by 4 oxygen and 2 hydroxyl ions, cis) to Fe^{3+}, in M_2 sites (cation coordinated by 6 oxygen ions). Charge transfer from Fe^{2+}, in M_1 sites, to Fe^{3+}, in M_3 sites (both sites contain four oxygen ions and two hydroxyl ions, the M_1 site being cis and the M_3 site being trans), gives rise to absorption between 2.1 eV ($\lambda = .6\mu$) and 2.5 eV ($\lambda = .5\mu$). In the orthopyroxene, the $.6\mu$ -$.7\mu$ charge transfer occurs from Fe^{2+}, in M_2 sites, to Fe^{3+}, in M_1 sites, both sites being free of OH. In the hematite spectrum (Figure 5b) both charge transfer features can be seen, indicating that OH substitutes for oxygen. A strong broad absorption feature can be seen in Figure 5c, with its band edge at 3.7 eV ($\lambda = .33\mu$), and centered at 5.7 eV ($\lambda = .22\mu$). No explanation has been given for this feature, except that it is a charge transfer feature (Gardner et al.,

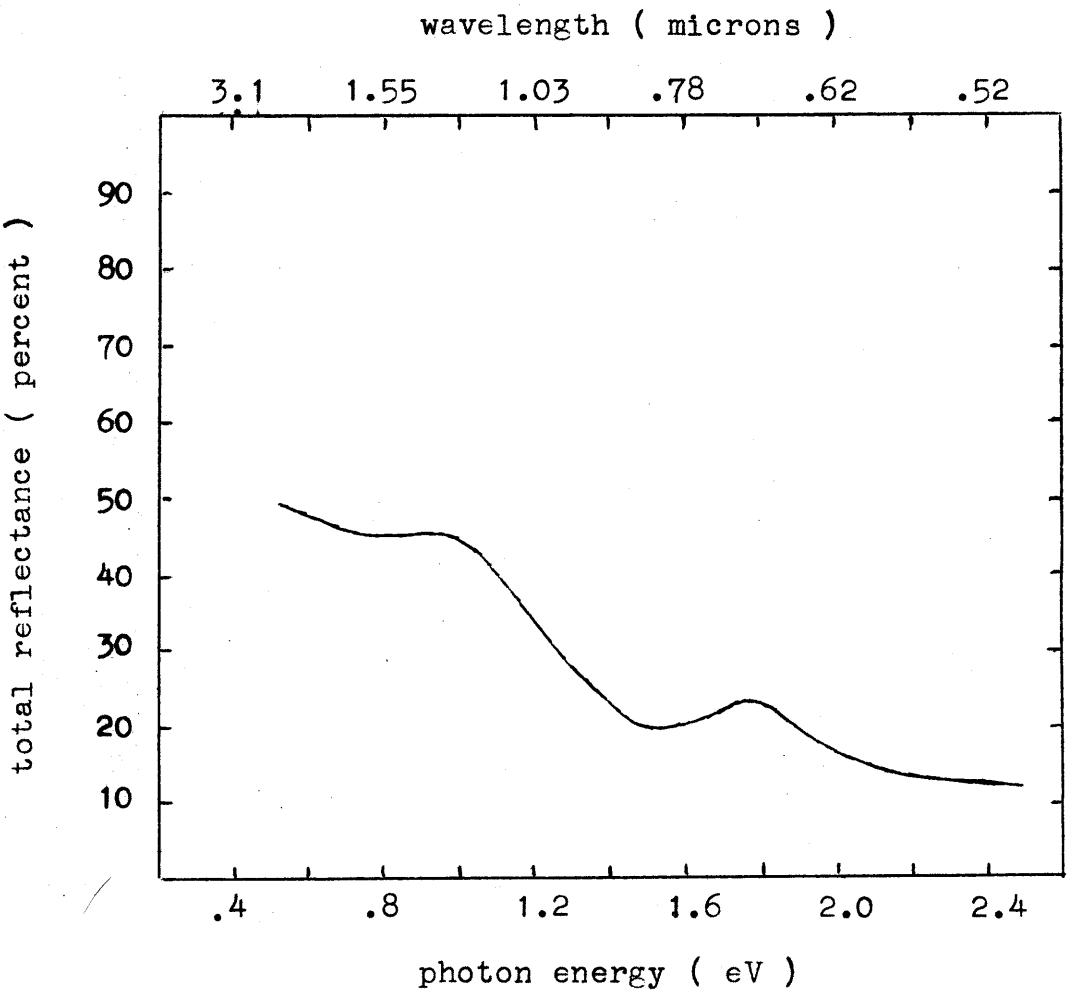

Figure 6. The reflectance spectrum of powdered natural hematite specimen, .5 eV to 2.5 eV (after Sagan et al., 1965).

1963). Sagan et al. (1965) measured the reflectance spectrum of a powdered natural hematite sample. His results are shown in Figure 6. The absorption bands at .85μ and between .5μ and .7μ give rise to a relative reflectance maximum, centered at .7μ, giving hematite its characteristic red color.

The formation of hematite. The surface oxidation of magnetite to hematite occurs as a result of oxygen chemisorption on the surface. Oxygen chemisorption occurs in two stages (Burshtein et al., 1964). The first stage of chemisorption is a rapid one, in which a monolayer of O is chemisorbed to the surface. The second stage is a much slower one, but the same amount of oxygen is chemisorbed in this in this stage, as there is in the first stage. The first stage of chemisorption leads to the formation of a protective oxide layer which prevents further oxidation.

Burshtein et al. (1964) found, however, that if H_2O is adsorbed on this first-stage protective oxide layer, its structure becomes disturbed and its protective properties are altered. This is observed to lead to the rapid formation of a thick oxide layer on the surface. In a .07 torr atmosphere of O_2, the first stage of adsorption on Ge, in the absence of adsorbed H_2O, for

example, occurs in as little as 10 minutes, while several days are required to complete the second stage. After 90 minutes of exposure to the .07 torr O_2 atmosphere with H_2O adsorbed to the surface, the amount of oxygen chemisorbed to the surface is more than 130 times that which is chemisorbed to the surface upon exposure to the H_2O-free O_2 atmosphere for 90 minutes. This is also observed to be true for Si and Fe. Burshtein et al. (1964) propose that the adsorbed H_2O promotes the migration of substrate cations to the surface, where they undergo first-stage chemisorption and oxidation.

The cations are leached from the magnetite substrate by the adsorbed H_2O. Removal of the ions from the magnetite depends on whether the water molecules can penetrate the oxygen environment about the cation. The cations at the surfaces of the magnetite crystals are the most susceptible to leaching because of the broken bonds there. In the presence of adsorbed water, an OH^- ion is bonded to the cation at a surface cation vacancy and the H^+ ion converts a second O^{2-} ion to a second hydroxyl ion (Blyholder and Richardson, 1964). A second water molecule approaches the cation along a surface t_{2g} orbital, forming a seven-coordinate transition state (Basolo and Pearson, 1958). This

transition state breaks down to form a two-hydroxyl, four-oxygen coordinated cation. The process is repeated four times, and the the cation goes into solution in the form of $Fe(H_2O)_6^{3+}$ or $Fe(H_2O)_6^{2+}$, depending on whether the cation is ferric or ferrous. A similar process leaches ferric cations from the tetrahedral sites. The hexahydrated cations migrate in the second layer of physically adsorbed H_2O molecules (McCafferty et al., 1970). Desorption of the H_2O, oxidation of the Fe^{2+} cations, and replacement of OH^- ions with O^{2-} ions, results in the incorporation of the ferric cations, and the growth of the ferric oxide structure. Crystallites of Hematite are formed in the Magnetite surface layer.

Once these Hematite crystallites are formed, in the Magnetite surface layer, the oxidation of Magnetite can proceed, in the absence of H_2O, through a process of " nucleation-disruption " of the protective oxide layer (Arkharov, 1966). The Hematite structure has a different spatial configuration than that of Magnetite. This different spatial configuration, of the Hematite, causes a spatial fluctuation in the structural configuration of the Magnetite, at the Hematite / Magnetite transition zone. Such a disruption, of the spatial configuration, disrupts the protective properties of the overlaying

first-stage oxide layer, and the crystallite grows latterally. The small displacements of the atoms closest to the center of initial rebuilding, induces displacements of other atoms, further removed from the center. The forces, inducing successive displacements, are then transferred, from atom to atom, in each crystallographic direction, radially from the crystallite center. When the magnitude of the displacements reaches some critical value, a rupture of coherence occurs, and hematite scales result.

The hematite islands are hexagonally shaped and polycrystalline (Takei and Chiba, 1960). Tallman and Gulbransen (1968a,b) have found that the α-Fe_2O_3 crystals, in these islands, are in the form of whiskers, blade-like platelets, and broad rounded platelets. The whiskers have an axial twist, characteristic of an axial screw dislocation. The blade-like platelet is a contact mirror twin, with the blade face being the rhombohedral face (010) of the primitive structural rhombohedron. The rounded platelets are sandwhich structures, with the faces parallel to the basal plane.

In both the H_2O-bearing and dry, O_2-bearing, atmospheres, the oxide whiskers are the first growths. In dry atmospheres the whiskers predominate ,

accompanied by separate areas of the broad rounded platelets. None of the blade-like platelets are observed, when the atmosphere is H_2O-free. In the H_2O-bearing atmospheres, the whiskers evolve into blade-like platelets. The platelets probably grow by rapid diffusion of iron cations along the twin interfaces, followed by incorporation into the oxide structure along the platelet edges (Tallman and Gulbransen, 1968b). No crystals are observed to grow in atmospheres free of H_2O.

Goethite and Limonite

Adsorption of H_2O to hematite, during its formation, can lead to the formation of goethite. Goethite is a ferric oxyhydroxide, denoted by the formula α-FeOOH. The structure of goethite is that of hexagonally close-packed oxygen and hydroxyl ions, with Fe^{3+} cations occupying octahedral interstices. The $Fe(O,OH)_6$ octahedra are arranged in strips, as shown in Figure 7 (Francombe and Rooksby, 1959). The strips are rigidly bonded, because of the presence of directed hydroxyl bonds. Dehydration of goethite occurs through removal of water molecules, or hydroxyl groups, in strips, running parallel to the c-axis, and lying in (0110) cleavage

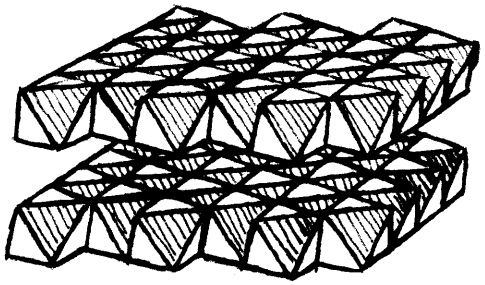

Figure 7. The goethite structure.

planes of the oxyhydroxide lattice (Francombe and Rooksby, 1959).

The goethite structure starts to lose water at about 230°C. On heating to 270°C, transformation to the alpha ferric oxide structure is completed, but ordering of the cations is incomplete. When the temperature reaches 600°C, the cations are completely ordered. These temperatures are for P = 1 atmosphere.

The reflectance spectrum of a natural goethite sample is shown in figure 8 (Sagan et. al., 1965). The reflectance minimum at .83μ to .85μ in hematite is shifted to .85μ to .87μ in goethite (Adams, 1968). The cation-cation charge transfer absorption feature, between .6μ and .7μ is reduced, because of the presence of abundant coordinate OH, while the .5μ to .6μ charge transfer feature can be readily seen. This results in a reflectance plateau between .6μ and .7μ, giving goethite its characteristic yellow-brown to red-brown color.

Adsorption of H_2O to hematite, during its formation can also lead to the formation of limonite. Limonite is essentially goethite, with physically bound water. The water molecules are probably doubly hydrogen-bonded to the goethite structure (McCafferty et. al., 1970).

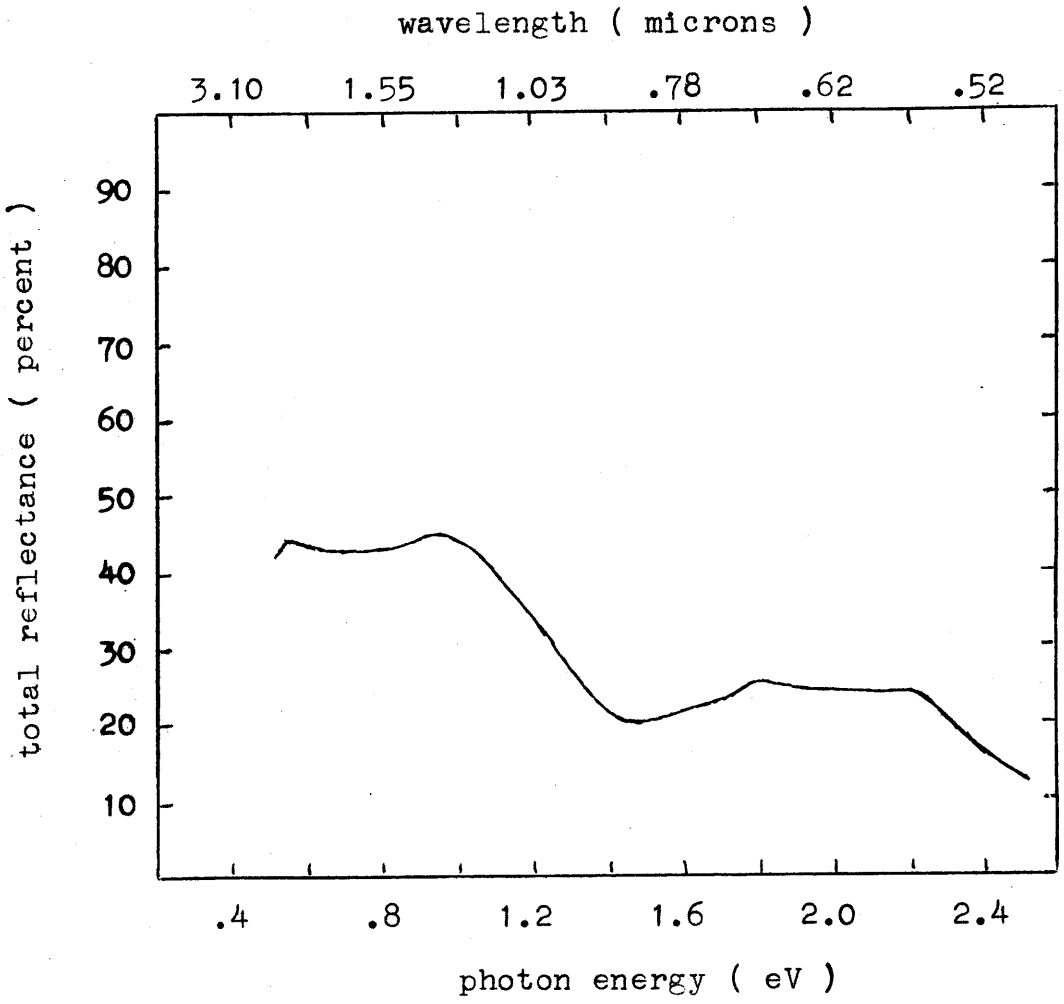

Figure 8. The reflectance spectrum of a powdered natural goethite specimen, .5 eV to 2.5 eV (after Sagan et al., 1965).

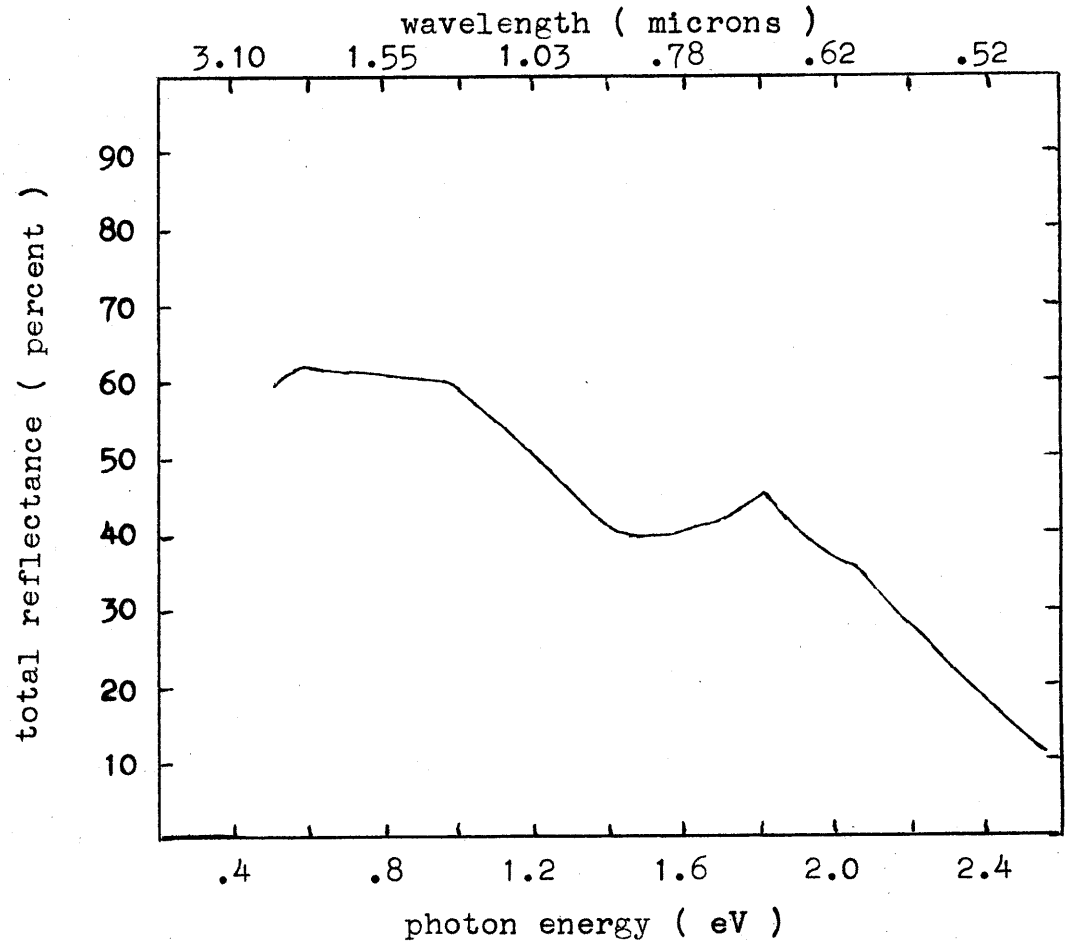

Figure 9. The reflectance spectrum of a powdered natural limonite specimen, .5 eV to 2.5 eV (after Sagan et al., 1965)

A natural limonite reflectance spectrum is shown in figure 9 (Sagan et. al., 1965).

Maghemite and Lepidocrocite

Maghemite (γ -Fe_2O_3) is a cubic form of ferric oxide. It has the spinel structure, with the ratio of the cations to oxygen ions falling between .625 and .67. This ratio is smaller than that in magnetite, which is .75. The unit cell has a formula, ranging between $Fe_8^{3+}\left[Fe_{12}^{3+}\square_4\right](OH)_4O_{28}$ and $Fe_8^{3+}\left[Fe_{13\ 1/3}^{3+}\square_{2/3}\right]O_{32}$ (David and Welch, 1956), where $\square$ represents a cation vacancy. The species included within the brackets are in octahedral sites, while the Fe^{3+} outside of the brackets are in tetrahedral sites. The 16 octahedral sites, in the unit cell, are occupied in such a way that each cation vacancy is surrounded by 6 ferric cations in a deformed octahedron, and each ferric cation, in an octahedral site, is surrounded by two vacancies and four ferric cations. The Fe^{3+}, in the tetrahedral sites, are distributed in the same manner as in magnetite.

The presence of cation defects in spinel structures, as in maghemite, normally causes the structure to break down into a more close-packed structure, but the presence of combined water, in the gamma oxide, provides an additional stability . The water contents, observed in typical γ -Fe_2O_3 samples, (.54 to .94 percent) correspond to the presence of one H atom, per 10 to 20 cations (David

and Welch, 1956). David and Welch propose that combined water is situated in the structure, such that the hydroxyl portion of the molecule replaces one of the O^{2-} ions, which bound a vacancy, and the H portion of the molecule occupies the vacancy, as an inclusion. Braun (1952) and Aharoni et al. (1962) propose that γ-Fe_2O_3 actually consists of a solid solution of $Fe_8^{3+}\left[Fe_{13}^{3+}\ {}_{1/3}\square_2\ {}_{2/3}\right]O_{32}$ and HFe_5O_8, the hydrogen ferrite stabilizing the structure.

Takei and Chiba (1966) report that the O^{2-} to Fe^{3+} charge transfer band edge in maghemite falls between 2.2 eV (λ = .56μ) and 2.5 eV (λ = .50μ), in contrast to the value of 1.8 eV (λ = .7μ) in α-Fe_2O_3. Takei and Chiba did not present their optical data in the 1966 paper, but it is expected that, instead of having such a high energy band edge, the .6μ to .7μ charge transfer feature, in maghemite, is weak or absent, as in goethite, and the .5μ to .6μ feature is strong, as it is in hematite, goethite and limonite. This would give the misleading appearance of a band edge between .5μ and .6μ. At any rate, the reflectance maximum between .6μ and .7μ gives Maghemite its characteristic brown color.

Lepidocrocite (γ-FeOOH) consists of parallel layers of maghemite, held together by weak hydrogen bonds. The dehydration of lepidocrocite, by heating,

gives δ-Fe_2O_3 at 350°C. Lepidocrocite powder is yellow to yellow-brown in color.

Maghemite formation. Colombo et al. (1965) have reported that γ-Fe_2O_3 is formed, in the magnetite surface layer, topotactically, i.e. that the δ-Fe_2O_3 is formed through internal cationic displacements, and removal, within the magnetite surface layer, such that there is accord, in three dimensions, between the initial and final lattices. The δ-Fe_2O_3 is in solid solution with the magnetite. Leaching of the cations, from the magnetite surface layer, during the formation of hematite, can lead to the formation of maghemite, under the hematite surface layer. Hematite can form, as a result of the disproportionation of γ-Fe_2O_3 into α-Fe_2O_3 and Fe_3O_4.

Magnetite-Maghemite-Hematite Stability

For temperatures between 50°C and 250°C, particles, with diameters less than about 1μ, oxidize, in the presence of water vapor and oxygen, to maghemite (David and Welch, 1956; Elder, 1965; Johnson and Merrill, 1972). Particles, with diameters between about 1μ and 25μ, oxidize to a mixture of maghemite and hematite, in this temperature range, while hematite forms, when the particle diameters exceed 25μ, in this temperature range.

For temperatures between 250°C and 580°C, the $< 1\mu$

particles oxidize to a mixture of maghemite and hematite, in the presence of water vapor (David and Welch, 1956). In this temperature range, the 1μ to 25μ particles also oxidize to the maghemite and hematite mixture, and the larger particles oxidize exclusively to hematite (Elder, 1965; Johnson and Merrill, 1972). Again, in the absence of water vapor, all of the samples oxidize exclusively to hematite in this temperature range.

Above 580°C all magnetite particles oxidize to Hematite exclusively, both with and without water vapor present. An exception to this was reported by Takei and Chiba (1966), however. They deposited a γ-Fe_2O_3 phase on an MgO substrate, which stabilized the maghemite to temperatures as high as 680°C. This high-temperature gamma phase was vacancy-disordered, however. Renshaw and Roscoe (1969) suggest that magnetite could provide an additional stability to maghemite, over that supplied by the combined water molecules.

The disproportionation of α-Fe_2O_3, into γ-Fe_2O_3 and Fe_3O_4, is irreversible. The disproportionation involves the restacking of the close-packed oxygen ion layers, with a synchronized displacement of the ferric ions (Kachi et. al., 1963). The transformation temperature decreases from 510°C, for .2μ particles to

370°C for .015u particles (Bando et al., 1965). The transformation temperatures, for aggregated particles, are lower than the temperatures for the separate unit particles, which make them up. The transformation temperature for the gamma phase, on the stabilizing MgO substrate, is considerably higher, than those gamma phases not on stabilizing substrates (Renshaw and Roscoe, 1969; Takei and Chiba, 1966).

III. UV-STIMULATED OXIDATION OF MAGNETITE: THE KINETIC RATE EQUATION AND PHASE IDENTIFICATION

EXPERIMENTAL DESIGN

Design Requirements

It was discovered by the author and Dr. Bruce Hapke, in 1969, that the illumination with ultraviolet light of magnetite, in air, resulted in the rapid alteration of the magnetite to a bright red phase. It was expected that the alteration phase was ferric oxide, but no positive identification of the alteration phase(s) was made. The present study is designed to determine the nature of the observed alteration phenomenon, and to identify the reaction product.

The mechanism of the alteration phenomenon is determined, through identifying the reactants and reaction products and by experimentally determining the kinetic rate equation. By knowing the reactants and products, a single reaction can be written, which describes the overall phase change. This reaction is stoichiometrically simple, in that its advancement is described by a single parameter: the extent of reaction.

Instead of a single reaction taking place, as written, however, the process proceeds through a network of reactions

which involve reactive intermediates, not appearing in the overall reaction. The central tasks, of determining the mechanism, are; (1) identify the reaction intermediates; (2) define the proper sequence of constituent reactions; and (3) determine the relative rates of the individual steps. The experimentally derived kinetic rate equation provides the information needed to solve these three tasks, by specifying the functional dependence of the reaction rate on the various parameters, which affect the rate. The kinetic rate equation also allows a prediction of the reaction rate in any specified environment.

The various environmental parameters, which may affect the rate, include atmospheric composition, pressure, and temperature, incident spectral radiation intensity distribution, magnetite particle size, and the amounts and types of adsorbed species present. The dynamic ranges over which these parameters must be investigated in order to determine the mechanism dictate the experimental design requirements.

The apparatus must be capable of attaining the values of the parameters, which obtained during the discovery of the alteration phenomenon by the author and Dr. Hapke. If, as was suspected during the design stages of this experiment, the process is an oxidation process,

then it is of special interest to determine whether the process can occur in the Martian environment. Hence, the apparatus should also attain the values of these parameters, that obtain in the Martian environment.

In air, the reaction took place in the presence of N_2, O_2, CO_2, H_2O, and other minor constituents, at a total pressure of 760 torr. The atmosphere and sample reached a temperature of $\sim 370^{\circ}K$. The spectral radiation intensity distribution, at the time of the observed alteration, is unknown. The particle diameter was $.04(\pm.02)\mu$. The principal adsorbed species were N_2 and H_2O, with minor quantities of O_2 and CO_2.

The present-day Martian lower atmosphere consists almost entirely of CO_2, with a surface pressure of between 1 and 13 torr (Fjeldbo and Eshleman, 1968; Fjeldbo et al., 1970; Kliore et al., 1972; Belton and Hunten, 1971), depending upon the surface elevation. The O_2 / CO_2 abundance ratio is 1.3×10^{-3}, and the O_2 / CO abundance ratio is approximately 2.0 (Traub and Carleton, 1972). The H_2O / CO_2 abundance ratio is on the order of 2×10^{-4} (Schorn et al., 1967; Kaplan et al., 1964). The diurnal temperature range, at the subsolar lattitudes, ranges between $185^{\circ}K$ and $305^{\circ}K$ (Morrison et al., 1969; Sinton and Strong, 1960). Since the atmosphere is

composed almost entirely of CO_2, at pressures ranging from about 1 torr to 13 torr, it will allow solar radiation to penetrate to the surface, nearly unattenuated, at wavelengths longward of about .195μ (Thompson et al., 1963).

An environmental chamber, in which the parameters can be manipulated, has been designed to accomodate atmospheres, with up to six compositional components, in any proportion. The total pressure can be adjusted to any value within the range $5.0(\pm.1) \times 10^{-3}$ torr to $1.0(\pm.1) \times 10^{3}$ torr. The temperature can be adjusted to within $\pm$ 2°K over the range 240°K to 380°K. The relative spectral radiation intensity distribution at the sample can be adjusted to any of the five curves, in Figure 10. These curves are scaled to 1.0 at .350μ. The intensity, at .350μ, can be adjusted to any value, up to $\mathbb{I}_{.350} = 2.8 \times 10^{19}$ photons-cm^{-2}-sec^{-1}-Å^{-1}, to within $\pm$10% accuracy. A comparison of the laboratory relative spectral intensity distribution to that of solar radiation is shown in Figure 11.

Environmental Chamber

The environmental chamber constructed for this experiment, is illustrated in Figure 12. It was designed by the author and machined from 316-stainless steel stock. The chamber includes a high-thermal-inertia 316-ss sample

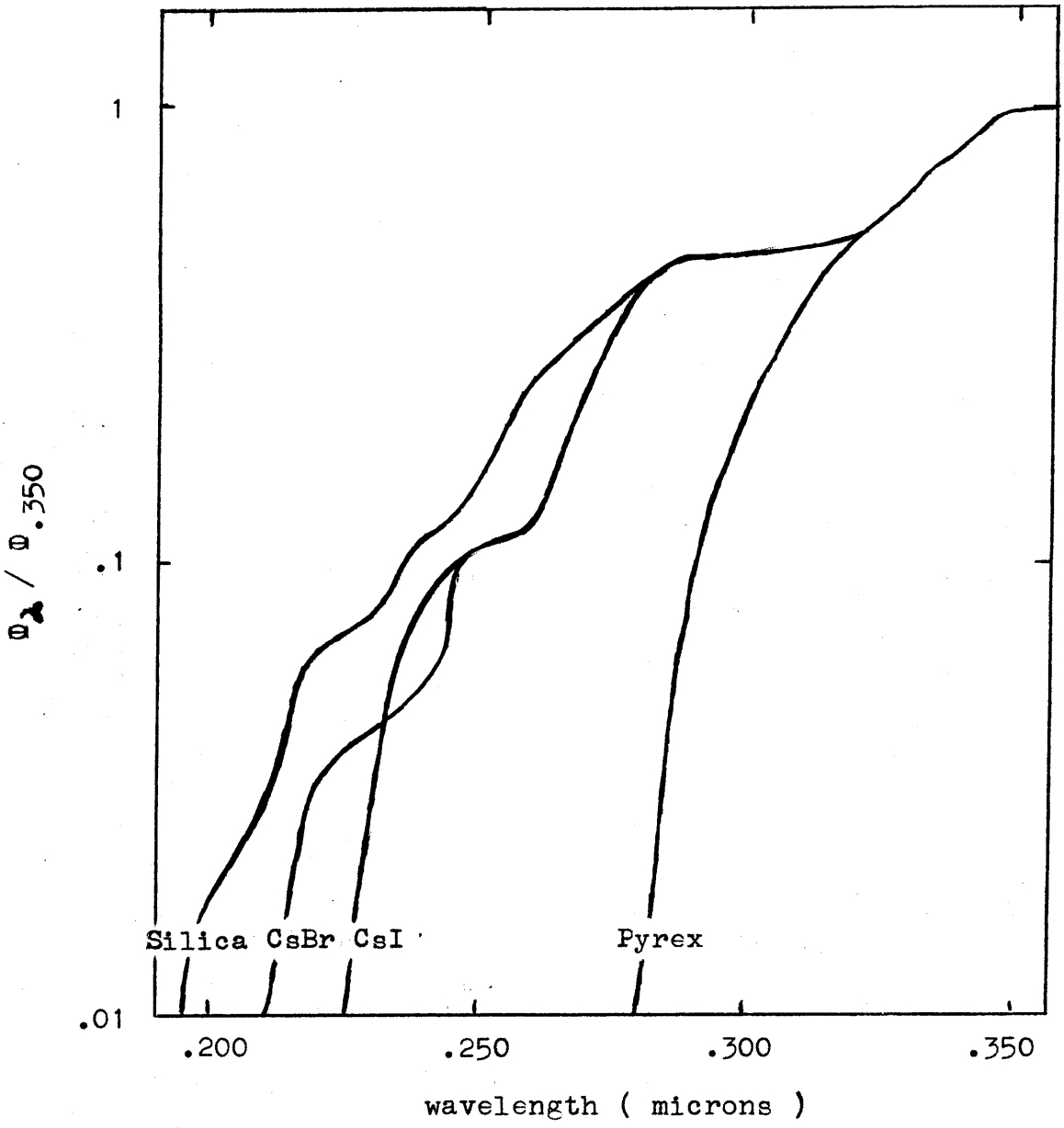

Figure 10. The relative spectral radiation intensity distribution, at the sample, using the fused silica, CsBr, CsI, or Pyrex window, scaled to 1.0 at $\lambda = .350\mu$.

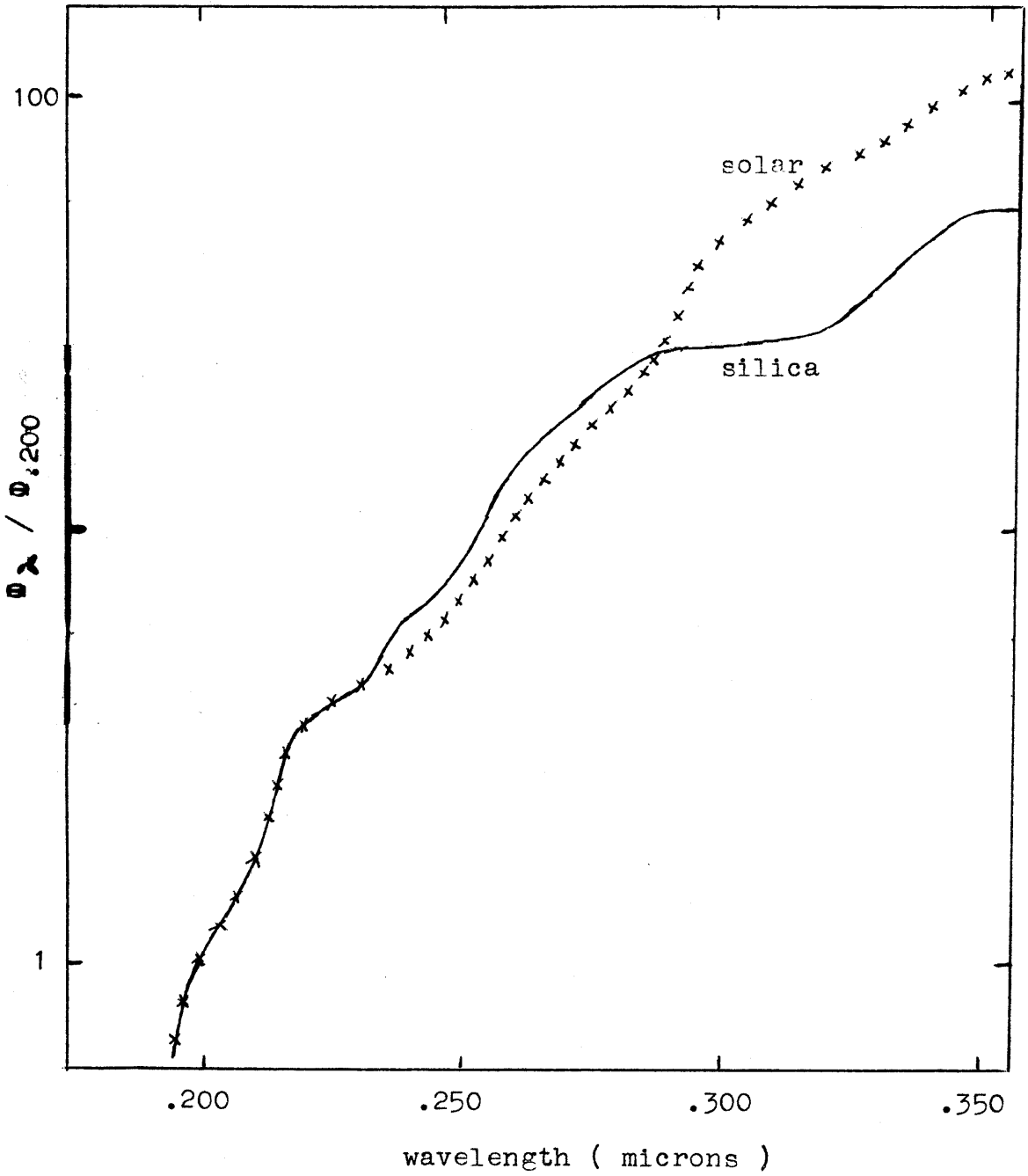

Figure 11. A comparison of the laboratory relative spectral radiation intensity distribution, using the silica window, to that of solar radiation, the two set equal to each other at $\lambda = .200\mu$.

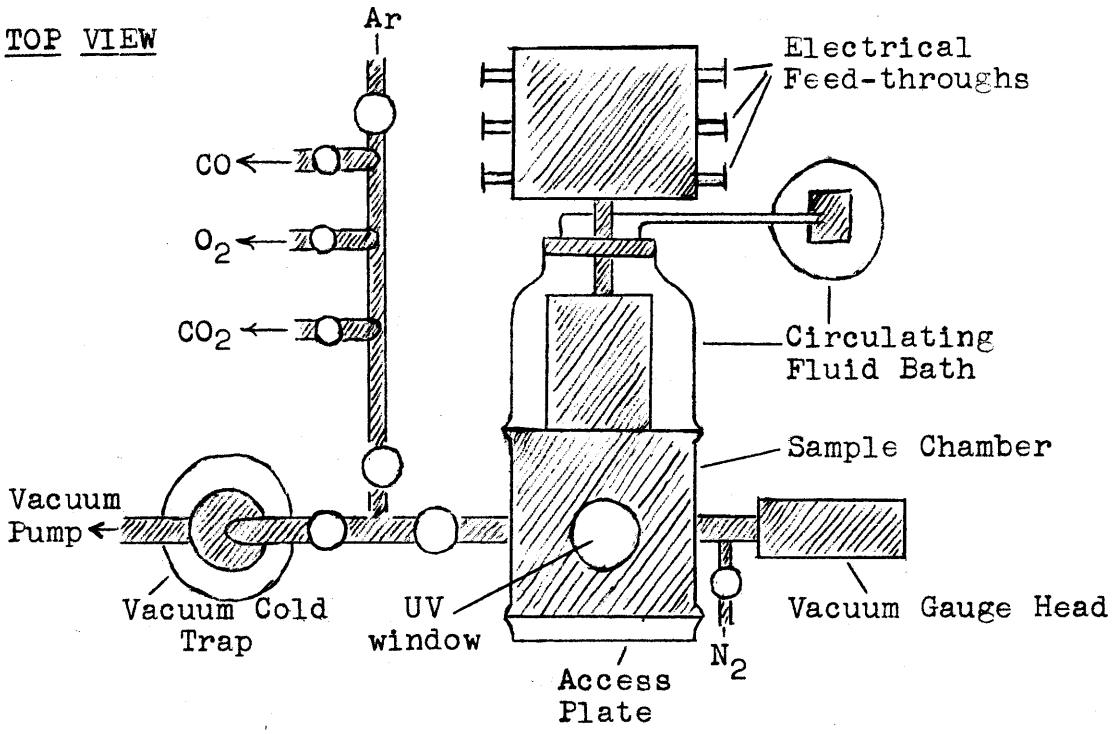

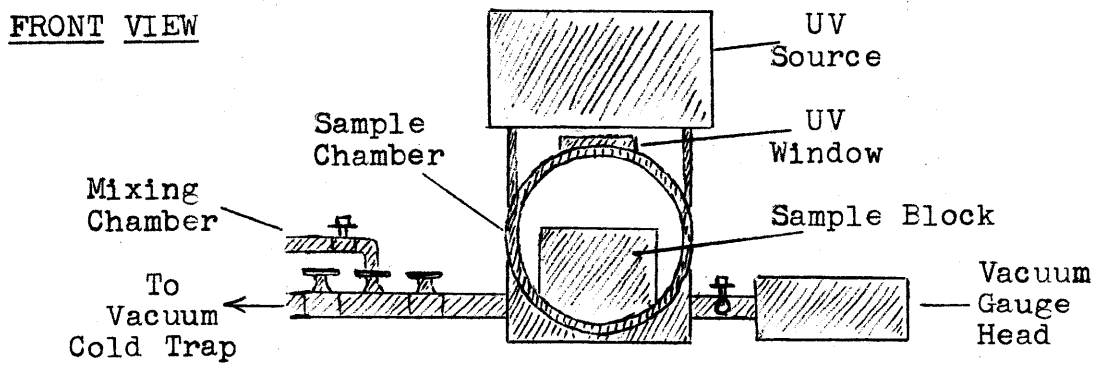

Figure 12. The environmental chamber.

block, which can be rotated, so that the incident radiation can illuminate the sample, at any desired angle, between 0^{o} and 90^{o}.

Connected to the environmental chamber is a mixing chamber, in which the composition of the atmosphere is set. The gases enter the chamber through a network of high-vacuum rough valves and needle valves. The composition is controlled through the use of an Edwards ED 330 two-stage mechanical pump, four Cenco vacuum / pressure gauges, and a Norton NRC 820 Alphatron Vacuum Gauge. The gases used are Matheson Research grade and Ultrahigh Purity grade CO_2, CO, O_2, N_2, and Ar. A stainless steel liquid nitrogen cold trap is located between the vacuum pump and the environmental chamber. Also attached to the chamber is an electrical feedthrough box, for the temperature sensors and general electrical connections. The electrical feedthrough box was also machined from 316-ss stock. The Norton NRC 820 Alphatron gauge is connected through a third inlet to the chamber. The same inlet is used for purging the system with Ar. Access to the chamber is accomplished with a removable 6-inch diameter Pyrex plate at the front of the chamber.

The UV radiation enters the chamber through a $1\frac{1}{2}$-inch diameter window, at the top of the chamber. The

relative spectral radiation intensity distribution can be modified, by replacing the fused silica window with a CsBr, CsI, or Pyrex window. The resultant intensity distributions are shown in figure 10. The radiation source is mounted directly above the UV window. It consists of a horizontally mounted Christie 300-watt Xenon lamp, and a 1-inch diameter fused silica lens. The net transmission factor, of the lens and fused silica window, source to sample, is .72 $\pm$.04, over the wavelength range .200$\mu \leq \lambda \leq$.400μ. The radiation intensity at the sample, at the standard wavelength (λ = .350μ), is computed using the formula,

$$\mathbb{I}_{.350} = .72(\pm.04)(1.1\text{x}10^{16})(\pi a^2/4\pi r^2) \;/\; A, \qquad (1)$$

where .72 ($\pm$.04) is the dimensionless transmission factor, 1.1 x 10^{16} is the source intensity at λ=.350μ (lamp output data was supplied by the manufacturer, Christie Electric) in photons - -sec^{-1}-Å^{-1}, the factor ($\pi a^2/4\pi r^2$) is the dimensionless fraction of the source intensity, which passes through the lens, of radius a, and located at a distance, r, from the source, and A is the cross-sectional area, in cm^2, of the incident radiation beam, at the sample. $\mathbb{I}_{.350}$ is adjusted to the desired intensity by varying r. a is fixed at 1.27 cm.

The chamber is cooled, and heated, through the use of a

fluid bath, which is circulated around the walls of the chamber. The fluid consists of a solution of alcohol and water, heated by a laboratory hot plate, or cooled with dry ice or liquid nitrogen. The temperatures of the circulating fluid, atmosphere, and sample are monitored with three remote thermistor probes, linked to a Simpson " Thermo-Meter," and calibrated with the use of distilled ice water.

Sample Preparation

The samples consisted of a synthetic precipitated magnetite powder, sorted by the manufacturer (Fisher Scientific) to be .04 ($\pm$.02)μ in diameter, with the formula $Fe^{2+}_{.762}Fe^{3+}_{2.24}O_4$. Impurities included < 2 ppm As and < 1 ppm Hg.

The samples were washed with acetone and methyl alcohol, to reduce the amount of organic impurities, and then with distilled water, to reduce the amount of water-soluble inorganic impurities. The washed magnetite was then placed in a dynamic N_2 atmosphere, at a pressure of 2.2 ($\pm$.05) x 10^{-2} torr, and a temperature of 302 ($\pm$2)^{o}K. The dried material was then pulverized in air, and formed into 1 cm x 1 cm x 1 mm portions, with a packing density of .91 ($\pm$.03) g-cm^{-3}.

The H_2O vapor pressure, in the ambient atmosphere,

was determined prior to each experimental session, by reducing the temperature of the chamber to the onset of H_2O condensation. The temperature of the chamber was then increased, until the ratio of the H_2O vapor pressure to the H_2O saturation vapor pressure, pH_2O/P, was .05. Assuming that the magnetite grains are spheres of diameter $d = .04\mu$, and density $\rho = 5$ g-cm^{-3}, the geometrical surface area of the magnetite is (Brunauer, 1937),

$$A_g = (6/d\rho) \text{ cm}^2\text{-g}^{-1} = 3 \times 10^5 \text{ cm}^2\text{-g}^{-1}. \qquad (2)$$

Since the grain diameter is so small, the true surface area is closely approximated by the geometrical surface area (Fanale and Cannon, 1971). With a surface area of 3×10^5 cm^2-g^{-1}, a pH_2O/P value of .05 corresponds to between 1 and 3 monolayers of adsorbed H_2O, on the grain surfaces (Dushman and Lafferty, 1966, p.469; Weast, 1969, p.D-108; Fanale and Cannon, 1971).

From the data of Lendle (1935), for activated charcoal, and with the ratio of the specific surface areas of Fe_3O_4 and activated charcoal of 3×10^{-5} (Brunauer, 1937), the volume of adsorbed O_2, from the air, is on the order of 10^{-5} to 10^{-4} cm^3-g^{-1}. With the surface area of the magnetite being 3×10^5cm^2-g^{-1}, the volume of O_2, adsorbed per unit surface area of magnetite, is 10^{-11} to

$10^{-10} cm^3 O_2\text{-}cm^{-2}$. The volume of O_2, in an adsorbed monolayer, per unit surface area of magnetite, is (Brunauer, 1945),

$$V_o = 3.72 \left(10^{-20}/S_s \right), \qquad (3)$$

where S_s is the surface area covered by an O_2 molecule, equal to $1.2 \times 10^{-15} cm^2$. V_o for O_2 is 3×10^{-5}, and, therefore, there is between 10^{-5} and 10^{-6} of a monolayer, of O_2, adsorbed on the magnetite grain surfaces.

The quantity of adsorbed N_2, on the grain surfaces, is 10^{-7} to 10^{-8} of a monolayer, while there is 10^{-6} to 10^{-7} of a monolayer of CO_2 on the magnetite (Rowe, 1926). The quantities of the other adsorbed gases, on the grain surfaces, are even more negligible.

The experiments were initiated in less than 15 seconds after the insertion of the experimental atmosphere. Therefore, it can be assumed that, at the onset of illumination, each sample had adsorbed, to its surface, 1 to 3 monolayers of H_2O, 10^{-5} to 10^{-6} monolayer of O_2 or O (O_2 dissociates into two O atoms on the surface), 10^{-6} to 10^{-7} of a monolayer of CO_2, and 10^{-7} to 10^{-8} of a monolayer of N_2.

EXPERIMENTAL DETERMINATION OF THE REACTION RATE DEPENDENCE ON THE ENVIRONMENTAL PARAMETERS

O_2 and UV as Necessary Constituents

Magnetite samples were placed in atmospheres of 1.0 ($\pm$.05) x 10^2 torr CO_2, N_2, and Ar, and irradiated for five hours, at an intensity corresponding to $\mathbb{D}_{.350}$ = 2.8 x 10^{19} photons-cm^{-2}-sec^{-1}-$\mathring{A}^{-1}$. In each case, there was no visible alteration of the sample, and an X-ray diffractometer pattern of the sample showed no alteration of the magnetite peaks, or additional peaks (see section on alteration phase identification). At the onset of irradiation, the partial pressure of O_2, pO_2, was less than 10^{-4} torr, and pH_2O was less than 2 x 10^{-2} torr. The experiment was repeated for 1.0 ($\pm$.05) torr atmospheres of CO_2, N_2, and Ar, and again there was no detectable alteration.

Samples were next placed in an atmosphere, composed of pO_2 = 1.0 ($\pm$.05) torr and pCO_2 = 760 ($\pm$5) torr, and the sample visibly altered to a bright red color after 8 minutes of irradiation at the same intensity. An equivalent amount of N_2 was substituted for the CO_2, and again, a sample became bright red after 8 minutes of irradiation. The sample was re-exposed to this environment twenty times, in order to accumulate a sufficient

amount of the red alteration material for identification. The alteration product was identified, through X-ray diffraction and reflectance spectroscopy, to be the ferric oxide phase, hematite, although some maghemite may be present (see section on alteration phase identification, for details).

Hence, it has been found that illumination with UV in any O_2-free atmosphere, composed of H_2O, CO_2, N_2, or Ar, cannot oxidize the magnetite. O_2 is a necessary constituent. Further it was found that in the absence of illumination, rapid oxidation of the magnetite does not occur in these atmospheres. UV and O_2 are necessary constituents.

Δt_o

In the O_2-bearing atmosphere, the sample turned bright red after 8 minutes of irradiation. Irradiation for an interval of 7 minutes 30 seconds left the sample unaltered to the unaided eye. Examination with the petrographic microscope (both reflected and transmitted light), after these two illumination intervals, revealed that, at the end of each of the intervals, there were particles of a transparent phase present. These particles were not present at the onset of irradiation.

In order to determine whether these transparent

particles were alteration products or foreign particles, several samples were irradiated, at the same intensity and in the same atmospheres. Each sample was thoroughly stirred, and a particle point count was taken of 10 random samples, of 300 particles each, using the petrographic microscope (transmitted light), with a resolution on the order of a micron. Eleven samples were irradiated, at an intensity corresponding to $\mathbb{D}_{.350} = 2.8 \times 10^{19}$ photons-cm^{-2}-sec^{-1}-$\mathring{A}^{-1}$, in an atmosphere composed of pO_2 = 1.0 ($\pm$.05) torr and pCO_2 = 760 ($\pm$5) torr, for intervals of 1, 2, 3, 5, 6, 7, 7.5, 8, 8.5, 15, and 30 minutes, respectively.

It was found that, after the 1 and 2 minute intervals of exposure to the environment, no transparent particles could be found. After 3 minutes of exposure, however, an average of 5 ($\pm$1) transparent particles (or aggregates of particles) each were found in 10 random samples of 300 particles. After 5 minutes of exposure, an average of 8 ($\pm$1) transparent particles were found in the 10 samples. After 6 minutes, the number of transparent particles climbed to 10 ($\pm$1). After 7 minutes there were 11 ($\pm$1) particles in each of the 10 samples of 300 particles each.

After both the 7.5 and 8 minute exposure intervals, an average of 13 ($\pm$1) transparent particles (or

aggregates of particles) were found. Some of the transparent particles approached 2μ in diameter, after exposure to the environment for 7.5 and 8 minutes. Up to this point, most of the particles were around a micron or less in diameter, although a few particles larger than a micron were found. These larger particles appeared orange to red in color, while the smaller ones appeared colorless. After 8 minutes of exposure, the unstirred sample had a slightly higher albedo to the unaided eye. Stirring the sample decreased its albedo.

After 8 minutes of exposure to the environment, the sample appeared brighter and red in color. Stirring the sample returned it to its original black color. With the microscope, it was found that there was an average of 14 (±4) transparent particles (or aggregates of particles) in the random samples of 300 particles each. After 15 and 30 minutes of illumination, there were 26 (±5) and 49 (±7) transparent particles present. The larger the aggregate of transparent particles, the more deeply colored it appeared in transmitted light. No aggregates of particles, smaller than about 1 to 2 microns in diameter, appeared colored.

It is concluded that the transparent particles are the alteration product of the magnetite, rather than

impurity phases. The number of these particles increases linearly with increased exposure interval, and it can be concluded, from the distribution of particle sizes after each of these intervals that the volume of the alteration product increases linearly with exposure time; i.e. the number of particles increases linearly with time, and the particle diameters were essentially the same (between 1 and 2 microns) for each exposure interval. A few of the particles exceeded about 2 microns in diameter, and were orange to red in color. It is concluded that these particles are of the same composition, as the smaller ones, but they exceed 1 or 2 optical depths in thicness ($\sim 1\mu$). The undisturbed sample appears red, to the unaided eye, when an accumulate layer of the alteration product reaches a thickness which exceeds 1 or 2 optical depths.

The minimum exposure interval which will produce a layer of the alteration phase, that is 1 to 2 optical depths thick ($\sim 1u$), is defined as Δt_o. Since the volume of alteration product increases linearly with time, the alteration rate is $(\Delta t_o)^{-1}$ microns per minute.

Δt_o was determined for ten other environments, and it was found that the interval, from the time when the sample last appeared black (to the unaided eye)

to the time when the sample appeared definitely red (Δt_o exceeded), is on the order of 8% to 10% of Δt_o, in all cases. Hence the uncertainty in determining Δt_o, with the unaided eye, is on the order of $\pm 5\%$ of Δt_o. The results are repeatable, to within $\pm 5\%$ of Δt_o, for several trials in a given environment, and it was decided that it is not necessary to resort to another, more sophisticated detection system for determining Δt_o.

Ar, N_2, CO, and CO_2

The effect on Δt_o of substituting Ar, N_2, or CO for the CO_2 in the atmosphere was next examined. First, the samples were irradiated, at an intensity corresponding to $\mathbb{I}_{.350} = 2.8 \times 10^{19}$ photons-cm^{-2}-sec^{-1}-Å^{-1}, and an O_2 partial pressure of 1 ($\pm$.05) torr. The total pressure, of each atmosphere, was 760 ($\pm$5) torr. It was found that Δt_o is the same, within the $\pm 5\%$ measurement uncertainty limits, for each of the atmospheres. The reaction rate, at this total pressure and oxygen partial pressure, was not affected by changes in the composition of the major atmospheric constituent.

The Total Pressure, P_T

Maintaining the same radiation intensity and O_2 partial pressure, the total atmospheric pressure, P_T,

was varied from a maximum of 800 (±5) torr to 100 (±5) torr. The results are shown in figure 13a. The CO_2 was then replaced with N_2, CO, and Ar, and the total pressure was again varied over the same range of values. For all four atmospheres, Δt_o was the same, at any given pressure, and the data presented in figure 13a apply to each of these atmospheres. The best fit to these data is given by the expression,

$$\Delta t_o = 1.4 \times 10^{-5} P_T^2 \qquad (4)$$

The Δt_o dependence on variations in P_T, for P_T less than 100 torr, was determined with $pO_2 = 1.0\ (\pm.05) \times 10^{-2}$ torr and $\mathbb{I}_{.350} = 4.8\ (\pm.5) \times 10^{18}$ photons-cm^{-2}-sec^{-1}-Å^{-1}. P_T was varied from 200 (±5) torr to 6.0 (±.05) torr, and the results are shown in figure 13b. The best fit to these results are given by the expression,

$$\Delta t_o = 2.0 \times 10^{-3} P_T^2. \qquad (5)$$

The error bars, in Δt_o, on the data points, in figures 13a and 13b, reflect the measurement uncertainty in Δt_o, and the error limits in P_T reflect the precision of the vacuum gauge. The leak rate of the system, during these measurements and the other measurements in this experiment, was low enough not to affect the results beyond the measurement uncertainty limits.

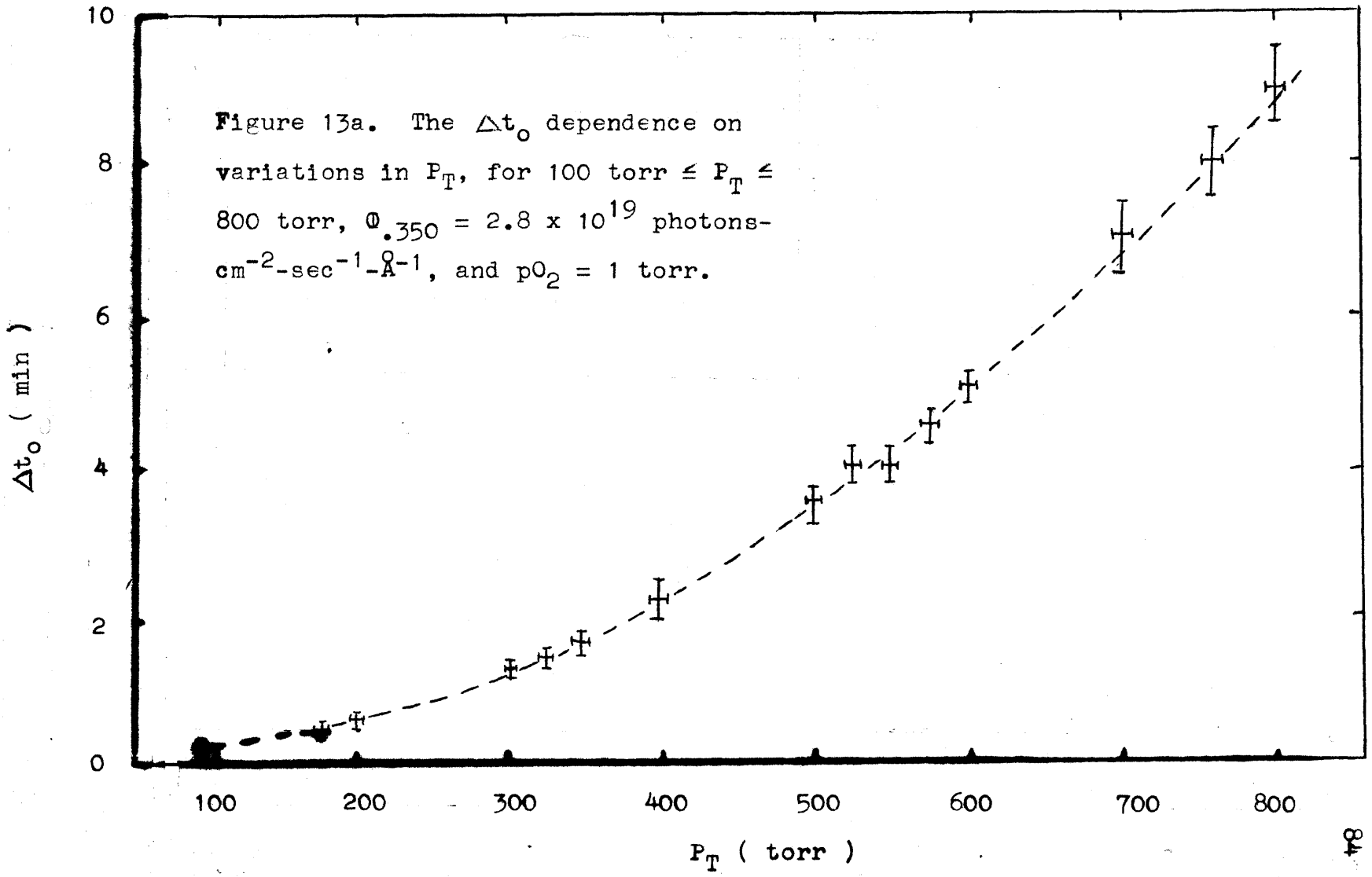

Figure 13a. The Δt_o dependence on variations in P_T, for 100 torr $\leq P_T \leq$ 800 torr, $\Phi_{.350} = 2.8 \times 10^{19}$ photons-cm^{-2}-sec^{-1}-$Å^{-1}$, and pO_2 = 1 torr.

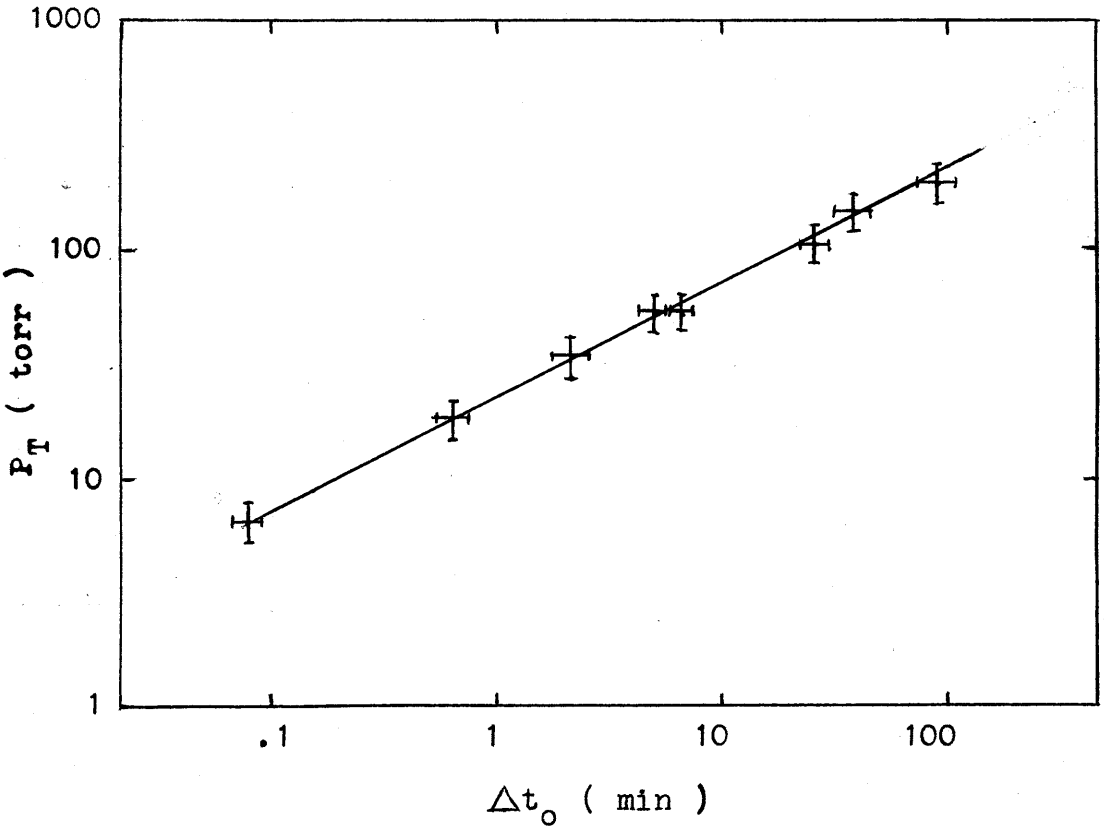

Figure 13b. The Δt_o dependence on variations in P_T, for 6 torr $\leq P_T \leq$ 200 torr, $\mathbb{D}_{.350} = 4.8 \times 10^{18}$ photons-cm^{-2}-sec^{-1}-Å^{-1}, and $pO_2 = 1 \times 10^{-2}$ torr.

Atmospheric O_2 Partial Pressure, pO_2

The effect on Δt_o of varying the O_2 partial pressure was next determined. For a total pressure of 760 ($\pm$5) torr and for $\mathbb{I}_{.350}$ = 2.8 ($\pm$.3) x 10^{19}photons-cm^{-2}-sec^{-1}-$\mathring{A}^{-1}$, pO_2 was varied from 100 ($\pm$5) torr to 1.0 ($\pm$.05) x 10^{-2} torr. The results are shown in figure 14a. The error bars on these data points are there for the same reasons as described for figures 13a and 13b. The best fit to these data points is provided by the function,

$$\Delta t_o = 8.0\ pO_2^{-\frac{1}{2}}. \qquad (6)$$

Again, the CO_2 was replaced by N_2, CO, and Ar, and for all four atmospheres , the best fit to these data is provided by the same function. Next, pO_2 was varied from 9.00($\pm$.05) x 10^{-3} torr to 1.00($\pm$.05) x 10^{-4} torr. The results are presented in figure 14b. The best fit to these data is provided by the function,

$$\Delta t_o = 7.4 \times 10^{-2}\ pO_2^{-\frac{1}{2}}. \qquad (7)$$

Incident Radiation Intensity, $\mathbb{I}_{.350}$

The response of Δt_o to variations in the incident radiation intensity was next determined. With pO_2 = 100 ($\pm$5) torr and P_T = 760 ($\pm$5) torr, $\mathbb{I}_{.350}$ was varied from

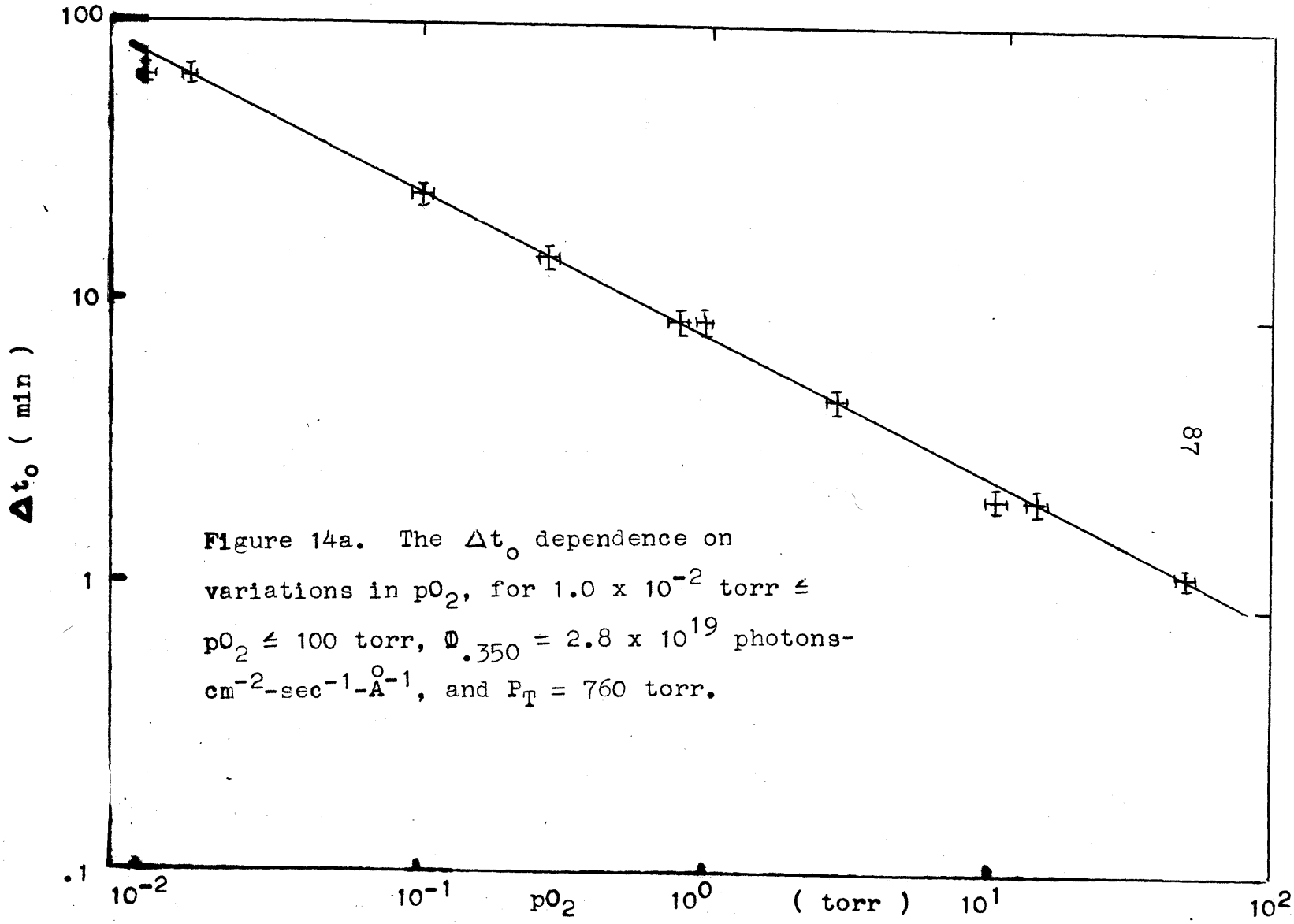

Figure 14a. The Δt_o dependence on variations in pO_2, for 1.0×10^{-2} torr $\leq$ $pO_2 \leq$ 100 torr, $\mathbb{D}_{.350} = 2.8 \times 10^{19}$ photons-cm^{-2}-sec^{-1}-$\mathring{A}^{-1}$, and P_T = 760 torr.

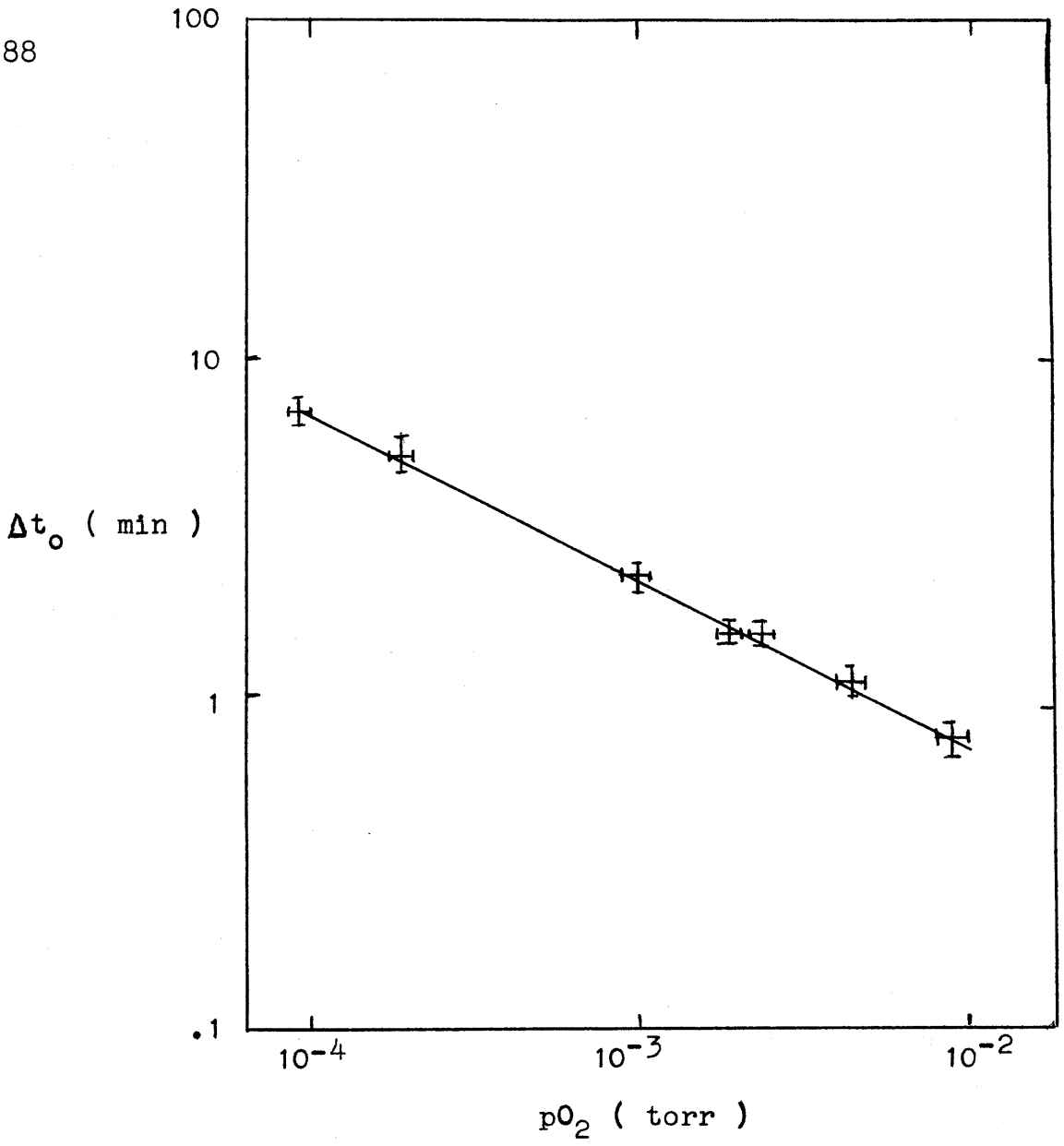

Figure 14b. The Δt_o dependence on variations in pO_2, for $1.0 \times 10^{-4} \leq pO_2 \leq 9.0 \times 10^{-3}$, $\mathbb{D}_{.350} = 5.0 \times 10^{18}$ photons-cm^{-2}-sec^{-1}-Å^{-1}, and $P_T = 20$ torr.

2.8 ($\pm$.3) x 10^{19} to 1.1 ($\pm$.1) x 10^{18} photons-cm^{-2}-sec^{-1}-Å^{-1}. The results are shown in figure 15a, from which it was found that

$$\Delta t_o = 1.2 \times 10^{29} \text{Ⅲ}_{.350}^{-3/2} \qquad (8)$$

A pure O_2 atmosphere was then used at a pressure of 10($\pm$.5) torr, and Ⅲ$_{.350}$ was varied from 1.2 ($\pm$.1) x 10^{17} to 8.6 ($\pm$.9) x 10^{15} photons·cm^{-2}·sec^{-1}·Å^{-1}. It was found that,

$$\Delta t_o = 6.5 \times 10^{25} \text{Ⅲ}_{.350}^{-3/2}, \qquad (9)$$

from the data in figure 15b. The range of intensities was further extended by using a pure O_2 atmosphere at a pressure of 1.00($\pm$.05) torr. Ⅲ$_{.350}$ was varied from 1.4 ($\pm$.1) x 10^{16} to 6.6 ($\pm$.7) x 10^{14} photons·cm^{-2}·sec^{-1}·Å^{-1}, and the results, shown in figure 15c, were best fit by the function,

$$\Delta t_o = 2.0 \times 10^{24} \text{Ⅲ}_{.350}^{-3/2}. \qquad (10)$$

The Relative Spectral Radiation Intensity Distribution

The response of Δt_o to variations in the relative spectral radiation intensity curve shape was next determined. The fused silica window, in the chamber, was replaced with CsBr, CsI, and Pyrex windows. Ⅲ$_{.350}$ was adjusted to a value of 2.8 ($\pm$.3) x 10^{19} photons-

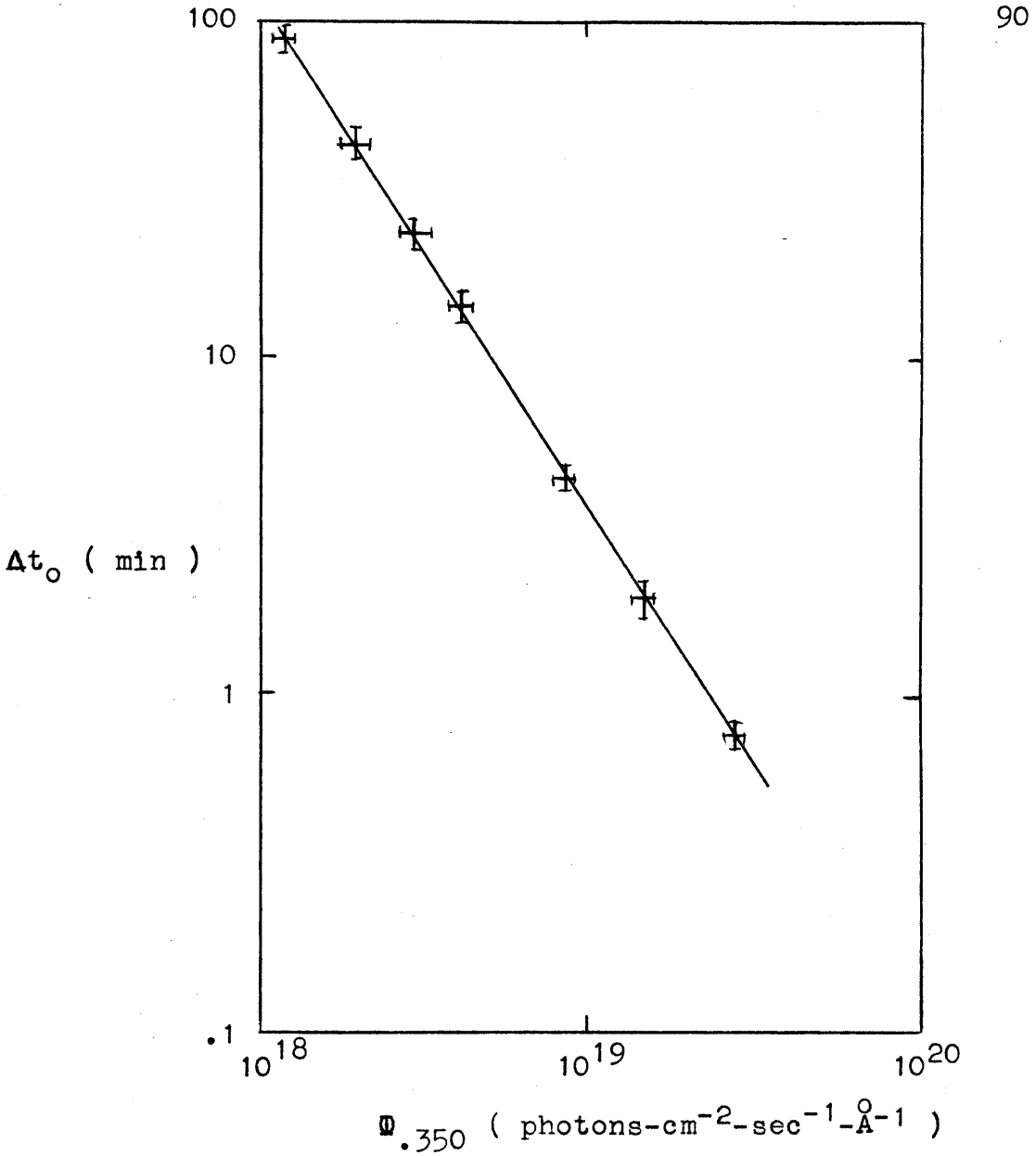

Figure 15a. The Δt_o dependence on variations in the incident radiation intensity, for $1.1 \times 10^{18} \leq \mathbb{D}_{.350} \leq 2.8 \times 10^{19}$ photons-cm^{-2}-sec^{-1}-Å^{-1}, P_T = 760 torr, and pO_2 = 100 torr.

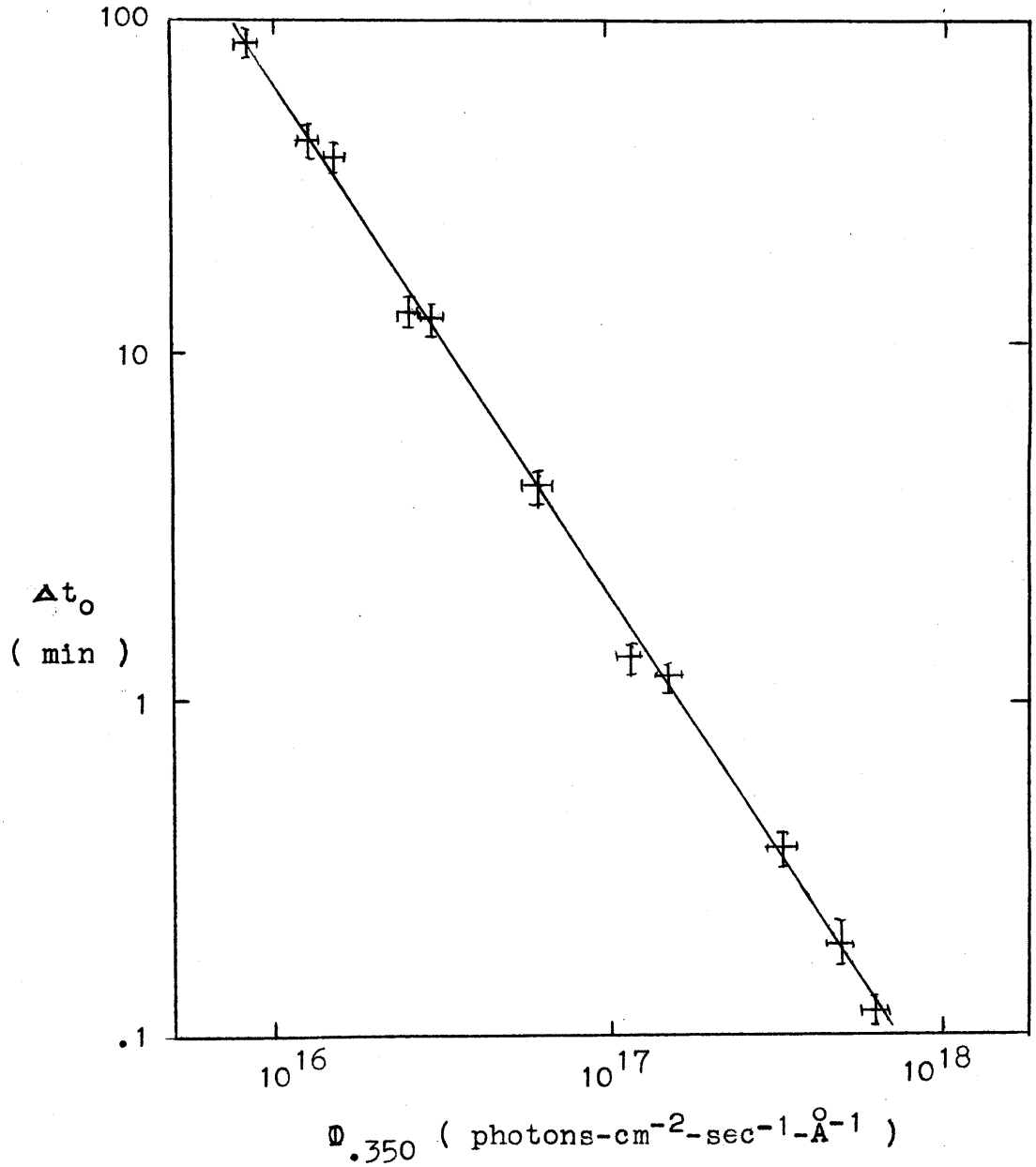

Figure 15b. The Δt_o dependence on variations in the incident radiation intensity, for $8.6 \times 10^{15} \leq \mathbb{D}_{.350} \leq 7.2 \times 10^{17}$ photons-cm^{-2}-sec^{-1}-Å^{-1}, and $P_T = pO_2 = 10$ torr.

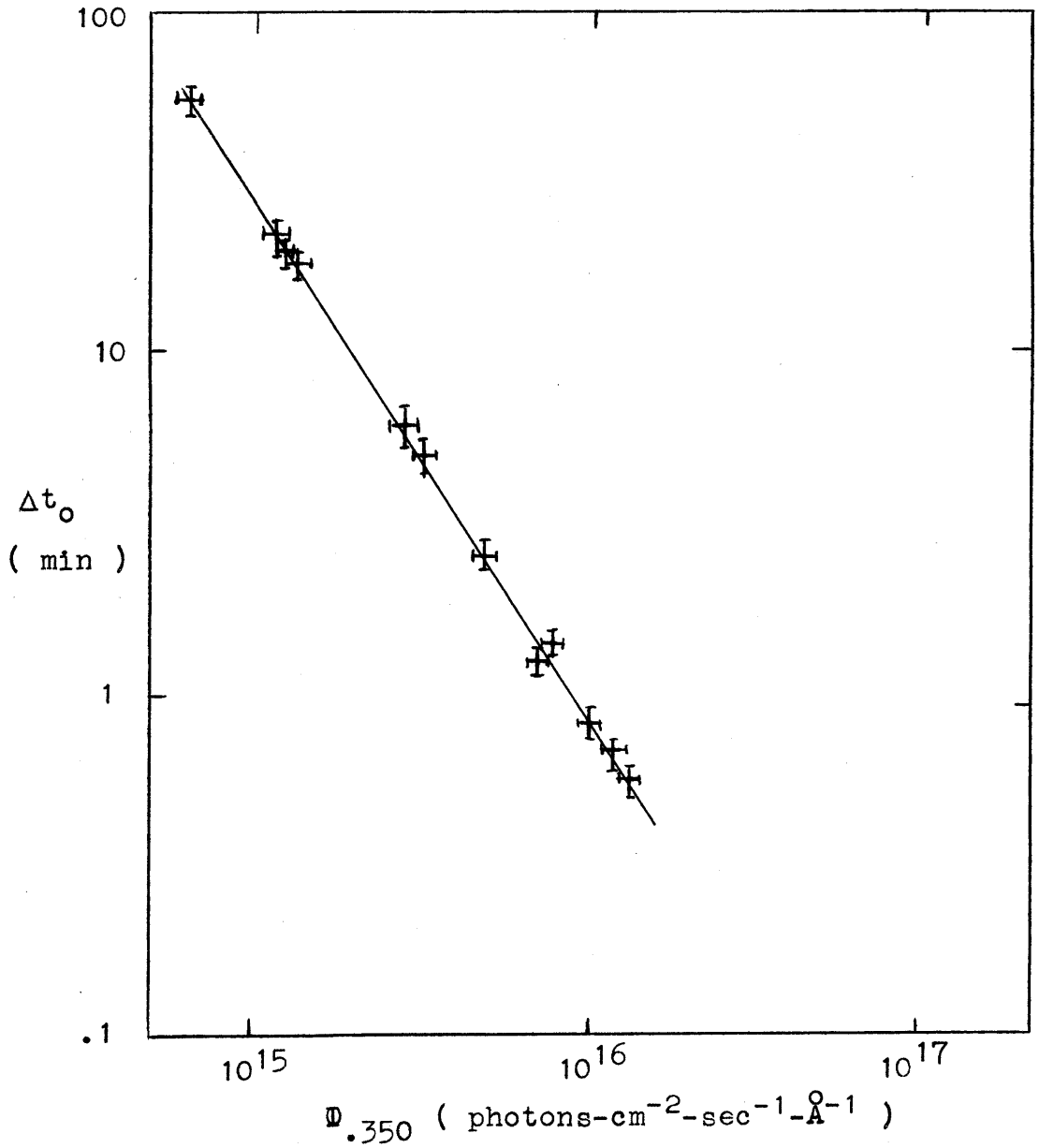

Figure 15c. The Δt_o dependence on variations in the incident radiation intensity, for $6.6 \times 10^{14} \leq \mathbb{D}_{.350} \leq 1.4 \times 10^{16}$ photons-cm^{-2}-sec^{-1}-Å^{-1}, and $P_T = pO_2 =$ 1 torr.

$cm^{-2} \cdot sec^{-1} \cdot \text{Å}^{-1}$ for each window. The relative spectral radiation intensity distribution at the sample for each of these windows, is shown in figure 10. The spectral transmission characteristics were provided by the manufacturer (Harshaw Optics). For pO_2 = 100 ($\pm$5) torr, and P_T = 760 ($\pm$5) torr, Δt_o for the fused silica window was measured to be 48 ($\pm$3) seconds. Δt_o for the CsBr window was 2min. 42($\pm$8)sec., for CsI it was 10min. 30($\pm$35)sec., and with the Pyrex window, Δt_o was 17min. 30($\pm$50)sec.

Since the quantity of alteration material increases linearly with exposure time, then, in a given period of irradiation, only .05 times as much of the alteration product is formed, by using the Pyrex window, as would be formed if the fused silica window was used. With the CsI window, only .08 times as much alteration product is formed, as would be formed with the fused silica window. With the CsBr window, .3 times as much would be formed.

Therefore, from figure 10, the radiation intensity can vary by a factor of $\pm$2 from the fused silica values for wavelengths longward of about .280μ, and change Δt_o by less than its $\pm$10% uncertainty limits. Similarly, by changing the intensity, longward of .230μ by a factor of $\pm$1.25, Δt_o varies by less than $\pm$10%. Longward of

.210μ, the intensity can be varied by a factor of ±.33. From this information, a $\mathbb{I}_\lambda$ region can be constructed, within which any spectral intensity distribution curve may lay and yield a Δt_o which is the same, within a ±10% uncertainty, as the Δt_o for the fused silica window. This is presented in figure 16. Also plotted in figure 16 is the solar UV spectral intensity distribution, set equal to the intensity of the radiation passed by the fused silica window at .200μ (Allen, 1965, p.171). Although the solar curve lays within the $\pm\Delta t_o$ curve, its value at .350μ is a factor of 2.2 higher than the Xenon/silica value at .350μ. Hence, a $\mathbb{I}_{.350}$ value for solar radiation is obtained by dividing by 2.2 at .350μ.

Atmospheric and Adsorbed H_2O, pH_2O/P

In each of the experiments discussed so far, the quantity of adsorbed H_2O at the onset of irradiation was that amount which is in equilibrium with a pH_2O/P ratio of .05 during sample preparation. The effect on Δt_o of variations in the quantity of adsorbed H_2O, at the onset of irradiation, was next determined. First, all of the physically adsorbed H_2O was removed from one of the samples through a chain of five 3-hour dynamic desorption environments. A dynamic desorption environment is characterized by a 2.2×10^{-2} torr flow of

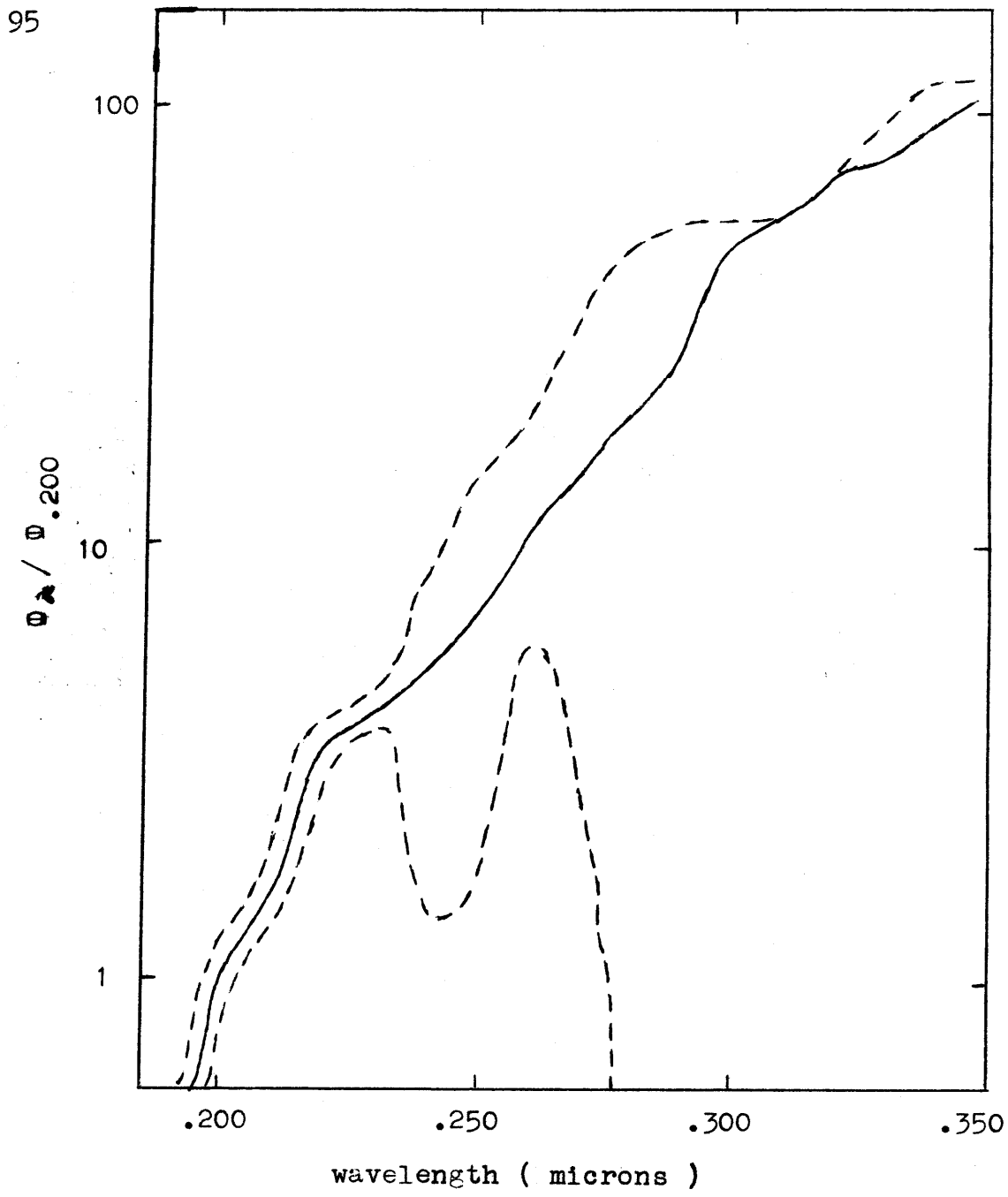

Figure 16. Φ_λ region, within which any relative spectral radiation intensity distribution may lay, and yield a Δt_0 value, which is the same, within a $\pm$10% uncertainty, as the Δt_0 for the fused silica window, scaled to 1.0 at $\lambda = .200\mu$.

Ultrahigh Purity grade Matheson N_2 gas at ambient temperature. The dried sample was then irradiated in a 760 ($\pm$5) torr atmosphere, containing 100 ($\pm$5) torr O_2, at an intensity corresponding to $\mathbb{I}_{.350} = 2.8 \times 10^{19}$ photons$\cdot cm^{-2} \cdot sec^{-1} \cdot \mathring{A}^{-1}$. Irradiation for 5 hours produced no observed alteration, while irradiation of a sample, which was prepared with $pH_2O/P = .05$, had a Δt_o of .80($\pm$.04) minute, in this environment. Therefore, in order for the reaction to occur, some H_2O was required to be adsorbed on the grain surfaces, at the onset of irradiation.

It was next investigated whether the H_2O was required on the grain surfaces throughout all of the Δt_o interval, or whether it was needed only for some initial interval. A sample was prepared in an atmosphere in which pH_2O/P was .05. It was irradiated for an initial interval of 10 seconds, at an intensity corresponding to $\mathbb{I}_{.350} = 2.8 \times 10^{19}$photons$\cdot cm^{-2} \cdot sec^{-1} \cdot \mathring{A}^{-1}$, in a 760 ($\pm$5) torr atmosphere with $pO_2 = 1.0(\pm.05)$ torr. The visibly unaltered sample was then exposed to the dynamic desorption chain, and reirradiated, at the same intensity, and in the same atmosphere. After 8.0($\pm$.5) minutes of exposure to this H_2O-free environment the magnetite reddened.

The experiment was repeated with the initial interval reduced to 5 seconds, and again $\Delta t_o = 8.0(\pm.4)$ minutes. When the initial interval was reduced to 1 second, however, irradiation in the H_2O-free environment left the sample visibly unaltered. No transparent particles could be found with the petrographic microscope (see section on Δt_o, earlier in this chapter). The experiment was repeated for other lengths of the initial interval, and it was found that the adsorbed H_2O was required for the initial 5 (± 1) seconds of the exposure to the UV radiation in the O_2-bearing atmosphere.

Investigations with various combinations of $\mathbb{I}_{.350}$, P_T, and pO_2 revealed that the initial interval, during which the adsorbed H_2O is required, is between 1 and 2 percent of Δt_o. This value for the initial interval applies to the case in which the adsorbed H_2O layer has a thickness corresponding to a pH_2O/P ratio of .05 during sample preparation.

A sample, prepared with the same pH_2O/P ratio, was irradiated for its initial interval of $.02\Delta t_o$ (10 seconds in this case), at an intensity corresponding to $\mathbb{I}_{.350} = 2.8 \times 10^{19}$ photons$\cdot cm^{-2}\cdot sec^{-1}\cdot \mathring{A}^{-1}$, in a 760 ($\pm 5$) torr atmosphere, containing 1.0($\pm$.05) torr O_2. It was then exposed to a chain of five 3-hour dynamic desorption

periods. It was re-exposed to the original environment for 30-second intervals, alternating with 15 second intervals of no irradiation or adsorbed H_2O, until the sample turned red. Δt_o was found to be 8 minutes $\pm$ 30 seconds, essentially the same as for an uninterrupted exposure interval in this environment. Irradiation for 30-second intervals, at the same intensity and in the same atmosphere, was repeated. However, instead of exposing the the sample to the desorption environment after exposure to the initial interval, the sample was exposed to the standard sample preparation environment ($pH_2O/P = .05$) prior to each 30-second exposure interval. In this case Δt_o was found to be 7.5 ($\pm$.5) minutes.

Hence, for previously un-irradiated samples, an adsorbed H_2O layer is required, at the onset of irradiation, in order for oxidation to occur. However, after having been irradiated for the initial $.01\Delta t_o$ or $.02\Delta t_o$ interval, the H_2O is no longer required. In addition, if the sample is exposed intermittantly to adsorbed H_2O, with a layer thickness corresponding to a pH_2O/P value of .05, the Δt_o value is shortened.

Next, the effect on Δt_o of varying the thickness of the adsorbed H_2O layer was investigated. Δt_o was determined as a function of the pH_2O/P ratio during sample preparation.

This was done for various combinations of T, pO_2, P_T, A_t, and $\mathbb{I}_{.350}$. It was found that, for samples prepared with pH_2O/P greater than .05, Δt_o increases with increasing pH_2O/P. Further, for pH_2O/P greater than .05, Δt_o has two components. During one of these intervals, oxidation occurs at a rate which is equivalent to the rate when pH_2O/P is .05 during sample preparation. Preceeding this oxidizing interval, there is another interval during which no oxidation occurs. The length of this non-oxidizing interval increases with increased pH_2O/P. The length of the non-oxidizing interval was found to decrease by increasing $\mathbb{I}_{.350}$ and T, and by decreasing A_t, but it was unaffected by variations in pO_2 or P_T.

The effect of adsorbed H_2O on Δt_o, for values of pH_2O/P which were less than .05 at the onset of irradiation, was investigated, using $\mathbb{I}_{.350} = 1.7 \times 10^{17}$ photons$\cdot cm^{-2} \cdot sec^{-1} \cdot \mathring{A}^{-1}$, in a pure 10.0($\pm$.5) torr O_2 atmosphere. For $pH_2O/P = .05$, Δt_o was found to be 55 ($\pm$3) seconds. The initial interval, during which adsorbed H_2O was required, was found to be less than 1 second. For pH_2O/P values of both .03 and .01, Δt_o remained at 55 ($\pm$3) seconds, and the initial interval was still less than 1 second. For $pH_2O/P = 5 \times 10^{-3}$, Δt_o increased to 9 minutes 15 seconds ($\pm$ 30 seconds). The initial interval, during which the

H_2O was required, increased to 6 ($\pm$1) second. For pH_2O/P = 1×10^{-3}, Δt_o was 45 min. $\pm$3 min., and the initial interval increased to 30 seconds. Finally, for $pH_2O/P \approx 0$, Δt_o increased to a value greater than 5 hours.

Next, the effect on Δt_o of varying the atmospheric H_2O partial pressure was determined. Samples were irradiated at an intensity corresponding to $\mathbb{I}_{.350} = 2.8 \times 10^{19}$ photons$\cdot cm^{-2} \cdot sec^{-1} \cdot \text{Å}^{-1}$, in atmospheres composed of various proportions of N_2, and air, with known H_2O partial pressures. The resultant H_2O partial pressures in these atmospheres ranged from values of 5.3 torr to 5.3×10^{-3}torr. The Δt_o for each of these atmospheres was determined, with the onset of irradiation occuring in less than 10 seconds after injection of the air into the chamber. These values of Δt_o were then compared with Δt_o values obtained for the H_2O-free atmospheres which had the same pO_2 and P_T values. It was found that Δt_o was not affected by changing the atmospheric H_2O content. In each of these cases, the amount of adsorbed H_2O corresponded to a pH_2O/P ratio of .05 during sample preparation.

Temperature, T.

The effect of temperature on Δt_o was next investigated. Since variations in surface temperature affect the

desorption rate of the adsorbed H_2O layer, the samples were all irradiated for the $.02\Delta t_o$ initial interval, and then they were exposed to the dynamic desorption environment. All Δt_o values were then determined in the H_2O-free environments.

The temperature of the sample, at the onset of irradiation, was varied over the range 263°K to 373°K, and Δt_o was observed to be unchanged, within the ±5% uncertainty limits. The experiment was repeated for a variety of environments, with $\mathbb{I}_{.350}$ ranging from 2.8×10^{19} to 7.3×10^{14} photons-cm^{-2}-sec^{-1}-$\mathring{A}^{-1}$, P_T ranging from 760 (±5) torr to 1 (±.05) torr, and pO_2 ranging from 100 (±5) torr to 1.0 (±.05) $\times 10^{-2}$ torr, and it was again found that Δt_o is independent of the temperature of the sample at the onset of irradiation.

In the 760 torr atmosphere, it was noticed that irradiation, at an intensity corresponding to $\mathbb{I}_{.350} = 2.8 \times 10^{19}$ photons-cm^{-2}-sec^{-1}-$\mathring{A}^{-1}$, caused an 18°K increase in the sample temperature, stabilizing after 6 minutes of exposure. To determine the effect of this temperature change during irradiation, a sample was dynamically cooled during the irradiation interval, and the temperature was constrained to increase by only 2°K over the 6 minute interval. Δt_o remained the same. When the temperature was made to

increase by 32°K over 6 minutes, Δt_o was also the same. The experiment was then repeated for various radiation intensities, repeating between $\mathbb{I}_{.350} = 2.8 \times 10^{19}$ and 7.3×10^{14} photons·cm^{-2}·sec^{-1}·Å^{-1}, and total pressures between 1 torr and 760 torr. Temperature changes were made to range from values of -30°K to +52°K, and Δt_o was found to be unchanged, as a result of altering the magnitude of the temperature change during irradiation, in every case. In summary, temperature has no apparent effect on the length of the oxidizing interval.

Surface Area, A_t

The next parameter that was investigated was particle size. Samples of the .04μ diameter magnetite grains were wetted with acetone, spread onto glass slides, dried, and scraped off into a mortar. The magnetite was then in the form of densely-packed aggregates of particles. They were sorted into various particle diameter ranges between .04μ and 10μ. The aggregates were irradiated at an intensity corresponding to $\mathbb{I}_{.350} = 2.8 \times 10^{19}$ photons·cm^{-2}·sec^{-1}·Å^{-1}, in a 760 torr atmosphere containing 100 (±5) torr O_2. Δt_o was determined as a function of the particle (aggregate) diameter, d, in microns. The results are shown in figure 17. The principle feature of the figure to note is that the Δt_o values deviate from a d^2 law,

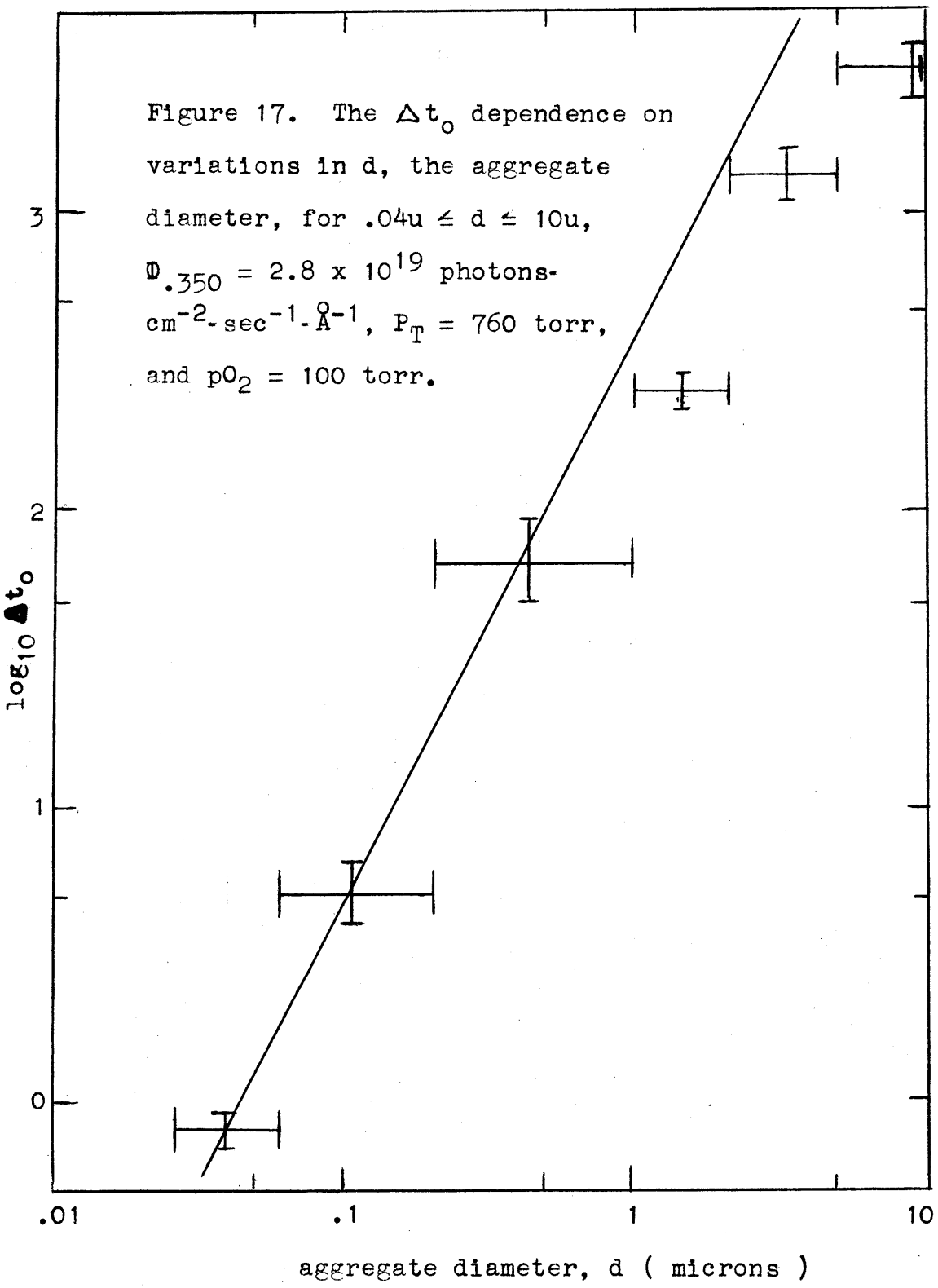

Figure 17. The Δt_o dependence on variations in d, the aggregate diameter, for .04u ≤ d ≤ 10u, $\mathbb{D}_{.350} = 2.8 \times 10^{19}$ photons-cm^{-2}-sec^{-1}-$Å^{-1}$, P_T = 760 torr, and pO_2 = 100 torr.

represented by the curve in the figure, at the higher d values. This observation is consistent with the fact that aggregates of particles have more complex surfaces, and therefore greater surface areas per gram, than the geometrical surface area of a smooth-surfaced sphere of diameter d. The .04μ diameter Magnetite particles have surface areas which are most closely approximated by the geometrical surface area of a sphere of diameter d (refer to section on sample preparation, in this chapter), given in equation 2 to be 3×10^5 $cm^2 \cdot g^{-1}$. The curve in figure 17 is fit to the datum point at .04μ, and the data at the other d values are consistent with the interpretation that,

$$\Delta t_o = 2.4 \times 10^5 \, A_t^{-1}, \qquad (12)$$

where A_t is the true surface area, per gram, of magnetite.

SUMMARY OF LABORATORY RESULTS: EMPIRICAL CONSTRAINTS ON THE REACTION MECHANISM

A model for the mechanism of the UV-stimulated alteration of magnetite is constrained to satisfy the results of the laboratory investigation. They include:

1. The presence of both atmospheric O_2 and ultraviolet light are required in order for the reaction to proceed.

2. The reaction rate is proportional to P_T^{-2}, where P_T is the total pressure of the atmosphere, but it is independent of whether the principle compositional constituent is Ar, N_2, CO_2, or CO. The range for which the P_T^{-2} dependence is valid is 6 torr $\leq P_T \leq$ 800 torr.

3. The reaction rate is proportional to $pO_2^{\frac{1}{2}}$, where pO_2 is the atmospheric O_2 partial pressure, over the range 1×10^{-4} torr $\leq pO_2 \leq 1 \times 10^{2}$ torr. Atmospheric O_2 also contributes to the P_T dependence.

4. The reaction rate is proportional to $\mathbb{I}_{.350}^{3/2}$, where $\mathbb{I}_{.350}$ is the incident radiation intensity, at the reference wavelength of .350μ, over the range $6.6 \times 10^{14} \leq \mathbb{I}_{.350} \leq 2.8 \times 10^{19}$. The units of $\mathbb{I}_{.350}$ are photons$\cdot cm^{-2} \cdot sec^{-1} \cdot \text{Å}^{-1}$.

5. The alteration rate is higher, with higher incident photon energies, for $h\nu \leq 6.2$ eV.

6. The reaction rate is independent of temperature, over the range $263^{\circ}K \leq T \leq 373^{\circ}K$.

7. The alteration rate is proportional to the surface area of the sample, A_t.

8. In order for the reaction to occur, with a previously unaltered magnetite sample, some H_2O must be adsorbed on the grain surfaces for an initial interval of $.01\Delta t_o$ or $.02\Delta t_o$, where Δt_o is the illumination interval that is required in order to form an accumulate layer of the alteration product to a thickness of 1 micron. Once a sample has been exposed to this initial interval, however, adsorbed H_2O is no longer required in order for the reaction to continue. Δt_o is the same, for both continuous and interrupted intervals, in the absence of adsorbed H_2O, while if H_2O is adsorbed to the surface during illumination interruptions, Δt_o is decreased. The amount of adsorbed H_2O on the grain surfaces, is that which is in equilibrium with the ratio of the atmospheric H_2O partial pressure to the H_2O vapor saturation pressure of the atmosphere, i.e. pH_2O/P. When $pH_2O/P < .01$, the reaction rate is proportional to pH_2O/P. For $.01 \leq pH_2O/P \leq .05$, the reaction rate is independent of pH_2O/P. For pH_2O/P greater than .05, Δt_o is composed of two intervals: an alteration interval, which is the same length as Δt_o for $.01 \leq pH_2O/P \leq .05$, and a non-reacting interval, Δt_n, which preceeds the alteration interval. The length of the non-reacting interval increases in a complex manner with increased pH_2O/P and A_t, and decreased $\mathbb{I}_{.350}$ and T.

THE KINETIC RATE EQUATION

It has been found that, upon illumination with ultraviolet radiation in an O_2-bearing atmosphere, magnetite has formed on it a surface layer of bright red alteration material. The interval of exposure to this environment which results in the formation of a surface layer 1 micron in thickness is defined as Δt_o. The rate of formation of this layer is linear with exposure time, and therefore the formation rate can be expressed as $(\Delta t_o)^{-1}$, in units of microns per minute. From the functional dependences of the formation rate on the various environmental parameters, which were experimentally derived and presented in this chapter, an expression for Δt_o can be formed for each of the three characteristic pH_2O/P ranges. The kinetic rate equation for the alteration process, which is operating in each of the characteristic pH_2O/P ranges, is simply the inverse of the experimentally derived Δt_o expression for that region. The expressions for Δt_o are:

For $pH_2O/P < .01$,

$$\Delta t_o = 6.0(\pm.6)\times10^{31} P_T^2 (pO_2)^{-1/2} (\text{Ⅲ}_{.350})^{-3/2} A_t^{-1} (pH_2O/P)^{-1}; \quad (13a)$$

For $.01 \leq pH_2O/P \leq .05$,

$$\Delta t_o = 6.0(\pm.6)\times10^{29}P_T^2(pO_2)^{-1/2}(\mathbb{I}_{.350})^{-3/2}A_t^{-1}; \qquad (13b)$$

For $pH_2O/P > .05$,

$$\Delta t_o = 6.0(\pm.6)\times10^{29}P_T^2(pO_2)^{-1/2}(\mathbb{I}_{.350})^{-3/2}A_t^{-1} + \Delta t_n. \qquad (13c)$$

In equations 13a, 13b, and 13c, Δt_o is in minutes, and

P_T = total atmospheric pressure, in torr.

pO_2 = partial pressure of atmospheric O_2, in torr.

$\mathbb{I}_{.350}$ = incident photon flux at the reference wavelength of .350μ, in photons-cm^{-2}-sec^{-1}-$\mathring{A}^{-1}$.

A_t = true surface area of the magnetite, in cm^2-g^{-1}, per gram of the sample.

pH_2O/P = ratio of the partial pressure of H_2O in the atmosphere, to the saturation H_2O vapor pressure in that atmosphere. This ratio is the value, which is in equilibrium with the amount of adsorbed H_2O, on the grain surfaces at the onset on illumination.

Δt_n = length of the non-reacting exposure interval, in minutes.

ALTERATION PHASE IDENTIFICATION

Identification of the oxidation product is extremely difficult. Although the structures of the two forms of ferric oxide are different (see chapter II), their X-ray diffraction patterns are similar. Differentiation between the two is made difficult by the broadening and shifting of the peaks, associated with the solid solution and small particle size effects. Further, since maghemite and magnetite are isostructural, their patterns are nearly indistinguishable, even for large end member crystals.

Bulk magnetic measurement is not a good technique, because of the various combinations arising from the mixing of different magnetic characters. Magnetite is ferrimagnetic, with a Curie point of 578°C and a saturation magnetization, at room temperature, of 92 - 93 e.m.u. / gm. (Nagata, 1961). Maghemite is also ferrimagnetic, with approximately the same Curie point, and with a saturation magnetization of 83.5 e.m.u. / gm. Hematite is only weakly magnetic, displaying ferromagnetism and paramagnetism, with a Curie point of 675°C. In the samples, the oxidation product is mixed with the magnetite, and therefore bulk magnetic measurements are not useful for the indentification of the alteration phase.

Differential Thermal Analysis (DTA) alone is also limited. Heat from the exothermic reaction, $Fe_3O_4 \rightarrow \gamma\text{-}Fe_2O_3$, triggers, to an unknown extent, the transformation, $\gamma\text{-}Fe_2O_3 \rightarrow \alpha\text{-}Fe_2O_3$. Adsorbed gases on the small particles lead to erroneous results for mass changes in thermogravimetric analyses of the powdered specimens. Wet chemical, microprobe, and Mössbauer analyses cannot differentiate between the two forms of Fe_2O_3.

The best single technique, although still not free of of ambiguity, is the color of the powder in reflected light. Magnetite is black to black-brown, in small particle reflectivity. Maghemite is yellow to yellow-brown, and hematite is red to red-brown. Ambiguity arises when the hematite has OH in substitution for some of its O ligands. The presence of $Fe(O,OH)_6$ octahedra causes hematite to become brown to yellow-brown in color, depending on the extent of the hydroxyl substitution (see section on hematite, in chapter II). Maghemite never is red or red-brown in color, however. Spectral reflectance curves distinguish hematite from the other ferric oxide and oxyhydroxides, since only hematite, possesses the .7μ reflectivity peak. The others exhibit a reflectivity plateau from .5μ, or .6μ, to .7u. The least ambiguous characterization method is the combination of the reflected color and the X-ray diffraction.

X-Ray Diffraction

A two gram sample of magnetite was prepared for oxidation, in the manner described in the section on sample preparation, in this chapter. The sample was illuminated at an intensity corresponding to $\mathbb{D}_{.350} = 2.8 \times 10^{19}$ photons$\cdot cm^{-2} \cdot sec^{-1} \cdot \mathring{A}^{-1}$, in a 760($\pm$5) torr atmosphere, composed of 20% O_2 and 80% N_2, for 5 min. The sample was then stirred, replaced in the sample preparation environment, and illuminated again in the O_2 / N_2 atmosphere, for 5 more minutes. This exposure cycle was repeated 20 times, in order to insure that there was sufficient alteration product in the sample for X-ray identification. A one-half gram portion of the sample was next placed in a mortar, where it was mixed with 18 drops of amyl-acetate and 6 drops of Collodion. It was then spread on a glass diffraction sample slide and allowed to dry for a half hour.

An X-ray diffractometer trace of the sample was taken. In addition, X-ray diffractometer traces of unoxidized magnetite and reagent grade (Fisher Scientific Co.) hematite, were taken, for comparison. Both the unoxidized magnetite and the hematite have the same mean particle diameter, .04 ($\pm$ .02) μ. The diffraction patterns of the three samples were

taken using the GE Unit #1 at the MIT X-Ray Metallography Lab. Chromium K-α radiation was used, at 35 kv and .14 ma, with a vanadium filter.

In figures 18a through 18g, the results are presented. In these figures, the positions of the diffraction peaks are presented in terms of 2θ, where θ is the Bragg angle. Not presented in these figures is the diffraction record of maghemite. The reason for this is that the maghemite peaks are positioned, for the most part, coincidently with the magnetite peaks. The maghemite structure differs from the magnetite structure in one important respect, however. It has a superstructure, due to the vacancy ordering, yielding characteristic 2θ peaks at 22.4° (d = 5.887 Å), 27.5° (d = 4.810 Å), 35.8° (d = 3.721 Å), and 39.4° (d = 3.398 Å). The other, not so characteristic, principal peaks occur at 45.8° (d = 2.944 Å), 54.2° (d = 2.510 Å), 66.8° (d = 2.082 Å), 78° (d = 1.818 Å), 91.4° (d = 1.602 Å), and 101.2° (d = 1.472 Å). Of the latter peaks, only the 78° peak is not coincident, or nearly coincident, with a magnetite peak. This peak is 80% of the intensity of the maximum intensity maghemite peak at 54.2°, and should be clearly visible if maghemite occupies greater than about 5% of the sample volume and is crystalline.

In figure 18e, it can be seen that there is no peak present at $2\theta = 78^{\circ}$. The characteristic peak at 22.4° would have an intensity which is 40% that of the maghemite maximum intensity peak, and it could not be seen on the record (figure 18a) even if it was present because of the noisy background at $2\theta = 22^{\circ}$. The characteristic peak at 27.5° is nearly coincident with the magnetite peak at 27.3°, and would not be distinguishable in the record. The characteristic peak at 35.8° has an intensity which is 60% that of the maghemite maximum intensity peak. A low-intensity peak at 35.7° may correspond to this maghemite peak, in figure 18b. An ambiguity arises, however, since hematite has a peak at 36°, in figure 18b. No peak at 39.4° can be seen in figure 18b, even though the intensity of the maghemite peak would be the same as the intensity of the 35.7° peak. On this evidence, the peak at 35.7° is assigned to Hematite.

In figure 18c, the 46.6° magnetite peak is seen in the oxidized magnetite record. However, the peak is shifted slightly toward a higher 2θ value. In addition, the peak is broader and more complex, than the unoxidized magnetite peak. The shifting and broadening are characteristic of the presence of small particles ($\sim$100 Å in

diameter), and the presence of two phases, with d spacings of similar value. Such mixing of the 44.6° (d = 2.966 Å) magnetite peak and a 50° (d = 2.69 Å) hematite peak could result in the observed shifting of the oxidized magnetite peak. A broad, low-intensity peak at 50° in the oxidized magnetite record, is visible in figures 18c and 18d. In figure 18d, the scan speed has been reduced to 0.4°/min., and the range is reduced from 1000 to 200. The scan speed in figure 18c is 2°/min. The complex peak at 54° in figure 18c demonstrates the small-particle and mixing effects. The mixing occurs as a result of the magnetite 53.8° (d = 2.530Å) and the hematite 54° (d = 2.510 Å) peaks.

In figure 18e, the magnetite 66.2° peak is seen in the oxidized magnetite record. Again it is broader and more complex than the unoxidized magnetite peak. The hematite peaks at 62.4° and 76.7° are not evident in the oxidized magnetite curves, due probably to the fact that the hematite peaks are so low in intensity.

In figure 18f, the peak at 84.4° in the oxidized magnetite record shows the effects of the 84.9 Å hematite peak and the magnetite 83.9° peak. A similar mixing of the 90.3° magnetite peak and the 91.5° hematite peak results in the 90.8° peak in the oxidized magnetite record.

Magnetite displays a peak at 101.1° and hematite displays peaks at 100.6°and 103.8°. As a result, the oxidized sample displays a single peak, resulting from the mixing of the magnetite and hematite peaks, 101.6°. In figure 18g the 84.4° oxidized Magnetite peak is shown in more detail. In this figure the assymetrical peak arising from the influence of the hematite peak at 84.9° is clearly seen.

Goethite and limonite display essentially the same X-ray diffraction records, highlighted by four intense peaks at 31.6° (d = 4.21 Å), 50° (d = 2.69 Å), 56° (d = 2.44 Å), and 26.5° (d = 5.0 Å). The first peak is not present in the record in figure 18b. The peak at 26.5° for goethite is not distinguihable from the magnetite peak at 27.3° due to mixing effects. The 50° peak is not characteristic only of goethite and limonite, it is also characteristic of hematite, and is therefore not diagnostic of goethite or limonite. No peak is present in the oxidized magnetite record at 56°.

From the X-ray diffraction record of the oxidized sample, it can be concluded that hematite is the principal oxidation product. If any maghemite is present in the alteration product, it either occupies less than about 5 volume percent of the sample, it is

amorphous, or it is vacancy-disordered. Goethite and limonite are apparently not present in the alteration product.

Reflected Color

The oxidation product was compared with a sample of hematite, both samples being of the same size and shape, and both being packed at the same density. Both samples appeared, visually, to have the same reflected color, bright red. Also present for comparison was a sample of goethite, prepared by steaming hematite in air for 72 hours, and then heating it in dry O_2 for 24 hours. Goethite and maghemite have the same reflected color, viz. brown to yellow-brown. It was evident that the oxidized sample is definitely red, not brown or yellow-brown, in color. This supports the X-ray diffraction evidence that hematite is the principal oxidation product.

Figures 18a - 18g. An X-ray diffraction record, for the hematite, unoxidized and oxidized magnetite samples, for $22^{o} \leq 2\theta \leq 86^{o}$. In figures 18d and 18g, the 2θ scan speed is $.4^{o}$/ min., while in the remaining figures, the 2θ scan speed is 2^{o} / min. Relative intensity is along the ordinate.

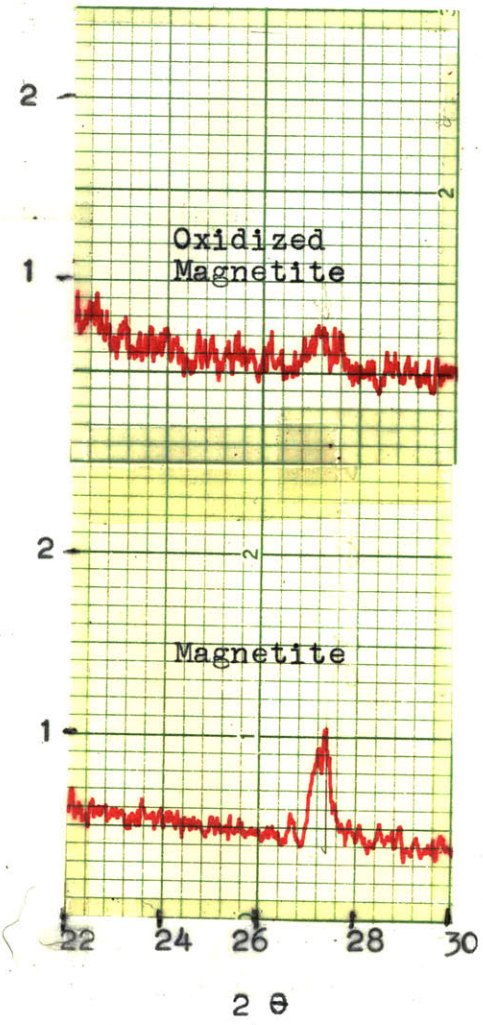

Figure 18a.

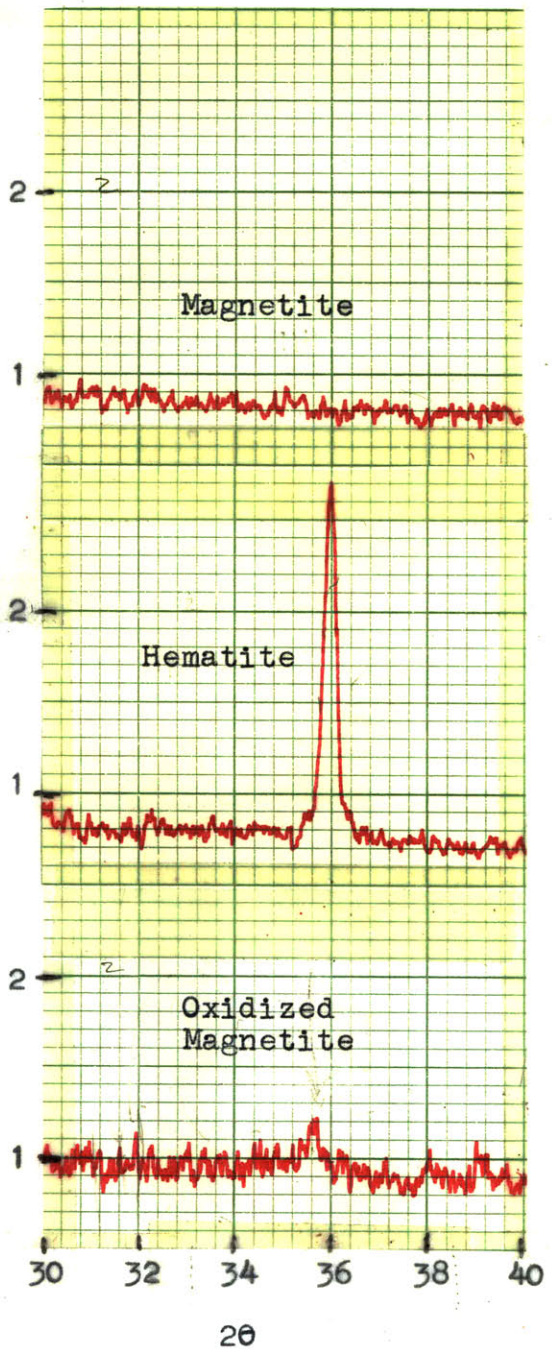
2
Magnetite
1
2
Hematite
1
2
Oxidized
Magnetite
1
30
32
34
36
38
40
2θ

Figure 18b

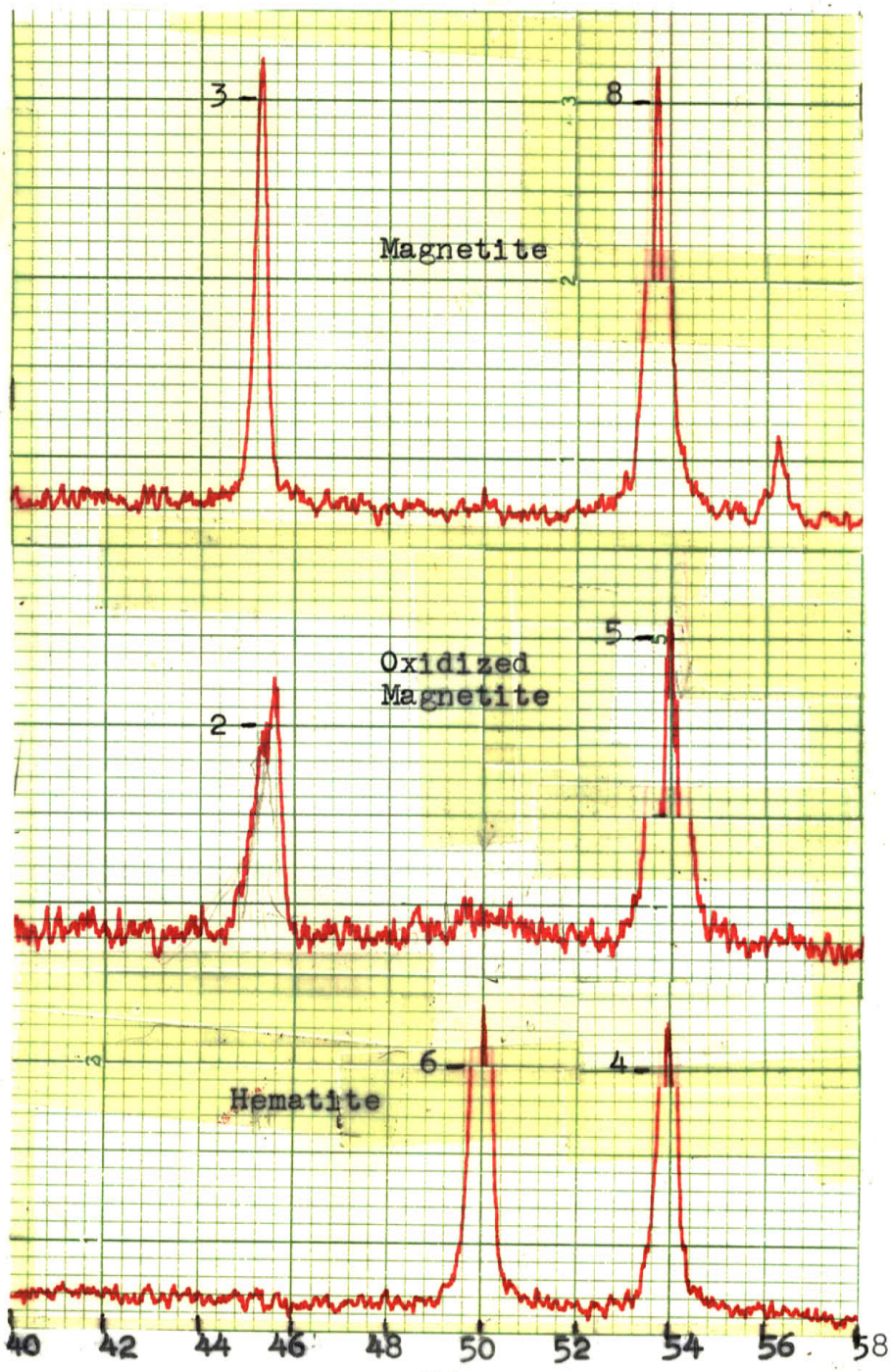
3
8
Magnetite
5
Oxidized
Magnetite
2
6
4
Hematite
40
42
44
46
48
50
52
54
56
58
2θ

Figure 18c

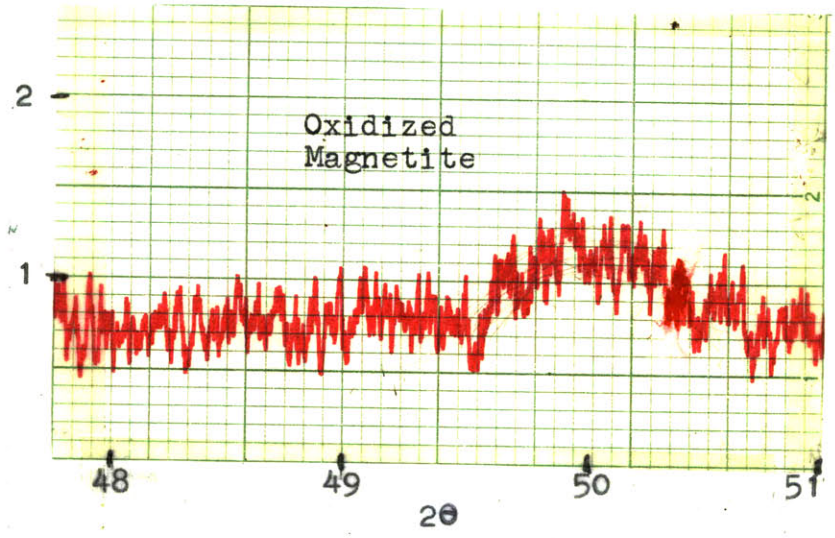

Figure 18d

Figure 18e.

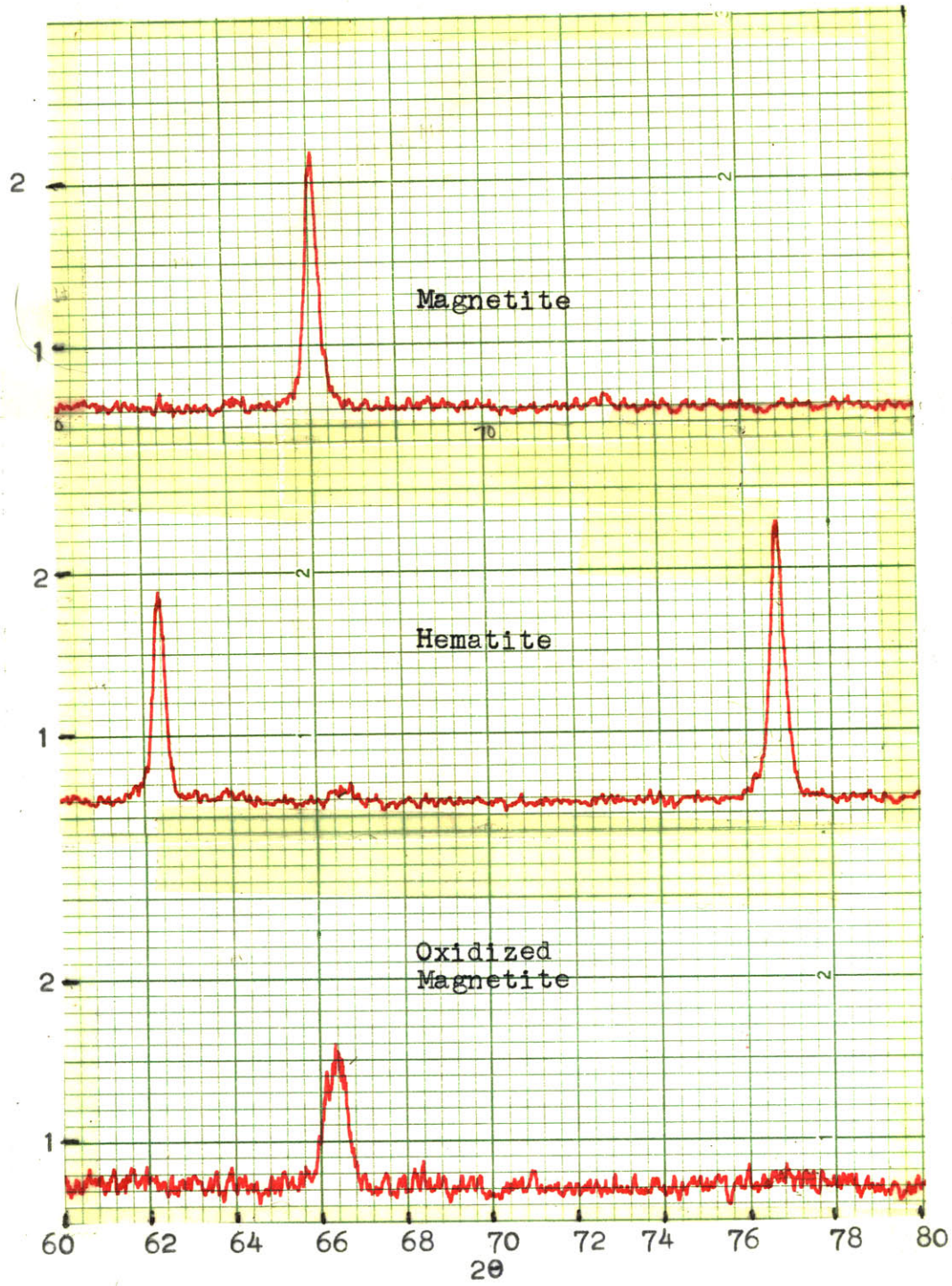
Magnetite
Hematite
Oxidized
Magnetite
2
1
60
62
64
66
68
70
72
74
76
78
80
2θ

Figure 18f.

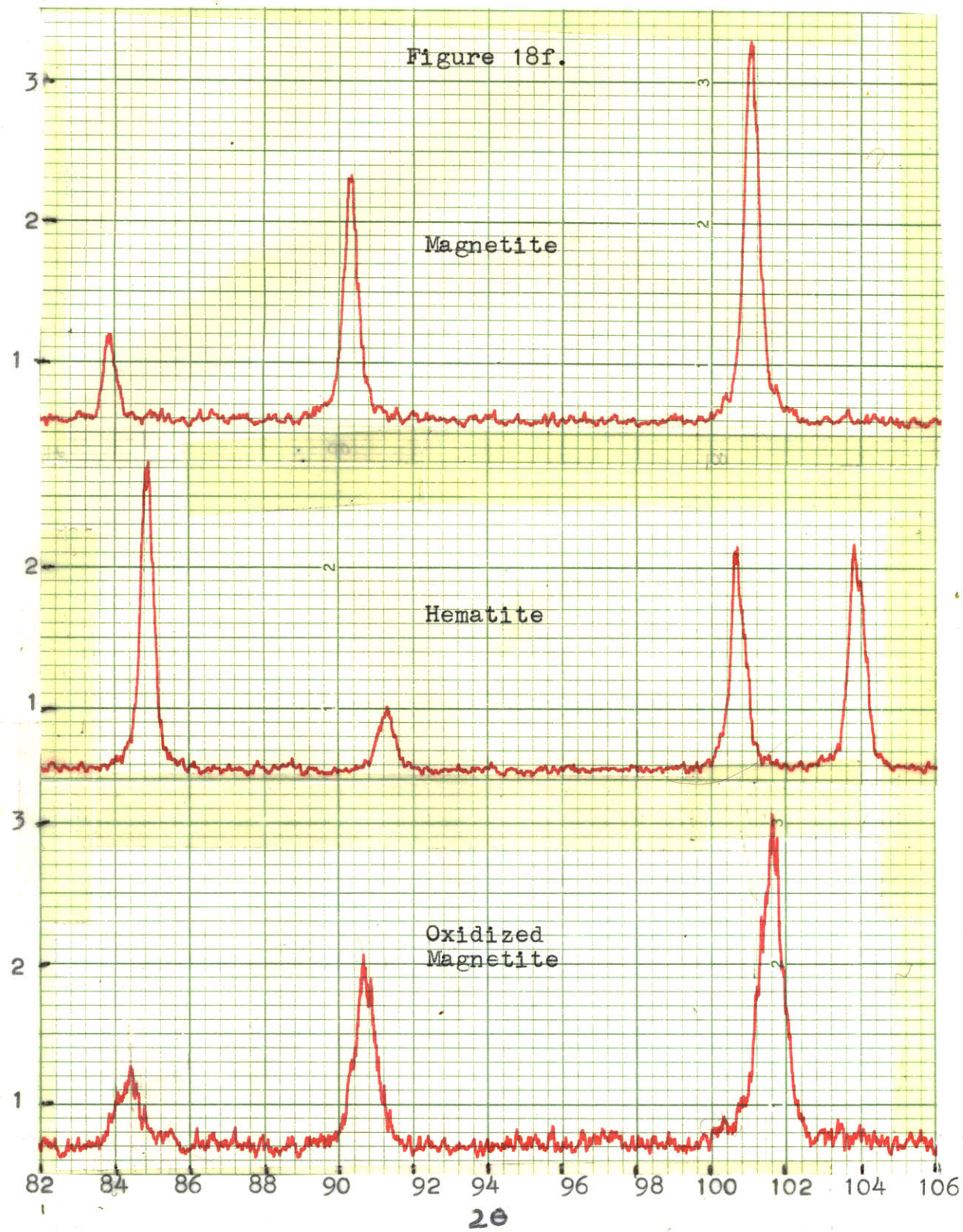
Magnetite
Hematite
Oxidized
Magnetite
1
2
3
82
84
86
88
90
92
94
96
98
100
102
104
106
2θ

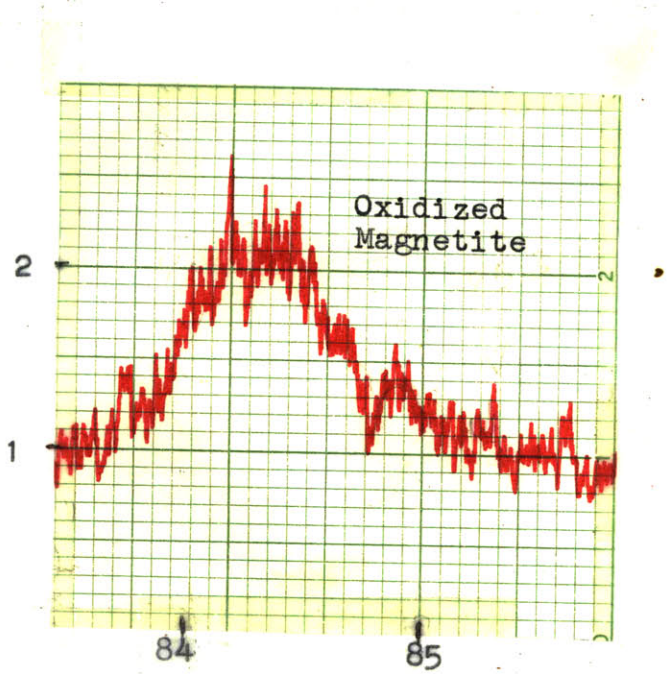

Figure 18g.

IV. UV-STIMULATED OXIDATION OF MAGNETITE: THE MECHANISM

THE OVERALL REACTION

It has been demonstrated in the laboratory that Magnetite (Fe_3O_4) can be oxidized to ferric oxide (Fe_2O_3), when it is illuminated with ultraviolet radiation in an O_2-bearing atmosphere. The ferric oxide is principally in the form of Hematite (α-Fe_2O_3), although some Maghemite (γ-Fe_2O_3) may be present. The overall reaction can be represented by the expression,

$$2Fe_3O_4(\text{ solid }) + \tfrac{1}{2}O_2(\text{ gas }) \xrightarrow{h\nu} 3a\alpha\text{-}Fe_2O_3 + 3(1-a)\gamma\text{-}Fe_2O_3 \qquad (14)$$

This reaction is stoichiometrically simple, in the sense that its advancement can be described by a single parameter: the extent of reaction. The extent of reaction is given by $(\Delta t_o)^{-1}$ times the length of time to which the magnetite is exposed to the oxidizing environment. Δt_o is given by equations 13a, 13b, and 13c.

THE CONSTITUENT REACTIONS: THE RATE DETERMINING STEP

It is apparent from equations 13a through 13c that instead of a single reaction taking place as written (equation 14), the phase change proceeds through a network of reactions which involve reactive intermediates:

i.e., the reaction rate is a complex function of the total atmospheric pressure, the atmospheric O_2 partial pressure, the ultraviolet radiation intensity, surface area per gram of the sample, and the amount of adsorbed H_2O on the grain surfaces.

Surface Controlled Rate Determining Step

One important result from the experiment is that the amount of ferric oxide formed from the magnetite increases linearly with time. A linear growth law indicates that the rate determining step in the oxidation mechanism is surface controlled, rather than diffusion controlled (Evans, 1947; Gulbransen and Wysong, 1947; Grimley and Trapnell, 1956; Ritchie and Hunt, 1969). When the rate determining step is diffusion controlled, the growth laws are parabolic, cubic or exponential (Mott, 1940, 1947), or logarithmic (c.f. Fromhold, 1963a,b). That the rate determining step is surface controlled is further supported by the direct proportionality of Δt_o to A_t in equations 13a through 13c.

The Rate Determining Step Follows O_2 Dissociation

Since the kinetic rate equation for this oxidation process demonstrates a dependence on the atmospheric O_2 partial pressure, the grain surfaces are not saturated

with adsorbed O_2 (Gulbransen and Wysong, 1947; Grimley and Trapnell, 1956; Ritchie and Hunt, 1969). Since the reaction rate is linear and it is proportional to $pO_2^{\frac{1}{2}}$, the rate determining step must follow O_2 dissociation (Ritchie and Hunt, 1969). If the rate determining step had involved undissociated O_2, the linear growth law would be proportional to pO_2 or L (pO_2), where L (pO_2^n) is the Langmuir function , $bpO_2^n/(1 + bpO_2^n)$. b is a constant.

The Electron Concentration is Independent of Oxide Thickness

If the growing ferric oxide layer remains mechanically intact on the magnetite core, the rate determining step can be either diffusion controlled or surface controlled. If the adsorbed ions on a mechanically intact oxide layer set up an electric field across the oxide layer, this electric field results in a Boltzman distribution of electron concentration across the layer (Collins and Nakayama, 1967; Ritchie and Hunt, 1969). This electron distribution gives rise to the diffusion of ions through the oxide layer. As pointed out earlier, if the rate determining step was controlled by the diffusion of these ions, the oxide layer growth law would be either parabolic,

cubic, exponential, or logarithmic. It has already been pointed out that the rate determining step is surface controlled and the growth law is linear. This indicates that the electron concentration at the surface of the magnetite is independent of the oxide thickness (Ritchie and Hunt, 1969). If the surface controlled rate determining step was controlled by the Boltzman electron distribution, a parabolic growth law would result, unless the ionization of oxygen is rate determining. In the latter case, a cubic or logarithmic law results.

It can be concluded that the rate determining step occurs either at a fresh magnetite surface, or on the surface of the ferric oxide. The first case requires that the ferric oxide layer fails mechanically, and is continually broken away from the magnetite surfaces to be contiuously exposed to the atmospheric Oxygen (Evans, 1947). The second case suggests that cations from the magnetite substrate diffuse rapidly to the surface of the ferric oxide layer, where the slower, rate determining, post-O_2-dissociation step occurs. In either case, the electron concentration would be independent of the oxide thickness, as required by the results of Ritchie and Hunt (1969).

O_2 Dissociation on the Surface

In the presence of ultraviolet radiation, with wavelengths shortward of .230μ, the O_2 can dissociate in the atmosphere (Kaufman, 1967),

$$O_2 \xrightarrow{h\nu} 2\,O, \tag{15}$$

with a photodissociation rate constant of $5.8 \times 10^{-10} sec^{-1}$. The atomic Oxygen can collisionally recombine by the three-body process (Kaufman, 1967),

$$2O + M \longrightarrow O_2 + M, \tag{16}$$

where M is a molecular atmospheric species. The recombination coefficient is $k_{16} = 3 \times 10^{-33} (T/300)^{-2.9} cm^6\text{-}sec^{-1}$. O can collisionally recombine with O_2 in a three-body process, to form O_3, by the process (Kaufman, 1967),

$$O + O_2 + M \longrightarrow O_3 + M, \tag{17}$$

with a rate coefficient of $k_{17} = 5.5 \times 10^{-34} (T/300)^{-2.9}$ $cm^6\text{-}sec^{-1}$. Ozone photodissociates by the reaction (Inn and Tanaka, 1959),

$$O_3 \xrightarrow{h\nu} O_2 + O, \tag{18}$$

with the photolysis rate $J_{18} = 4.2 \times 10^{-3}$ sec^{-1} for $.200\mu \leq \lambda \leq .300\mu$. Further, O and O_3 recombine by the

reaction (Kaufman, 1967),

$$O + O_3 \longrightarrow 2O_2, \qquad (19)$$

with the recombination rate coefficient $k_{19} = 1.4 \times 10^{-12}$ exp(-1500/T) cm^3-sec^{-1}. Hence, the three principal neutral atmospheric oxygen species are O, O_2, and O_3.

Upon approaching the surface, a portion of the these three species of oxygen can collide with photoelectrons emitted from the magnetite. The photoelectric work function of magnetite is on the order of 3.8 eV to 4.2 eV, as described earlier (see section on photoemission, from the chapter on magnetite and its oxidation products). The number of emitted electrons per incident photon ranges from about 10^{-7} at the work function to around 10^{-2} to 10^{-3} for the 6 eV photons.

For photoelectrons with kinetic energies between .03 eV and 1.3 eV, electron attachment to O can occur by the process (Branscomb, 1964),

$$e_p^- + O\ (\ ^3P\ ) \longrightarrow O\ (\ ^2P\ )^- + h\nu, \qquad (20)$$

with the radiative attachment coefficients ranging between $1.2 \times 10^{-15} cm^3 \cdot sec^{-1}$ and $1.9 \times 10^{-15} cm^3 \cdot sec^{-1}$. These low energy photoelectrons can also attach to O_2,

by the process (Chanin et al., 1959),

$$e_p^- + O_2 + M \longrightarrow O_2^{-*} + M \longrightarrow O_2^- + M + h\nu, \qquad (21)$$

with the three body attachment coefficients ranging between $1 \times 10^{-30} cm^6 \cdot sec^{-1}$ and $7 \times 10^{-30} cm^6 \cdot sec^{-1}$. For photoelectron kinetic energies greater than .4 eV, electron attachment to ozone can occur by the reactions (Meyer and Neldel, 1937),

$$e_p^- + O_3 \longrightarrow O^- + O_2 \qquad (22)$$

and

$$e_p^- + O_3 \longrightarrow O + O_2^-, \qquad (23)$$

with the rate coefficients for these two reactions being on the order of $10^{-10.5} cm^3 \cdot sec^{-1}$. O_3^- is formed by collision clustering of O^-, O_2 and M (Burch and Geballe, 1957),with a clustering collision rate coefficient of $8.8 \times 10^{-31} cm^6 \cdot sec^{-1}$,

$$O^- + O_2 + M \longrightarrow O_3^- + M. \qquad (24)$$

For electron kinetic energies greater than 1.3 eV, O^- is produced by electron attachment to O_2 (Chanin et al., 1959),

$$e_p^- + O_2 \longrightarrow O + O^-, \qquad (25)$$

with the attachment coefficients ranging from $4 \times 10^{-13} cm^3 \cdot sec^{-1}$ for the 1.3 eV electrons to about 6×10^{-12} $cm^3 \cdot sec^{-1}$ for the 2 eV electrons. Also above 1.3 eV, radiative attachment to O_2 will produce O_2^- (Branscomb, 1964),

$$e_p^- + O_2 \longrightarrow O_2^- + h\nu \ , \qquad (26)$$

with the radiative attachment coefficients on the order of $10^{-16} cm^3 sec^{-1}$. Electron attachment to ozone for electron kinetic energies greater than 1.3 eV is given by reactions (22) and (23).

Detachment of electrons from O^- occurs collisionally, by reaction 24, and by photodetachment. Electron photodetachment from O^- results in $O(^3P)$ formation, for photon energies between 1.4 eV and 3.4 eV, with cross sections ranging from $2 \times 10^{-19} cm^2$ at 1.4 eV. to $6 \times 10^{-18} cm^2$ at 3.5 eV (Klein and Brueckner, 1958). Photodetachment produces $O(^1D)$, for incident photon energies between 3.5 eV and 5.7 eV, with detachment cross sections of $10^{-17} cm^2$ (Henry et al., 1969). Above 5.7 eV, photodetchment from O^- produces $O(^1S)$, with photodetachment cross sections of $10^{-17} cm^2$. (Henry et al., 1969).

Photodetachment of electrons from O_2^- occurs for photon energies above .5 eV (Branscomb, 1964), with photodetachment cross sections ranging from $10^{-20} cm^2$

for 0.5 eV photons to 10^{-18} for 2.9 eV photons. The cross sections from 2.9 eV to 6 eV increase at a rate which compensates for the decrease in photon flux beyond 2.9 eV (Branscomb, 1964). Collisional detachment of electrons from O_2^- occurs (Phelps and Pack, 1961),

$$O_2^- + M \longrightarrow O_2 + e^- + M, \qquad (27)$$

with a collisional detachment coefficient of 4×10^{-20} $cm^3 \cdot sec^{-1}$ at T = 230°C, decreasing with T by the factor exp (-.46 /kT).

The number of molecules of O_2 that collide with the surface per cm^2 per second range from 10^{16} molec-cm^{-2}-sec^{-1} for the 10^{-4} torr O_2 partial pressure experimental atmospheres, to 10^{22} molec$\cdot cm^{-2} \cdot sec^{-1}$, for the 10^2 torr O_2 partial pressure experimental atmospheres. The number of molecules of the M species (CO_2, CO, N_2, Ar, H_2O, and O_2), which collide with the surface per cm^2 per second range from 10^{18} molec$\cdot cm^{-2} \cdot sec^{-1}$ to 10^{22} molec$\cdot cm^{-2} \cdot sec^{-1}$, for the 10^{-2} torr and 10^2 torr total pressure atmospheres, respectively. The maximum photon flux at .350μ (4 eV), in the experimental environments was 2.8×10^{19} photons$\cdot cm^{-2} \cdot sec^{-1} \cdot Å^{-1}$. At 6 eV, the flux was around 10^{17} photons$\cdot cm^{-2} \cdot sec^{-1} \cdot Å^{-1}$ (see figure 10). The minimum photon flux at .350μ that was reached in the

experiment was 6.6 x 10^{14} photons$\cdot cm^{-2}\cdot sec^{-1}\cdot \mathring{A}^{-1}$, with the corresponding minimum at 6eV being on the order of 10^{12} photons$\cdot cm^{-2}\cdot sec^{-1}\cdot \mathring{A}^{-1}$. The maximum emitted electron flux ranged from 10^{17} electrons $\cdot cm^{-2}\cdot sec^{-1}$ for the 6eV photons to 10^{10} electrons$\cdot cm^{-2}\cdot sec^{-1}$ for the 4eV photons. The emitted electron flux was five orders of magnitude lower than these values when the low intensity radiation levels were used.

The steady state concentration of O at the surface is governed by reactions (15) through (19), with $k_{17}k_{19}[O_2]/k_{16}J_{18} \gg 1$:

$$[O] = \left\{ \frac{J_{15}[O_2]}{k_{16}[M](1 + k_{19}k_{17}[O_2]/k_{16}J_{18})} \right\}^{\frac{1}{2}}$$

$$= (J_{15}J_{18}/ k_{17}k_{19}[M])^{\frac{1}{2}}. \qquad (28)$$

The steady state ozone concentration is governed by reactions (17) through (19), with $k_{19}[O] \ll J_{18}$:

$$[O_3] = k_{17}[O][O_2][M] / (J_{18} + k_{19}[O])$$

$$= k_{17}[O][O_2][M] / J_{18}$$

$$= (k_{17} J_{15}[M]/ J_{18}k_{19})^{\frac{1}{2}}[O_2]. \qquad (29)$$

The steady state concentrations of O^-, O_2^-, and O_3^- are negligible in comparison to the O_2 and O_3 concentrations, due to the low photoelectron fluxes relative to the photon fluxes, and to the short mean free paths of the electrons in the atmosphere (c.f. Sommer and Spicer, 1965).

Hence, O_2 and O_3 are the principal atmospheric Oxygen species which collide with the Magnetite grain surfaces, although some O, O^-, O_2^-, and O_3^- will also be colliding with the surfaces. In addition to these six atmospheric Oxygen species, the atmosphere also consists of various combinations of CO_2, N_2, CO, Ar and H_2O. These species all compete for occupancy of the surface adsorption sites.

The CO_2, CO, N_2, Ar, H_2O, O, O^-, O_3, and O_3^- species all adsorb as individual units. That is, each atom, molecule or ion adsorbs at a single site (Langmuir, 1918). The forces which hold the O_2 and O_2^- species to the surface act principally on the individual atoms, rather than on the molecule or ion, however. If two adjacent adsorption sites aren't vacant for the dissociation of the O_2

and O_2^- species and chemisorption of the two atoms, the O_2 molecule desorbs. The O_2^- ion gives up its electron to the surface and desorbs as an O_2 molecule, before chemisorption of one of the atoms can occur (Langmuir, 1918). It is also possible for the O_2^- ion to desorb before giving up its electron to the surface. Therefore, in order for the chemisorption and subsequent incorporation of oxygen to occur as a result of collisions by O_2 or O_2^- two adjacent surface adsorption sites must be vacant.

Langmuir (1918) found that the number of adsorbed molecules and atoms per cm^2 of surface area reaches a steady state value. At steady state, the number of molecules and atoms which adsorb to the surface per cm^2 per second equals the number of molecules and atoms which desorb from the surface per cm^2 per second. The number of species, M, which are adsorbed to the surface per cm^2 at steady state, is proportional to the number of species which are colliding with the unit surface area per second, ν_M, and to the fraction of the surface not covered by the other adsorbed atoms and molecules.

From kinetic theory, the number of molecules colliding with a unit surface area per second is,

$$\nu_M = pM / (2\pi mkT)^{\frac{1}{2}} = 3.5 \times 10^{22} pM / (m'T)^{\frac{1}{2}} = c_M pM, \qquad (30)$$

where pM is the partial pressure of the species, in torr, m is the mass of the molecule or atom, m' is the molecular or atomic mass, in grams, T is the temperature, and k is Boltzman's constant. ν_M is in cm^{-2}-sec^{-1}. For all of the species, c_M is on the order of 10^{20} at 300°K.

If α_M = fraction of the incident molecules and atoms that adsorb to the surface, and μ_M = number of adsorbed molecules and atoms, which desorb per cm^2 per sec, then at steady state,

$$\alpha_M \nu_M = \mu_M \tag{31}$$

Let σ_1 be the total number of sites per cm^2 available for adsorption on a clean (free of adsorbed species) surface, and let σ_M be the number of adsorbed molecules or atoms per cm^2, that is in steady state with the atmospheric pressure of that species. Assuming that a single adsorbed molecule or atom occupies a single site, then the fraction of surface sites which are occupied, in steady state with the atmospheric pressure of that species is,

$$\theta_M = \sigma_M / \sigma_1 . \tag{32}$$

If it is assumed that, (1) the adsorption sites are all identical, and (2) the potential energy of an adsorbed atom or molecule at a site is independent of the

presence of adsorbed atoms and molecules at other sites, then,

$$\mu_M = \mu_{1,M}\,\theta_M, \tag{33}$$

where $\mu_{1,M}$ is the rate of evaporation, in molecules·cm^{-2}·sec^{-1}, for a surface completely covered by the M species.

With θ_O being the fraction of the surface sites already occupied by oxygen atoms, i.e. $\theta_O = \sigma_O/\sigma_1$, then the fraction of sites available for adsorption is $1 - \theta$, where $\theta = \theta_O + \theta_M$. Therefore, the number of atoms or molecules, which adsorb to the surface per cm^2 per second, i.e. $\alpha_M \nu_M$, is given by the relation,

$$\alpha_M \nu_M = \alpha_{O,M}\,(\,1-\theta\,)\,\nu_M, \tag{34}$$

where $\alpha_{O,M}$ is the fraction of incident atoms or molecules that would adsorb on a surface which is free of any previously adsorbed molecules or atoms. At steady state,

$$\mu_{1,M}\,\theta_M = \alpha_{O,M}\,\nu_M\,(\,1 - \theta\,). \tag{35}$$

In order for oxygen chemisorption to occur, as a result of collision of an O_2 molecule with the surface, the O_2 (or O_2^-) molecule must collide with a pair of adjacent vacant surface sites, as described earlier. The probability that one of these sites is available is proportional to

$1 - \theta$. The probability that both are available for the adsorption of the O atoms is $(1 - \theta)^2$. The rate of adsorption of the O atoms, resulting from collisions by O_2 or O_2^-, is therefore,

$$\alpha_{O_2} \nu_{O_2} = \alpha_{o,O_2} (1 - \theta)^2 \nu_{O_2}, \qquad (36)$$

where $\alpha_{O_2} \nu_{O2}$ is the number of O_2 molecules which collide with a pair of adjacent vacant surface adsorption sites per cm^2 per second, dissociate, and adsorb as a pair of O atoms, and α_{o,O_2} is the fraction of incident O_2 (or O_2^-) molecules that would adsorb (as two O atoms) on a surface, which is free of any previously adsorbed atoms or molecules.

The rate of desorption of isolated adsorbed O atoms is negligibly small, while adjacent O atoms can combine together more readily. The desorption of atoms from the surface occurs only in pairs, as molecules. The probability that an adsorbed O atom will be in one of these adjacent spaces is proportional to θ_o, and that both sites are occupied by the O atoms is proportional to θ_o^2. The rate of desorption of these two atoms as an O_2 molecule is

$$\mu_{O_2} = \mu_{1,O_2} \theta_o^2, \qquad (37)$$

where μ_{1,O_2} is the rate of evaporation, in molecules$\cdot$cm^{-2}.

sec^{-1}, for a surface completely covered by the O atoms.

For the steady state,

$$\alpha_{o,O_2}(1 - \theta)^2 \nu_{O_2} = \mu_{1,O_2} \theta_o^2 , \qquad (38)$$

or,

$$\theta_o^2 = \alpha_{o,O_2} \nu_{O_2} (1 - \theta)^2 / \mu_{1,O_2} \qquad (39)$$

Let $b = \alpha_{o,O_2} c_{O_2} / \mu_{1,O_2}$, then

$$\theta_o^2 = b\, pO_2 (1 - \theta)^2. \qquad (40)$$

But, $1 - \theta = 1 - \theta_M - \theta_o$, so that

$$\theta_o + \theta_o (b\, pO_2)^{\frac{1}{2}} = (b\, pO_2)^{\frac{1}{2}} (1 - \theta_M), \qquad (41)$$

or,

$$\theta_o = \left\{ (b\, pO_2)^{\frac{1}{2}} / \left[1 + (b\, pO_2)^{\frac{1}{2}} \right] \right\} (1 - \theta_M). \qquad (42)$$

For the adsorbed molecules and isolated atoms, steady state occurs when (equation 35),

$$\mu_{1,M} \theta_M = \alpha_{o,M} \nu_M (1 - \theta). \qquad (35)$$

The adsorbed molecules (including O_2 and O_2^-) and isolated atoms at single sites occupy significantly more spaces per cm^2 than the adsorbed O atoms at adjacent surface sites, and

$\theta_M \cong \theta$. Hence, equation 35 becomes,

$$\mu_{1,M}\,\theta_M = \alpha_{o,M}\,\nu_M\,(\,1 - \theta_M\,). \tag{43}$$

Subtracting $\mu_{1,M}\,\theta_M$ from both sides of the equation, and adding $\mu_{1,M}$ to both sides yields the expression,

$$\mu_{1,M} = \mu_{1,M} - \mu_{1,M}\,\theta_M + \alpha_{o,M}\,\nu_M\,(\,1 - \theta_M\,), \tag{44}$$

or,

$$(\,1 - \theta_M\,) = \mu_{1,M} / (\,\mu_{1,M} + \alpha_{o,M}\,\nu_M\,). \tag{45}$$

Letting $b' = \alpha_{o,M}\,c_M / \mu_{1,M}$, equation (45) becomes,

$$(\,1 - \theta_M\,) = 1 / (\,1 + b'pM\,). \tag{46}$$

Substituting (46) into (42),

$$\theta_o = \left\{(\,b\,pO_2\,)^{\frac{1}{2}} / \left[1 + (\,b\,pO_2\,)^{\frac{1}{2}}\right]\right\} \cdot \left[1 / (1 + b'\,pM)\right] \tag{47}$$

From equation (39),

$$b\,pO_2 = \alpha_{o,O_2}\,\nu_{O_2} / \mu_{1,O_2} = \theta_o^2 / (\,1 - \theta\,)^2, \tag{48}$$

where θ_o is the number of sites occupied by O atoms at adjacent sites, and (1 - θ) is the total number of sites available for adsorption per cm^2. If $\theta_o \ll (\,1 - \theta\,)$ and therefore $(\,b\,pO_2\,)^{\frac{1}{2}} \ll 1$, and if

$$b' \, pO_2 = \alpha_{o,M} \nu_M / \mu_{1,M} = \theta_M / (1 - \theta_M) \gg 1, \quad (49)$$

then equation (47) becomes

$$\theta_o \cong (b \, pO_2)^{\frac{1}{2}} / b'pM, \quad (50)$$

or,

$$\theta_o = \frac{(\alpha_{o,O_2})^{\frac{1}{2}}}{(\mu_{1,O_2})^{\frac{1}{2}}} \cdot \frac{\mu_{1,M}}{\alpha_{o,M}} \cdot \frac{c_{O_2}^{\frac{1}{2}}}{c_M} \cdot \frac{(pO_2)^{\frac{1}{2}}}{pM}, \quad (51)$$

The terms α_{o,O_2} and $\alpha_{o,M}$ are the fractions of incident molecules on a surface, which is free of any previously adsorbed species, and are proportional to the rate constants of the reactions

$$O_2 \ (\text{gas}) + 2 \, S \longrightarrow S - O + S - O \quad (52a)$$

and

$$M \ (\text{gas}) + S \longrightarrow S - M, \quad (52b)$$

i.e. $\alpha_{o,O_2} \propto k_{52a}$ and $\alpha_{o,M} \propto k_{52b}$. In these reactions, S is a vacant surface site, 2 S is a pair of adjacent vacant surface sites, and S-O and S-M are adsorbed O and M. k_{52a} is in $cm^6\text{-}sec^{-1}$ and k_{52b} is in $cm^3\text{-}sec^{-1}$, while α_{o,O_2} and $\alpha_{o,M}$ are both unitless.

Samorjai (1964) has demonstrated that illumination,

at wavelengths shortward of the optical bandgap, results in more rapid desorption of atoms and molecules from the surfaces of semiconductors than that arising from thermal energy. Hence, $\mu_{1,M}$ and μ_{1,O_2} are proportional to the rate constants of the reactions,

$$S\text{-}O + S\text{-}O \xrightarrow{h\nu} O_2 \text{ (gas)} + 2\ S \qquad (53a)$$

and

$$S - M \xrightarrow{h\nu} M \text{ (gas)} + S, \qquad (53b)$$

i.e. $\mu_{1,O_2} \propto J_{53a}$ and $\mu_{1,M} \propto J_{53b}$. μ_{1,O_2}, $\mu_{1,M}$, J_{53a}, and J_{53b} all have the units $cm^{-2}\text{-}sec^{-1}$. c_{O_2} and c_M are proportional to $T^{-\frac{1}{2}}$ from equation (30), and they have the units $cm^{-2}\text{-}sec^{-1}\cdot torr^{-1}$.

Therefore,

$$\theta_o = K_{54} \frac{k_{52a}^{\frac{1}{2}}}{J_{53a}^{\frac{1}{2}}} \cdot \frac{J_{53b}}{k_{52b}} \cdot \frac{T^{-\frac{1}{4}}}{T^{-\frac{1}{2}}} \cdot \frac{pO_2^{\frac{1}{2}}}{pM}, \qquad (54)$$

where K_{54} is a constant which incorporates all the proportionality constants in going from the $\propto$ factors to the k factors, from μ to J, and from the c factors to $T^{-\frac{1}{2}}$. K_{54} has the units $torr^{\frac{1}{2}}\text{-}cm\text{-}{}^oK^{-\frac{1}{4}}$.

θ_o is the ratio of the number of adsorbed O atoms per cm^2 on the grain surfaces, σ_{O_2}, to the number of sites per cm^2 available for adsorption, σ_1. Hence, the steady state

surface concentration of adsorbed oxygen atoms is,

$$\sigma_{O_2} = K_{54} \cdot \frac{k_{52a}^{\frac{1}{2}}}{J_{53a}^{\frac{1}{2}}} \cdot \frac{J_{53b}}{k_{52b}} \cdot \frac{T^{-\frac{1}{4}}}{T^{-\frac{1}{2}}} \cdot \frac{pO_2^{\frac{1}{2}}}{pM} \cdot \sigma_1 , \qquad (55)$$

where σ_1 is a characteristic of the grain surfaces of Magnetite, assumed to be a constant for magnetite. For the O_2^- species, pO_2 is replaced with pO_2^- in equation (55).

For the case when the principal adsorbing oxygen species is one of the odd oxygen species, viz. O, O^-, O_3, or O_3^-, then equation (38) becomes,

$$\alpha_{o,0} \nu_0 (1 - \theta) = \mu_{1,0} \theta_0, \qquad (56)$$

where the subscript 0 refers to any of the odd oxygen species, not just atomic oxygen. Then, equation (42) becomes,

$$\theta_0 = \left[b\ pO / (1 + b\ pO) \right] (1 - \theta_M), \qquad (57)$$

where pO is the atmospheric partial pressure of the odd Oxygen species under consideration. Equation (51), for the case of odd oxygen, becomes,

$$\theta_0 = \frac{\alpha_{o,0}}{\mu_{1,0}} \cdot \frac{\mu_{1,M}}{\alpha_{o,0}} \cdot \frac{c_0}{c_M} \cdot \frac{pO}{pM} . \qquad (58)$$

The terms $\alpha_{o,O}$ and $\alpha_{o,M}$ are the fractions of incident odd oxygen and the other molecules, respectively, that adsorb to the surface, which is free of any previously adsorbed species. These terms are proportional to the rate constants of the reactions,

$$O\ (\text{gas}) + S \longrightarrow S - O \tag{59}$$

and

$$M\ (\text{gas}) + S \longrightarrow S - M, \tag{52b}$$

i.e. $\alpha_{o,O} \propto k_{59}$ and $\alpha_{o,M} \propto k_{52b}$. In these reactions, S is a vacant surface site, and S - O and S - M are adsorbed odd oxygen (either O, O^-, O_3, or O_3^-) and adsorbed M, respectively. k_{59} and k_{52b} are in $cm^3 \cdot sec^{-1}$, while $\alpha_{o,O}$ and $\alpha_{o,M}$ are unitless. $u_{1,M}$ and $u_{1,O}$ are proportional to the rate constants of the reactions

$$S - O \xrightarrow{h\nu} O\ (\text{gas}) + S \tag{60}$$

and

$$S - M \xrightarrow{h\nu} M\ (\text{gas}) + S, \tag{53b}$$

i.e. $\mu_{1,O} \propto J_{60}$ and $\mu_{1,M} \propto J_{53b}$. The $\mu_{1,O}$, $\mu_{1,M}$, J_{60}, and J_{53b} all have the units $cm^{-2}\text{-}sec^{-1}$. c_O and c_M are

proportional to $T^{-\frac{1}{2}}$, from equation (30), and they have the units $cm^{-2} \cdot sec^{-1} \cdot torr^{-1}$.

Therefore,

$$\theta_0 = K_{61} \frac{k_{59}}{J_{60}} \cdot \frac{J_{53b}}{k_{52b}} \cdot \frac{pO}{pM} , \qquad (61)$$

and equation (55) becomes,

$$\sigma_0 = K_{61} \cdot \frac{k_{59}}{J_{60}} \cdot \frac{J_{53b}}{k_{52b}} \cdot \frac{pO}{pM} \cdot \sigma_1 . \qquad (62)$$

For the O^-, O_3, and O_3^- species, pO is replaced with pO^-, pO_3, and pO_3^-, respectively, in equation (62). It is evident from expressions (28) and (29), and the discussion which follows them, that the principal odd oxygen species is O_3. As discussed later, the electron concentration is greatest at the surface, and electron attachment occurs there at a higher rate than it does in the atmosphere. The principal atmospheric oxygen species that collide with the surface are O_2 and O_3. From expression (29) $pO_3 \propto pO_2\, pM^{\frac{1}{2}}$ and

$$\sigma_{O_2} = K_{63}\, J^{\frac{1}{2}}\, T^{\frac{1}{4}}\, pO_2^{\frac{1}{2}}\, pM^{-1}\, \sigma_1 , \qquad (63)$$

and

$$\sigma_{O_3} = K_{64}\, pO_2\, pM^{-\frac{1}{2}}\, \sigma_1 , \qquad (64)$$

where K_{63} and K_{64} are proportionality constants. J is proportional to the incident UV radiation intensity. The pressure dependence of atmospheric O_2 is not affected by any of the subsequent steps of the oxidation mechanism (shown later in this chapter), and so it can be seen from expressions (63) and (64) that the square root dependence of the O_2 partial pressure in the kinetic rate equation arises from the surface dissociation of O_2 on the Magnetite grain surfaces. The next step in the oxidation process is Oxygen chemisorption, i.e. electron attachment to physically adsorbed Oxygen, forming a bond with a surface cation.

Electron Attachment to Physically Adsorbed Oxygen

After O_2 collides with the surface, and dissociates into two Oxygen atoms, physically adsorbed, at two adjacent surface adsorption sites, the Oxygen atoms chemisorb to the surface. Oxidation of the Magnetite occurs, when the chemisorbed Oxygen is incorporated into the surface layer, i.e. when it coordinates a cation as an O^{2-} ligand.

Electron attachment to physically adsorbed Oxygen, to form S - O^-, occurs through the reaction,

$$S - O + e_p^- \longrightarrow S - O^-, \tag{65}$$

where e_p^- is a photoelectron. Electron attachment can be followed by electron photodetachment,

$$S - O^- \xrightarrow{h\nu} S - O + e^-, \tag{66}$$

where $e^- = \alpha e_p^- + (1 - \alpha) e_c^-$, i.e. a fraction, $1 - \alpha$, of the photodetached electrons return directly to the crystal as conduction or valence electrons, and the remaining portion, α, are emitted as photoelectrons. Electron attachment can also be followed by the attachment of a second electron,

$$e_p^- + S - O^- \longrightarrow S - O^{2-}. \tag{67}$$

Again, $S\text{-}O^{2-}$ may suffer photodetachment before being incorporated,

$$S - O^{2-} \xrightarrow{h\nu} S - O^- + e^-, \tag{68}$$

or,

$$S - O^{2-} \xrightarrow{h\nu} S - O + 2e^-. \tag{69}$$

The principal source of electrons for the electron attachment is photoemission from an Fe - Fe B-site cation pair (see section on the electronic properties of magnetite) in magnetite. Photoemission from magnetite

can be represented as,

$$Fe_3O_4 \xrightarrow{h\nu} Fe_3O_4^+ + \alpha e_p^- + (1 - \alpha) e_c^- . \qquad (70)$$

The work function of magnetite is between 3.8 eV and 4.2 eV, and the photoelectric yield, α, ranges from 10^{-7} e_p^- per incident photon for photon energies around the work function, to around 10^{-3} to 10^{-2} e_p^- per incident photon for photon energies around 6 eV (see section on electronic properties of magnetite).

Photoelectrons, e_p^-, that do not attach to the adsorbed oxygen, may either (1) collide with another adsorbed atom or molecule, lose kinetic energy, and recombine with the $Fe_3O_4^+$,

$$Fe_3O_4^+ + S - M + e_p^- \longrightarrow S - M + Fe_3O_4; \qquad (71)$$

or (2) penetrate the adsorbate, lose kinetic energy through collisions with atmospheric species, and subsequently return to the crystal,

$$Fe_3O_4^+ + M (gas) + e_p^- \longrightarrow M (gas) + Fe_3O_4. \qquad (72)$$

Those photoelectrons which return to the solid recombine with $Fe_3O_4^+$ through the reaction,

$$Fe_3O_4^+ + e_c^- \longrightarrow Fe_3O_4 . \qquad (73)$$

Incorporation

Those chemisorbed oxygen ions, $S - O^{2-}$, which do not undergo electron photodetachment, are incorporated into the magnetite surface layer, to form hematite (α-Fe_2O_3), and possibly some maghemite (γ-Fe_2O_3),

$$2\ Fe_3O_4^{+} + S - O^{2-} \longrightarrow 3a\ \alpha\text{-}Fe_2O_3 + 3\ (1 - a)\ \gamma\text{-}Fe_2O_3 \qquad (74)$$

The structures and electronic properties of these ferric oxide phases were discussed earlier.

The Rate Determining Step

The linear growth law of the kinetic rate equation, and the $pO_2^{\frac{1}{2}}$ dependence of the oxidation rate reveal that the rate determining step (the slowest step of the process) is a surface-controlled, rather than diffusion-controlled, reaction, and that it follows O_2 dissociation. Therefore, the rate determining step is either one of the electron attachment processes, or incorporation. All the steps which preceed the rate determining step are much faster than the rate determining step, and the kinetic problem is reduced to the consideration of the kinetics of the rate determining step and the steady state of all the preceeding steps.

Assume $S\text{-}O^-$ formation as rate determining. If electron attachment to S-O is rate determining, then, from reaction (65),

$$d[Fe_2O_3]/dt = (1/3)\, d[S\text{-}O]/dt = k_{65}[S\text{-}O][e_p^-]\, A_t, \quad (75)$$

where $d[Fe_2O_3]/dt$ is the rate formation of Fe_2O_3, in sec^{-1}, $d[S\text{-}O^-]/dt$ is the rate formation of $S\text{-}O^-$, in sec^{-1}, $[S\text{-}O]$ is the steady state concentration of adsorbed O atoms, in cm^{-2}, $[e_p^-]$ is the steady state photoelectron concentration at the surface, in cm^{-2}, and A_t is the surface area per gram of the sample. k_{65} is the rate constant of reaction (65), in $cm^2 \cdot g \cdot sec^{-1}$. Since $[S\text{-}O] = \sigma_{O_2}$, from expression (55),

$$d[Fe_2O_3]/dt = (1/3)\, k_{65}\sigma_{O_2}[e_p^-]\, A_t . \quad (76)$$

The emission rate of photoelectrons is given by reaction (70). The principal photoelectron cooling processes are given by expressions (20), (21), (22), (23), (25), (26), (65), (67), (71), and (72). The assumption that $S\text{-}O^-$ formation is rate determining eliminates (65) as a principal cooling process. Further, (20) is eliminated because of the low abundance of O and the low attachment coefficient. (26) is inefficient relative to (25). (25) is negligible relative to (21), because of the short

mean free path and low abundance of the high energy photoelectrons. Since the ozone to O_2 abundance ratio ranged between 1 and 10^{-3} in the experiment, the attachment coefficients for the remaining gas phase attachment processes reduces the choice to (22), (23), or to the non-attachment collisions with the atmospheric M species, (72). In addition, collisions with adsorbed species remain for consideration. Since the surface is not saturated with adsorbed oxygen, and since (65) is assumed to be slow, (67) is negligible with respect to (71). Finally, the ratio of the abundance of ozone to [M] is always less than one, and the choice is reduced to (71) and (72). Hence,

$$d[e_p^-]/dt = J_{70}[Fe_3O_4] - k_{71}[S\text{-}M][Fe_3O_4^+][e_p^-] - k_{72}[M][e_p^-] \qquad (77)$$

and the steady state concentration of photoelectrons at the surface is,

$$[e_p^-] = J_{70}[Fe_3O_4]/[Fe_3O_4^+](\, k_{71}[S\text{-}M] + k_{72}[M]\,). \qquad (78)$$

$[Fe_3O_4]$ is a constant. $[Fe_3O_4^+]$ is a steady state volume concentration, controlled by reactions (70) and (73),

$$[Fe_3O_4^+] = (\, J_{70}/k_{73}\,)[Fe_3O_4]. \qquad (79)$$

It is to be noted that reaction (73) is included implicitly in expressions (71) and (72). The steady state surface concentration of S-M is controlled by reactions (52b) and (53b),

$$[\text{S-M}] = (k_{52b}/J_{53b})\, c_M\, pM\, \sigma_1, \qquad (80)$$

where $c_M\, pM$ is the number of molecules colliding with the surface per cm^2 per second, and σ_1 is the total number of surface sites available for adsorption. Finally, from kinetic theory, the volume concentration of the atmospheric species, $[M]$, is given by the expression,

$$[M] = 9.656 \times 10^{18}\, pM / T, \qquad (81)$$

where pM is in torr, and $[M]$ is in cm^{-3}. T is the temperature of the gas, in ^{o}K.

Substituting (79), (80) and (81) into (78) gives the expression,

$$[e_p^-] = J_{70}[Fe_3O_4] / \left\{ (J_{70}/k_{73})\cdot[Fe_3O_4]\cdot\left[(k_{52b}k_{71}/ J_{53b})\cdot c_M\, pM\sigma_1 + (k_{72}\, k_{81})\cdot pM/T\right]\right\} . \qquad (82)$$

It can be seen that if reaction (71) is the principal photoelectron cooling process, substitution of expression (82) and (63) into (76) yields an expression which is in agreement with the kinetic rate equation

which was derived experimentally, except for a factor of $T^{\frac{3}{4}}$ and for a factor accounting for variations in the amount of adsorbed H_2O on the grain surfaces:

$$d\left[Fe_2O_3\right]/dt = K_{83}\, J^{\frac{3}{2}}\, pO_2^{\frac{1}{2}}\, pM^{-2}\, T^{\frac{3}{4}}\, A_t\, f(H_2O). \quad (83)$$

$K_{83} = k_{65}K_{63}k_{73}/3\, k_{71}k_{52b}(\, c_M T^{\frac{1}{2}}\,)$ and $J^{\frac{3}{2}} = J_{53b}{}^2/\, J_{53a}{}^{\frac{1}{2}}$. The factor of $T^{\frac{3}{4}}$ appears in equation (83) but not in the experimentally derived rate equation. In the experiment the temperature was varied from 263°K to 373°K, and no effect on Δt_o was observed. As shown below, the $f(H_2O)$ factor in expression (83) is proportional to $T^{-\frac{1}{2}}$ and the temperature dependence of (83) is actually $T^{\frac{1}{4}}$. A $T^{\frac{1}{4}}$ dependence over the 263°K to 373°K range would result in less than a $\pm$10% change in Δt_o (the measurement uncertainty). Therefore, the $T^{\frac{1}{4}}$ factor in equation (83) is not in disagreement with the measured temperature independence of Δt_o in expression (13). Further, the assumption that $S\text{-}O^-$ formation is rate determining satisfies the empirical kinetic rate equation constraints only if (71) is the principal electron cooling process, rather than (72), and (49) is true.

Assume $S\text{-}O^{2-}$ formation is rate determining. Then,

$$d[Fe_2O_3]/dt = (1/3)\, d[S\text{-}O^{2-}]/dt = k_{67}\,[S\text{-}O^-][e_p^-]A_t, \quad (84)$$

where all the preceeding steps are assumed to be in steady state. The steady state concentration of $S\text{-}O^-$ is controlled by reactions (65) and (66), and is given by the expression,

$$[S\text{-}O^-] = (k_{65} / J_{66})[S\text{-}O][e_p^-], \tag{85}$$

so that with $\sigma_{O_2} = [S\text{-}O]$,

$$d[Fe_2O_3]/dt = (k_{67}\, k_{65}/ 3\, J_{66})\, \sigma_{O_2} [e_p^-]^2\, A_t. \tag{86}$$

In this case, from (82) and (63), the intensity factor would be $J^{\frac{1}{2}}$ or $J^{-\frac{1}{2}}$, depending on whether reaction (71) or (72), respectfully, is the principal photoelectron cooling process. In addition the total pressure dependence is pM^{-3}, and σ_1 appears explicitly in the expression. Also, the temperature dependence would be either $T^{\frac{1}{4}}$ or $T^{\frac{7}{2}}$, depending on whether (71) or (72) is dominant, respectfully.

Assume incorporation is the rate determining step. If incorporation is chosen as the rate determining step, then all the the previous reactions are in steady state, and deviations from the experimentally derived rate equation are even more profound than in the previous case.

The kinetic rate equation is consistent with $S\text{-}O^-$ formation as the rate determining step. From reaction

(63), it is still unspecified whether O_2 or O_2^- dissociates on the surface. In expression (63), if O_2^- was the dissociative species , then σ_{O_2} would be proportional to $(pO_2^-)^{\frac{1}{2}}$, rather than $pO_2^{\frac{1}{2}}$, as written. The O_2^- concentration is a steady state concentration, governed by reactions (21), (26), (27) and photodetachment,

$$[O_2^-] = (k_{21}[O_2][e_p^-][M] + k_{26}[O_2][e_p^-])/(k_{27}[M] + J_{26a}), \quad (87)$$

where J_{26a} is the photodetachment rate coefficient. If (21) and (27) are chosen as dominant over (26) and photodetachment, then σ_{O_2} demonstrates a J, rather than $J^{\frac{1}{2}}$, dependence, or $T^{\frac{3}{4}}$ dependence, rather than $T^{\frac{1}{4}}$ dependence, depending on whether (71) or (72) is dominant in $[e_p^-]$. In addition, σ_{O_2} would demonstrate a $pM^{-\frac{3}{2}}$, rather than a pM^{-1}, dependence. If (26) and (27) are dominant in (87),then σ_{O_2} demonstrates a $pM^{-\frac{3}{2}}$ dependence, and a J or $T^{\frac{3}{4}}$ dependence, depending on whether (71) or (72) is dominant in $[e_p^-]$. If (21) and photodetachment are dominant in (87), then σ_{O_2} demonstrates a $T^{\frac{3}{4}}$, rather than $T^{\frac{1}{4}}$ dependence, for O_2^- the dissociative species, if (71) is dominant in $[e_p^-]$. If (72) is dominant, then σ_{O_2} demonstrates an independence on J and a $T^{\frac{3}{2}}$ dependence. If (26) and photodetachment are dominant in (87), then σ_{O_2} demonstrates either an independence on J,

or a $T^{\frac{3}{4}}$ dependence, depending on whether (71) or (72) is dominant in $[e_p^-]$. It also demonstrates a $pM^{-\frac{3}{2}}$ dependence.

The surface dissociation of O_2^- would result in the direct formation of S-O^-, however, and S-O^- formation would not be the rate determining step. In this case, either S-O^{2-} formation or incorporation would be the rate determining step. In the former case, S-O^- would be a steady state value, governed by the reaction,

$$O_2^- \text{ (gas)} + 2S \longrightarrow S\text{-}O^- + S\text{-}O \,, \qquad (88)$$

and reaction (66). Following the format of (55),

$$[S\text{-}O^-] = (K_{89}\, k_{88}^{\frac{1}{2}} J_{53b} / J_{66}^{\frac{1}{2}}\, k_{52b})\, T^{\frac{1}{4}}\, pO_2^{-\frac{1}{2}} pM^{-1} \sigma_1 . \qquad (89)$$

The formation rate of the ferric oxide would therefore be,

$$d[Fe_2O_3]/dt = (1/3)\, k_{67}\, [S\text{-}O^-][e_p^-]\, A_t \,. \qquad (90)$$

From (87) and (81),

$$pO_2^- = pO_2\, [e_p^-]\, (k_{21}\, k_{81}^{-1} pM\, T + k_{26})/(k_{27}\, k_{81}^{-1} pM\, T + J_{26a}). \qquad (91)$$

The closest that the theoretical kinetic rate equation comes to reproducing the experimentally derived equation, viz. (21) and photodetachment dominant in (91) and (71) dominant in (82), demonstrates a $T^{\frac{1}{4}}$ and a $\sigma_1^{-\frac{1}{2}}$ dependence. Hence, S-O^- formation is rate determining.

The Role of Adsorbed H_2O

Included in the empirical rate equations, but not included in the previous section, is a dependence on adsorbed H_2O. It was observed in the experiment that magnetite samples which were previously unexposed to the ultraviolet light in an O_2-bearing atmosphere require the presence of adsorbed H_2O at the onset of illumination in order for the reaction to proceed. After this initial exposure, with adsorbed H_2O on the grain surfaces, H_2O is no longer required in order for the reaction to proceed. The reaction rate is increased, however, if H_2O is adsorbed to the grain surfaces intermittantly, viz. during intervals of non-illumination.

The surface oxidation of magnetite occurs as a result of oxygen chemisorption ($S\text{-}O^{2-}$ formation), and subsequent incorporation into the magnetite surface layer. Oxygen chemisorption occurs in two stages (Burshtein et. al., 1964). The first step is a rapid one, in which a monolayer of O is chemisorbed to the surface. The second stage is a much slower one, but the same amount of oxygen is chemisorbed in this stage, as in the first stage. The first stage leads to the formation of a protective oxide layer, which prevents further oxidation.

However, Burshtein et al. (1964) found that if H_2O

is adsorbed onto this first-stage protective layer, its structure is disturbed and its protective properties are altered. This is observed to lead to the formation of a thick oxide layer on the surface. They propose that the adsorbed H_2O promotes the migration of substrate cations to the surface, where they are submitted to first-stage oxygen chemisorption, and subsequent oxidation.

The cations are leached from the substrate by the adsorbed H_2O. The process starts at the surface of the magnetite crystal, where the cations are most susceptible to leaching, because of the broken bonds there. An OH^- ion is bonded to the cation at a surface anion vacancy, and the H^+ ion converts a surface O^{2-} ion to a second hydroxyl ion (Blyholder and Richardson, 1964).

A second H_2O molecule approaches the cation along a surface t_{2g} orbital (cationic 3d electron orbital, which is situated between the ligands, rather than being directed toward the ligands, as are the e_g orbitals), forming a seven-coordinate transition state (Basolo and Pearson, 1958). The transition state breaks down to form a two-hydroxyl, four-oxygen coordinated cation. The process is repeated four times, and then the cation goes into solution in the form of $Fe(H_2O)_6^{3+}$ or $Fe(H_2O)_6^{2+}$,

depending on whether the cation is ferric or ferrous. A similar process leaches ferric cations from the tetrahedral sites.

The hexahydrated cations migrate in the mobile second layer of the adsorbed H_2O (McCafferty et al., 1970). Upon illumination in an O_2-bearing atmosphere, the H_2O is desorbed (Samorjai, 1964), the Fe^{2+} cations are oxidized to Fe^{3+}, and the cations are coordinated by the O^{2-} ligands. There results a ferric oxide crystallite in the magnetite surface layer.

For the magnetite, however, the presence of adsorbed H_2O is only required during the initial 1 or 2 percent of Δt_o. Beyond this initial interval, the reaction can proceed in the absence of adsorbed H_2O. Arkharov (1966) proposes that the oxidation can proceed in the absence of H_2O through the process of "nucleation-disruption" of the protective oxide layer.

"Nucleation-disruption" requires the presence of nuclei of different spatial configuration than that of magnetite in the magnetite surface layer, however. Such nuclei are formed during the initial .01 Δt_o interval, during which H_2O is adsorbed to the grain

surfaces. These nuclei would have to be hematite, rather than maghemite, because only the hematite has a different spatial configuration than the magnetite. If the nuclei were Maghemite, the protective properties of the first-stage oxide layer would not be disrupted, and " nucleation-disruption" could not proceed. It is expected that the nuclei have the hematite structure, since hematite grows epitaxially, as the nuclei do, while maghemite forms topotactically, i.e. the maghemite crystal structure has a 3-dimensional accord with the magnetite surface layer, within which it grows. (Colombo et. al., 1965).

The different spatial configuration of the hematite nucleus causes a fluctuation in the magnetite surface layer at the hematite / magnetite transition boundary. Such a disruption of the spatial configuration disrupts the protective properties of the overlaying first-stage oxide layer, and the crystallite grows laterally. The small displacements of the atoms which are closest to the center of the initial rebuilding. induces a displacement of other atoms which are situated further from the center. The forces which induce successive displacements are transferred from atom to atom, radially from the crystallite center. The absolute value of the displacements increases proportionally to the distance from the

center of the nucleus. When the magnitude of the displacements reaches the interatomic distance of the magnetite lattice, a rupture of coherence in the surface layer occurs, and hematite scales result. Takei and Chiba (1960) found that the hematite nuclei are polycrystalline, and generally hexagonal in shape. When the hematite scales are abraded away, fresh magnetite surfaces are exposed, and the oxidation process continues.

Since the migration of the cations occurs in the second monolayer of adsorbed H_2O (McCafferty et al., 1970), the number of nucleation centers per cm^2 should increase with increased surface coverage, until completion of the second monolayer. This accounts for the observed decrease in Δt_o with increased values of pH_2O / P, for pH_2O / $P < .01$. For pH_2O/P between .01 and .05, however, Δt_o is the same as that for $pH_2O/P = .01$. For $pH_2O/P > .05$, Δt_o is composed of an oxidizing interval, which is equivalent to that for $pH_2O/P = .01$ at the onset of irradiation, and a non-oxidizing interval, which is proportional to pH_2O/P. The length of the non-oxidizing interval is decreased for increased radiation intensity and temperature. This suggests that, for $pH_2O/P > .01$ at the onset of irradiation, the quantity of adsorbed H_2O is increased beyond the

second monolayer, and therefore the time required to desorb the H_2O before the oxidation can occur increases. In the range $.01 \leq pH_2O/P \leq .05$ the decrease in Δt_o due to increased surface coverage is apparently balanced by the increase in length of the non-oxidizing interval, Δt_n. For $pH_2O/P > .05$, Δt_n becomes the dominant of the two opposing effects.

The pH_2O/P value corresponds to a sample preparation environment temperature of 300°K. As the temperature is increased, the H_2O desorbs from the grains such that the quantity of adsorbed H_2O is proportional to $(pH_2O/P)\ T^{-\frac{1}{2}}$ from kinetic theory. Therefore the function $f(H_2O)$ in equation (83) becomes;

$$f(H_2O)=\begin{cases} k_{91a}(pH_2O/P)\ T^{-\frac{1}{2}} \ ; \ pH_2O/P < .01 \\ k'_{91a}T^{-\frac{1}{2}} \ ; \ .01 \leq pH_2O/P \leq .05 \\ \left[k'^{-1}_{91a}\ T^{\frac{1}{2}} + k''_{91a}pM^{-2}T^{\frac{3}{4}}\ pO_2^{\frac{1}{2}}\ J^{\frac{3}{2}}\ A_t\ \Delta t_n\right]^{-1}; \ pH_2O/P > .05 \end{cases} \qquad (91a)$$

The Possible formation of Maghemite

During the formation of the hematite nuclei in the magnetite surface layer, cations are leached from the magnetite substrate, leaving the substrate cation deficient, stabilized by interstitial H_2O and the surrounding magnetite. Vacancy-disordered maghemite would probably result. The vacancy disordering eliminates the structure

which yields the only identifying peaks for maghemite in the X-ray diffraction record. Otherwise, the X-ray diffraction record is the same as that of magnetite. The absence of such peaks in the X-ray diffraction record of the samples in this experiment indicates that, if there is any maghemite present at all in the alteration product it is either vacancy-disordered, occupies less than 1 or 2 volume percent of the X-rayed sample, or it is amorphous.

SUMMARY OF THE OXIDATION MECHANISM

The principal oxidation product of magnetite in this experiment is hematite, although there may be some maghemite formed. If maghemite is present in the X-rayed samples, it is either vacancy-disordered, occupies less than 1 or 2 volume percent of the samples, or it is amorphous.

The overall reaction is represented by the expression,

$$2\ Fe_3O_4\ (\text{solid}) + \tfrac{1}{2}\ O_2\ (\text{gas}) \xrightarrow{h\nu} 3a\ \alpha\text{-}Fe_2O_3 + 3(1-a)\ \gamma\text{-}Fe_2O_3 \qquad (14)$$

Even though this reaction is stoichiometrically simple, it has been found that instead of a single reaction taking as written, the phase change proceeds through a network of reactions.

Upon exposure to the O_2-bearing atmosphere, the magnetite surface becomes covered with adsorbed species. The atmospheric O_2 competes with the other atmospheric species for vacant adsorption sites. The adsorption of Oxygen is in the form of chemisorbed O, and in order for Oxygen chemisorption to occur, two adjacent vacant adsorption sites are required. The other atmospheric species require only single sites for their adsorption. The surface dissociation of O_2 is represented by the expression,

$$O_2 \text{ (gas)} + 2S \longrightarrow S\text{-}O + S\text{-}O, \qquad (52a)$$

where S is a vacant surface site, and S-O is a physically adsorbed O atom. The number of physically adsorbed O atoms reaches a steady state concentration, the desorption being represented by the expression,

$$2\ S\text{-}O \xrightarrow{h\nu} O_2 \text{ (gas)} + 2S. \qquad (53a)$$

Electron attachment to S-O, to form $S\text{-}O^-$, occurs through the reaction,

$$S\text{-}O + e_p^- \longrightarrow S\text{-}O^-, \qquad (56)$$

where e_p^- is a photoelectron. It was found that reaction (56) is the rate determining step, i.e. it is the

slowest reaction of the oxidation sequence.

Following $S\text{-}O^-$ formation, attachment of the second electron rapidly occurs,

$$S\text{-}O^- + e_p^- \longrightarrow S\text{-}O^{2-}, \qquad (58)$$

in the presence of photoelectrons. Following $S\text{-}O^-$ and $S\text{-}O^{2-}$ formation, desorption in the presence of UV may occur by the reactions,

$$S\text{-}O^- \xrightarrow{h\nu} S\text{-}O + e^-, \qquad (57)$$

$$S\text{-}O^{2-} \xrightarrow{h\nu} S\text{-}O^- + e^-, \qquad (59)$$

or,

$$S\text{-}O^{2-} \xrightarrow{h\nu} S\text{-}O + 2e^-, \qquad (60)$$

although incorporation of the chemisorbed oxygen ($S\text{-}O^{2-}$) occurs rapidly after $S\text{-}O^{2-}$ formation,

$$S\text{-}O^{2-} + 2\ Fe_3O_4^+ \longrightarrow 3a\alpha\text{-}Fe_2O_3 + 3(\ 1\text{-}a\ )\gamma\text{-}Fe_2O_3. \qquad (65)$$

In this reaction, $Fe_3O_4^+$ represents a formula unit of magnetite, from which the β-electron of the octahedral Fe-Fe pair has been photoejected, i.e. all the cations in $Fe_3O_4^+$ are Fe^{3+}.

This sequence of reactions results in a theoretically derived kinetic rate equation, except for a factor of $T^{\frac{1}{4}}$.

The uncertainty, in Δt_o, is $\pm 10\%$, however, and a $T^{\frac{1}{4}}$ dependence over the temperature range investigated would result in less than a $\pm 10\%$ change in the reaction rate. Therefore, the $T^{\frac{1}{4}}$ factor in the theoretical expression does not disagree with the apparent temperature independence in the experimentally derived kinetic rate equation.

Incorporation leads to the formation of a protective ferric oxide layer on the magnetite surface, which prevents any further oxidation. In the presence of adsorbed H_2O, however, the protective properties of this layer are disturbed, and the formation of ferric oxide can further proceed. The H_2O leaches cations from the magnetite substrate, and promotes their migration to the surface, where they are submitted to oxygen chemisorption and incorporation. This results in the formation of a hematite crystallite in the magnetite surface layer, possibly underlain by a layer of (vacancy-disordered) maghemite.

Once the hematite crystallite is formed, oxidation can proceed in the absence of adsorbed H_2O. The crystallite serves as a nucleus for oxide growth by "nucleation-disruption" of the protective oxide layer. The different spatial configuration of the hematite nucleus causes a fluctuation in the spatial configuration of the magnetite surface layer, at the hematite / magnetite transition boundary. Such a

disruption of the spatial configuration disrupts the protective properties of the overlaying oxide layer, and the crystallite grows laterally. A rupture of coherence in the surface layer eventually occurs, and hematite scales form. This reveals fresh magnetite surfaces, and the oxidation process continues.

The migration of the cations from the magnetite substrate, during nucleus formation, occurs in the second (mobile) layer of adsorbed H_2O. Since the oxidation rate is proportional to the number of nucleation centers, per cm^2, in the surface layer, the rate should increase with increased coverage of the surface by adsorbed H_2O (rate$\propto pH_2O/P$), until completion of the second monolayer of adsorbed H_2O. This accounts for the observed increase in oxidation rate with increased pH_2O/P, for $pH_2O/P < .01$ at the onset of irradiation. For $pH_2O \geq .01$, at the onset of irradiation, the quantity of adsorbed H_2O is increased beyond the second monolayer. The time required to desorb the H_2O before oxidation can occur, Δt_n, is therefore increased. In the range $.01 \leq pH_2O/P \leq .05$, the decrease in Δt_o (oxidation rate$\propto \Delta t_o^{-1}$), due to increased surface coverage and nucleus formation, is balanced by the increase in Δt_n. This accounts for the observed independence of the oxidation rate on pH_2O/P,

for $.01 \leq pH_2O/P \leq .05$, at the onset of irradiation. For $pH_2O/P > .05$, Δt_n becomes the dominant of the two effects.

OXIDATION OF OTHER Fe^{2+}-BEARING MINERALS

One important result of the mechanism is that it is not unique to magnetite. The constituent reactions in the mechanism simply involve the chemisorption of oxygen at vacant surface adsorption sites, simultaneously with the oxidation of Fe^{2+} to Fe^{3+}, and the incorporation of the adsorbed oxygen in the surface layer to form ferric oxide. This is characteristic of the oxidation of most minerals, which contain ferrous iron. Further, the mechanism, or a similar one, could apply to any cation that is not in its lowest naturally-occuring oxidation state, such as Ti^{3+}. The factor which makes this oxidation process occur in environments, which are otherwise non-oxidizing, is the presence of ultraviolet light. The UV illumination increases the rate of Fe^{2+} oxidation, and the attachment of electrons to oxygen, as a result of photoemission.

Hence, the oxidation rates of Fe^{2+}-bearing silicates, ilmenite, ülvospinel, and other minerals are also expected to be high, in the presence of small amounts of atmospheric O_2 and ultraviolet light. Ferric oxide is expected to be one of the oxidation products of all of the Fe^{2+}-bearing minerals, although a laboratory experiment would have to

be carried out to determine if that is true. In addition, the rate determining step in these other minerals may not be the electron attachment to S-O. In this case, the kinetic rate equation would have a different form. Before making any estimates of the surface mineralogy, or the actual ferric oxide formation rate on Mars, the rates of ferric oxide formation from minerals other than magnetite will have to be investigated.

In the next chapter, the oxidation rate of magnetite in an environment such as that which exists on Mars today is predicted from the kinetic rate equation. Although it is not predicted accurately how much ferric oxide is in the Martian surface layer, it does indicate whether the presently described mechanism could account for the proposed degree of oxidation (Adams and McCord, 1969) of the Martian surface materials.

V. PREDICTED OXIDATION RATE IN A MARS-LIKE ENVIRONMENT

INTRODUCTION

The surface environment of Mars contains the necessary constituents for the UV-stimulated oxidation of Magnetite, and probably several other minerals as well. The atmosphere is O_2-bearing, and solar radiation penetrates to the Martian surface, attenuated only by a factor of about 1/e at a wavelength as short as .195μ. In this chapter, the Martian surface environment is described, and a simple prediction of the oxidation rate from the kinetic rate equation is made. The other factors which would affect the rate but that could not be determined explicitly in the experiment are discussed. The probable oxidation rate, with these additional considerations, is then compared with the rate required to account for the extent of oxidation that is proposed by Adams and McCord (1969) for the Martian surface layer.

This chapter is not intended to make any statements about the presence, or absence, of magnetite, or any other Fe^{2+}-bearing minerals in the Martian surface materials. It is only intended to provide an oxidation mechanism, which could be responsible for the formation of ferric oxides on the Martian surface.

THE MARTIAN SURFACE ENVIRONMENT

The reaction rate is estimated with the use of the kinetic rate equation. To do this, the total atmospheric pressure, the atmospheric O_2 partial pressure, the radiation intensity, the magnetite surface area per gram, and pH_2O/P_j must be specified.

The Total Pressure, P_T

The Martian lower atmosphere consists almost entirely of CO_2, as indicated by ground-based spectroscopic measurements (Belton and Hunten, 1966; Owen, 1966; Spinrad et al., 1966; Belton et al., 1968), the Mariner 9 IRIS detection of the 15μ CO_2 band (Hanel et al., 1972), and the UV spectrometer observations by Mariners 6,7, and 9 of the CO and O airglow (Barth et al., 1971; Barth et al., 1972). The surface pressure, P_T, of the atmosphere, as deduced from the S-band occultation experiments of Mariners 4, 6, 7, and 9 (Fjeldbo and Eshleman, 1968; Fjeldbo et al., 1970; Kliore et al., 1972), and from the ground-based observations of Belton and Hunten (1971), ranges between 1 and 10 millibars, i.e. between 1 and 13 torr.

Atmospheric O_2 Partial Pressure, pO_2

From the telescopic measurements of Traub and Carleton (1972), the O_2/CO_2 abundance ratio is 1.3×10^{-3} and,

from the discussion of Belton and Hunten (1968) on the the mixing of O_2 to the surface from the upper atmosphere, the O_2 partial pressures at the surface range between 1.7×10^{-3} torr and 1.7×10^{-2} torr, depending on P_T.

The Surface Area, Per Gram, of the Magnetite

From their comparisons of the Martian spectral reflectance curves with the laboratory curves of pulverized oxidized basalts, Adams and McCord (1969) conclude that the mean particle diameter of the darker Martian regions is between .05mm and .1mm, and for the brighter regions it is less than .05mm. Fanale and Cannon (1971) measured A_t for a similar pulverized basalt, having a mean particle diameter of .012mm, to be 5.8×10^4 $cm^2 \cdot g^{-1}$. A scanning electron micrograph of the basalt used by Fanale and Cannon (1971) indicates that there is some surface subdivision as fine as .1μ in their samples. With such extensive subdivision, the difference between the mean particle diameters of the Adams and McCord and the Fanale and Cannon basalts should result in a negligible difference between the A_t for the two basalts. If it is assumed that the magnetite has the same particle diameter and degree of surface subdivision as the rest of the Martian surface materials, A_t becomes 3×10^4 $cm^2 \cdot g^{-1}$ for the magnetite.

Adsorbed H_2O, pH_2O/P

The precipitable H_2O content of the atmosphere is on the order of 10 to 30 microns (Spinrad et al., 1963; Kaplan et al., 1964; Schorn et al., 1966), corresponding to an atmospheric H_2O/CO_2 abundance ratio, at the surface, of around 2×10^{-4}. The H_2O partial pressure ranges from about 3×10^{-4} torr at the 1 mb elevation level to about 3×10^{-3} torr at the 10 mb level. The H_2O vapor saturation pressure, P, depends on the temperature, and therefore varies across the Martian surface. The H_2O vapor saturation pressures, for which pH_2O/P falls below .05, occur for temperatures greater than 225°K, at the 1 mb elevation level, and 250°K, at the 10 mb elevation level, assuming that the photodesorption of the H_2O is negligible in the low intensity Martian radiation environment, relative to the thermal desorption rate. The temperature will vary with longitude, latitude, and elevation on Mars, and in order to determine the pH_2O/P ratio for a region on Mars, the variation of temperature across the surface must be determined.

Martian surface temperatures. Morrison et al. (1969) and Sagan and Veverka (1971) have derived expressions which are intended to give the temperature of any point on the Martian surface. These expressions are based on the telescopic 8μ to 13μ observations of Sinton and Strong

(1961). They found that the temperature of a point, located at an angle ϕ ($\phi = 0^{o}$ at midday) on the equator, could best be described with the relation,

$$T_s(0) = 197 + 104 \cos (\phi - 7^{o}). \qquad (92)$$

The observed lattitude dependence is given by them to be,

$$T_s(\lambda) = T_s(0) \cos^{\frac{1}{2}}\lambda . \qquad (93)$$

These two expressions are valid for the case when the subsolar point, S, is at the equator, i.e. the equation applies during the Vernal and Autumnal Equinoxes. At all other times during the year, the subsolar point falls on la titudes other than the equator, and it is apparent that the equations must be modified, in order to accomodate these other cases.

Assume that the subsolar point, S, is located at la titude γ. γ is positive in the Northern hemisphere, zero at the equator, and it is negative in the Southern hemisphere. When $\gamma = 0$, for which expressions (92) and (93) apply, the surface of the planet is illuminated for one half of the rotational period, P_o, at all lat itudes exclusive of the poles. When $\gamma \neq 0$, however, the daily illumination period, P, is only equal to $\frac{1}{2}P_o$ at the equator, and expressions (92) and (93) no longer apply.

Expression (93) indicates that the maximum temperature on the surface, at any hour angle, occurs at the equator, and that, with increased distance from the equator, the temperature decreases uniformly by the same amount in both the Northern and Southern hemispheres. This is only true for $\gamma = 0$, however. When $\gamma \neq 0$, the maximum temperature occurs at $\lambda = \gamma$, not at $\lambda = 0$, and the temperatures are warmer in the hemisphere that contains the subsolar point, than they are in the other hemisphere, due to the assymetry of P in the two hemispheres, about the equator.

The geometry for determining the illumination period, as a function of λ and γ, is shown in figures 19a and 19b. In figure 19a is presented the latitudinal plane of Mars, which contains a point A. The rotational axis of Mars passes through the center of this plane. The rotational period of Mars is P_o, and the illumination period is P. It can be seen in the figure, that for $-1 \leq \sin\lambda/\cos\gamma \leq 1$, $P = \pi + 2\alpha$, where $\alpha = \sin^{-1}(d/f)$. d and f can be determined as a function of λ and γ from figure 19b. In this figure is presented the longitudinal plane of Mars, which contains the subsolar point, S. From 19a and 19b, $d = e \tan\gamma$, where $e = r_o \sin\lambda$, and $f = r_o \cos\lambda$, for $-1 \leq \sin\lambda/\cos\gamma \leq 1$. Hence, for

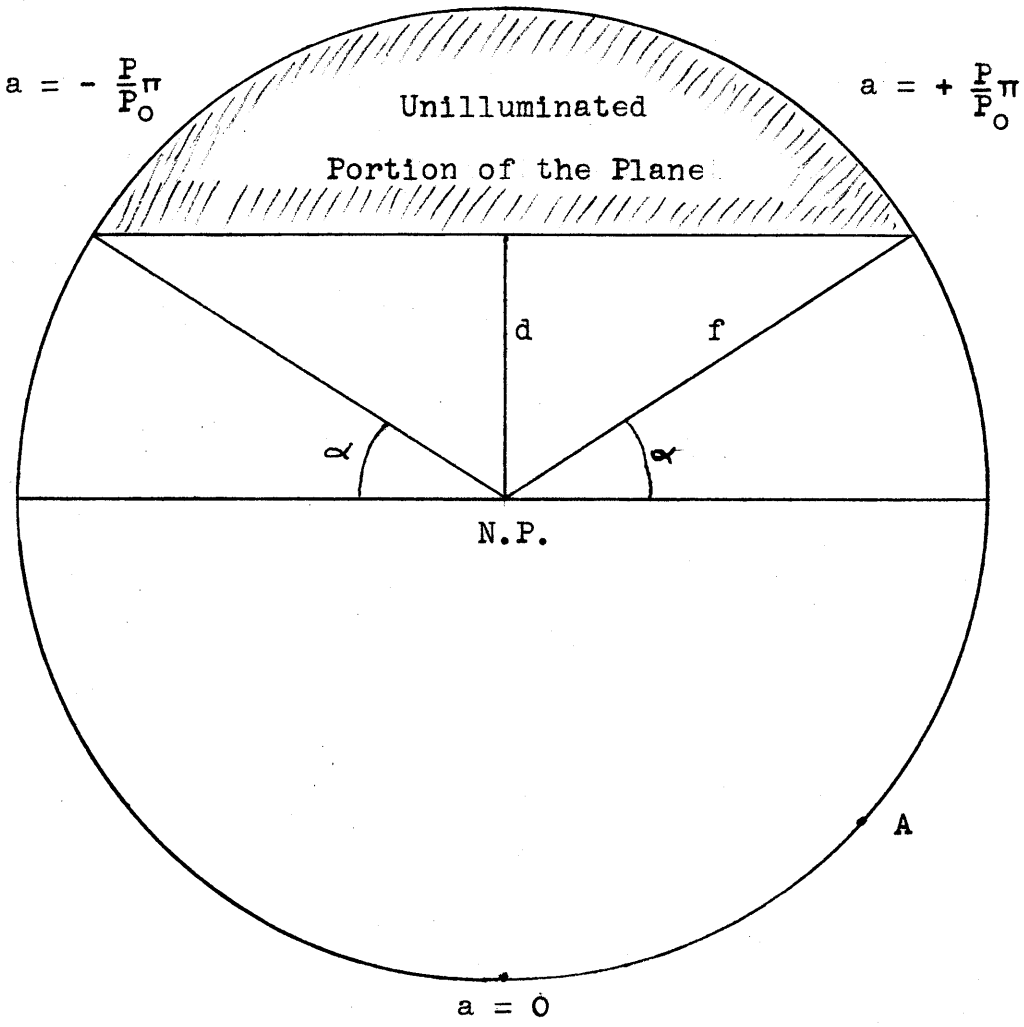

Figure 19a. The latitudinal plane of Mars, which contains point A and geometry for obtaining the illumination period, P, of Mars.

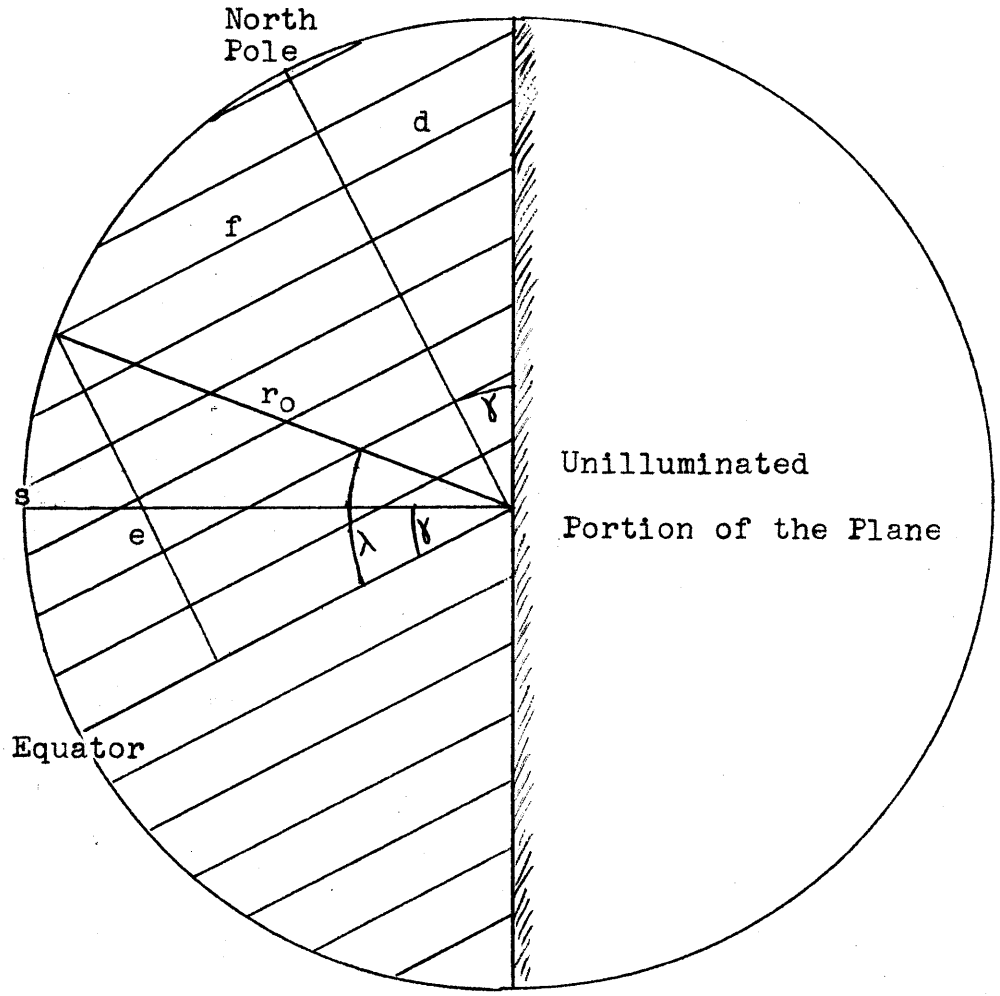

Figure 19b. The longitudinal plane of Mars, which contains the subsolar point, s, and geometry for obtaining the illumination period of Mars.

$-1 \leq \sin\lambda/\cos\gamma \leq 1, \alpha = \sin^{-1}(\tan\lambda \tan\gamma)$ and,

$$P = \pi + 2 \sin^{-1}(\tan\lambda \tan\gamma). \qquad (94)$$

For $\sin\lambda/\cos\gamma \leq -1$, $P = 0$, and for $\sin\lambda/\cos\gamma \geq 1$, $P = 2\pi$.

In figure 20 is shown the geometry for obtaining an expression for γ. Since the rotational axis of Mars is tilted at an angle of $\epsilon = 24^{o}$, with respect to a normal to the orbital plane of Mars about the Sun, the rotational axis traces out a cone, during one period of revolution about the Sun, Ω_o. In figure 20, this cone is shown. In this figure, the apex of the cone is the South Pole, ϵ is the inclination of the rotational axis to a normal to the orbital plane (the normal to the orbital plane is the axis of the cone), and the base of the cone is circumscribed by the trace of the North Pole during Ω_o. The length of the cone edge (and axis) is the diameter, d_o, of Mars. The Vernal Equinox is chosen as the origin of the trace of the North Pole. After Ω days into the orbit, the North Pole will have moved an arc distance of $\delta = (\Omega/\Omega_o) \times 2\pi$ radians. From the figure,

$$\gamma = \sin^{-1}\left[.407 \sin (2\pi\Omega/\Omega_o) \right], \qquad (95)$$

where $.407 = \sin\epsilon$. γ is zero at the Vernal Equinox,

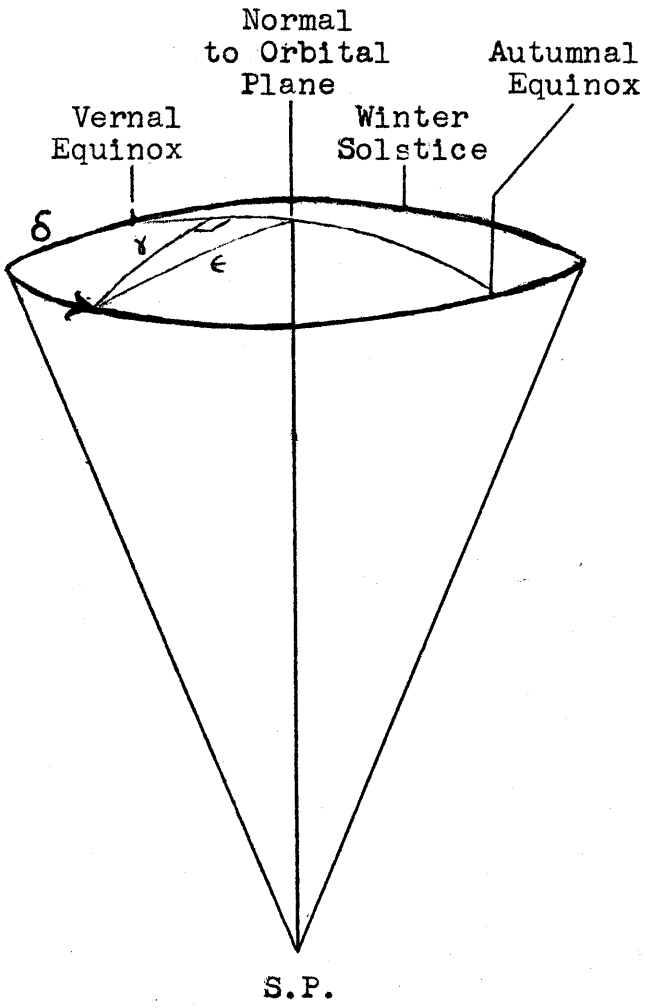

Figure 20. The cone, which is traced out by the planet's rotational axis, with respect to a normal to the orbital plane of Mars, during one period of revolution about the Sun.

increases to $+24^{o}$, at the Summer Solstice, passes through 0^{o}, at the Autumnal Equinox, extends to -24^{o}, at the Winter Solstice, and returns to 0^{o}, at the Vernal Equinox, over an orbital period of Ω_{o}.

From figure 19a, it can be seen that at γ, the lat i-tude which contains the subsolar point, the daily illumination period, P, is longer than it is at the equator, for $\gamma \neq 0$. As a result, the surface becomes illuminated earlier, and remains illuminated longer, than it does at the equator, while at γ, the maximum temperature is assumed to be the value specified in equation (92) for $\phi = 7^{o}$. Further, the phase lag factor of 7^{o} in the equation is applied to $\lambda = \gamma$. Finally, equations (92) and (93) apply to the average surface elevation. If it is assumed that the average surface elevation is at the 5 mb pressure level, an expression to describe the temperature at a point on the surface is,

$$T_{s}(\lambda,\gamma, P) = \left\{197 + 104 \cos\left[(P_{o}\,\phi/2P) - 7^{o}\right]\right\}\cos^{\frac{1}{2}}(\lambda-\gamma) + \Delta T(P_{r}), \qquad (96)$$

where P is the daily illumination period, for a specified set of values for λ and γ, and $\Delta T(P_{r})$ is the variation in temperature, due to changes in elevation. From the Mariner 9 Infrared Spectroscopy Experiment (Hanel et al.,

1972), the thermal lapse rate over the South polar region is -3.8°K/mb, from 10 mb to 2 mb, and +1.0°K/mb from 2 mb to 1 mb. Equation (96) is only valid for $-1 < \sin\lambda/\cos\gamma$.

If it is assumed that the principal factor controlling the steady state adsorption of H_2O on the surface is the temperature, then the oxidation process could only occur when $pH_2O/P \geq .05$. From equation (96), and using the Mariner 9 lapse rate, $\Delta T(P)$, the latitudes over which the oxidation can occur, i.e. the latitudes for which pH_2O/P falls below .05 for a portion of the year, can be determined. To determine this, the warmest hour of the day ($P_o \phi / 2P = 7^o$), at the Summer Solstice ($\gamma = 24^o$), is chosen, and the latitude is found, for which $pH_2O/P = .05$. At the 1 mb elevation level, $pH_2O/P = .05$ at $T = 225^oK$ (Dushman and Lafferty, 1966, p.469; Weast, 1969, p.D-108; Fanale and Cannon, 1971). From the Mariner 9 lapse rate, $\Delta T(1\ mb) = -10^oK$. Hence, at the 1 mb elevation level, oxidation will not occur poleward of $\pm 83^o$. At the 10 mb elevation level, pH_2O/P is always less than .05, at latitudes poleward of $\pm 77^o$ ($pH_2O/P = .05$ at 250^oK, and $\Delta T(P) = +19^oK$).

Hence, the oxidation process can proceed only within the approximate latitude range, $-80^o \leq \lambda \leq 80^o$. Further, the oxidation can occur within this latitude range, only

when the solar radiation has heated the surface above the temperature for which $pH_2O/P = .05$. From expression (96), the oxidation will begin when the hour angle reaches a minimum value of,

$$\phi_{min} = \frac{2P}{P_o}\left\{ 7^o - \cos^{-1}\left[\frac{T(P_T)_{min}}{104^oK \cos^{-\frac{1}{2}}(\lambda-\gamma)}\right] - 1.9\right\}, \quad (97)$$

and a maximum value of,

$$\phi_{max} = \frac{2P}{P_o}\left\{ 7^o + \cos^{-1}\left[\frac{T(P_T)_{min}}{104^oK \cos^{-\frac{1}{2}}(\lambda-\gamma)}\right] - 1.9\right\}. \quad (98)$$

In these equations, $T(P_T)_{min}$ is the temperature, due to insolation, which will result in a surface temperature, for which $pH_2O/P = .05$. It is calculated by subtracting from the temperature, for which $pH_2O/P = .05$, the temperature change, $\Delta T(P_T)$, induced by the difference in elevation of the region from the 5 mb level. For example, at the 3 mb elevation level, $pH_2O/P = .05$ at 238^oK. However, the 3 mb region is 8^oK cooler than the 5mb elevation level, with the same amount of insolation. Therefore, the solar radiation must heat the region to a temperature, which is 8^oK higher than that needed to heat a 5 mb level region, in order for $pH_2O/P = .05$, i.e. $T(\lambda, P_T)_{min}$ is 246^oK, for

3 mb regions.

Radiation Intensity, $\mathbb{I}_{.350}$

Since the atmosphere is composed almost entirely of CO_2, at pressures ranging from 1 torr to 13 torr, the solar radiation intensity, at the surface, is reduced by a factor of 1/e from the intensity outside the atmosphere, at a wavelength of .195μ (Thompson et al., 1963). The relative solar spectral radiation intensity distribution is shown in figure 16, with the absolute solar flux, at .350μ, equal to 9×10^{11} photons-cm^{-2}-sec^{-1}-$\mathring{A}^{-1}$ (Allen, 1955, p. 172). In this figure, the solar flux, at .350μ, is not scaled to 1.0. It is set equal to the intensity of the laboratory source at .200μ. Hence, in order to translate the incident solar flux into a value for $\mathbb{I}_{.350}$, the solar intensity at .350μ must be divided by a factor of 2.2.

Hence, $\mathbb{I}_{.350}$, at the subsolar point on the Martian surface, is 4.2×10^{11} photons$\cdot$cm$^{-2}\cdot$sec$^{-1}\cdot\mathring{A}^{-1}$. The solar flux at a point, A, located at an arc distance, ρ, away from the subsolar point, s, will have an intensity, at .350μ, of,

$$\mathbb{I}_{.350,\rho} = \mathbb{I}_{.350,s}\cos\rho \,. \qquad (99)$$

The geometry for obtaining an expression for ρ, in terms of the known parameters λ, γ, and ϕ, is given in figure 21.

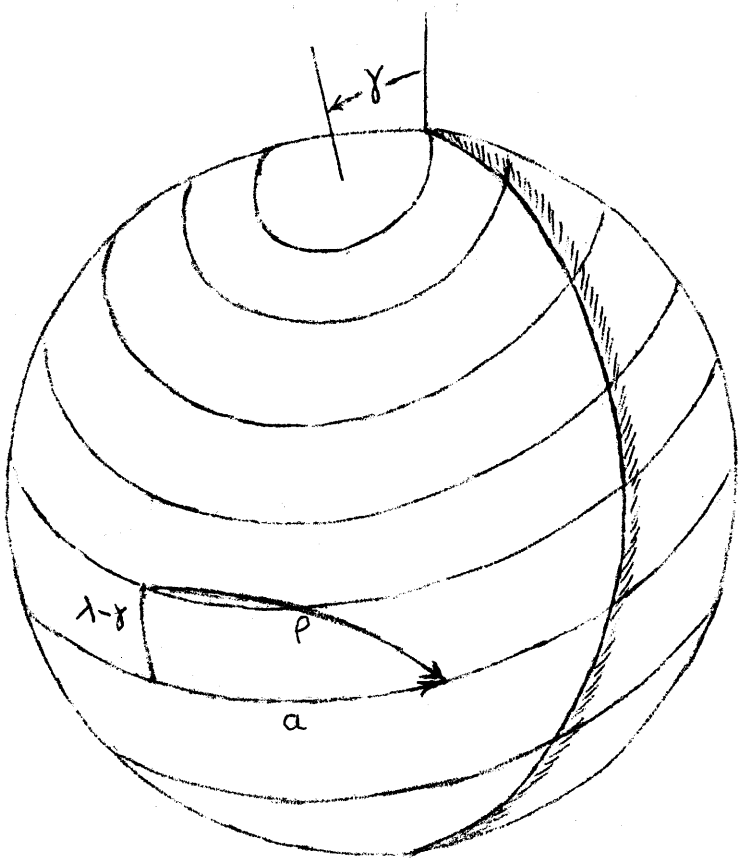

Figure 21. The geometry for obtaining an expression for ρ.

From this figure,

$$\tan\left(\frac{|\phi| - \lambda + \gamma}{2}\right) / \tan\left(\rho/2\right) = \sin\left(\frac{|\phi| - \lambda + \gamma}{2}\right) / \cos\left(\frac{|\phi| + \lambda - \gamma}{2}\right),$$

or,

$$\rho = 2 \tan^{-1}\left[\sin\left(\frac{|\phi|}{2} + \frac{\lambda - \gamma}{2}\right) / \cos\left(\frac{|\phi|}{2} - \frac{\lambda - \gamma}{2}\right)\right]. \quad (100)$$

To obtain a value of $\mathbb{I}_{.350}$, for use in the kinetic rate equation, the daily average of $|\phi|$ can be determined, and substituted into the expression for ρ, and then $\cos\rho$ can be averaged over an orbital period, with respect to γ. During a single rotational period, the oxidation occurs for only $(\phi_{max} - \phi_{min})/ 2\pi$ of that period, centered around $\phi = 0^{o}$. From equations (97) and (98), the average daily value of $|\phi|$ is

$$|\phi|_{av} = (\phi_{max} - \phi_{min}) / 2\pi = \frac{2P}{\pi P_o} \cos^{-1}\left[\left(\frac{T(P_T)_{min}}{104^{o}K \cos^{-\frac{1}{2}}(\lambda-\gamma)}\right) - 1.9\right], \quad (101)$$

where,

$$P = \begin{cases} 0 \; ; \; \sin\lambda / \cos\gamma \leq -1 \\ \pi + 2 \sin^{-1}(\tan\lambda \tan\gamma); \; -1 \leq \sin\lambda/\cos\gamma \leq 1, \\ 2 \; ; \; \sin\lambda / \cos\gamma \geq 1 \end{cases} \quad (96)$$

and $T(P_T)_{min}$ is equal to the temperature, for which pH_2O/P is equal to .05, minus the temperature change, $\Delta T(P_T)$, arising from the elevation difference from the 5 mb level. The average yearly value of $\mathbb{I}_{.350}$, for a point at latitude λ, and at the elevation level, corresponding to P_T, is,

$$\mathbb{I}_{.350,av}(\lambda,P_T) = \mathbb{I}_{.350,s} \cdot \frac{1}{48^o} \int_{\gamma=-24^o}^{\gamma=24^o} \cos\left(|\phi|_{av}, \lambda, \gamma \right) d\gamma . \quad (102)$$

At the equator, a point, at the 5 mb elevation level would have a yearly average radiation intensity of $\mathbb{I}_{.350,av}(0,5) = 3.9 \times 10^{11}$ photons $\cdot cm^{-2} \cdot sec^{-1} \cdot \mathring{A}^{-1}$. Some other average radiation intensities over the surface include: $\mathbb{I}_{.350,av}(\pm 30, 5) = 2.8 \times 10^{11}$; $\mathbb{I}_{.350,av}(\pm 60,5) = 1.6 \times 10^{11}$; $\mathbb{I}_{.350,av}(\pm 75, 5) = 1.4 \times 10^{11}$, all at the 5 mb pressure level.

During a single rotational period, the oxidation occurs during only $(\phi_{max} - \phi_{min}) / 2\pi$ of the day, as mentioned earlier. Averaged over the year, the oxidation therefore only occurs during a fraction, $f(\lambda,P_T)$, of the year, where,

$$f(\lambda,P_T) = \frac{1}{48} \int_{\gamma=-24}^{+24} (\phi_{max} - \phi_{min}) / 2\pi \; d\gamma , \quad (103)$$

and therefore, the rate of oxidation is $f(\lambda,P_T)$ times the

oxidation rate, derived by using $\mathbb{D}_{.350,av}(\lambda,P_T)$ in the kinetic rate equation (13b). Several values of $f(\lambda,P_T)$, across the surface, are: $f(0,5) = .44$, $f(\pm30,5) = .42$, $f(\pm60,5) = .13$, and $f(\pm75,5) = .10$, all at the 5 mb elevation level.

CONCLUSION: OXIDATION RATE ON MARS

If any magnetite is on the surface of Mars, it can be assumed to have been previously exposed to the oxidizing environment, and, therefore, to have had formed on it at least a small amount of ferric oxide. The oxidation rate can therefore be determined through the use of equation (13b). Equation (13b) gives the time, Δt_o, required to accumulate a 1 micron thick layer of ferric oxide on the surface of a pure magnetite sample. The rate of formation of this layer is given by $(\Delta t_o)^{-1}$, in microns per minute. The thickness of a layer of the ferric oxide, accumulated over a period of 10^9 years of exposure, the assumed age of the Martian environment and surface, is (10^9years/Δt_o) in microns. $\Delta t_o(\lambda,P_T)$ for a λ,P_T region on Mars is calculated by using the pO_2, P_T, A_t, and $\mathbb{D}_{.350,av}(\lambda,P_T)$ values for that region in equation (13b), and dividing by $f(\lambda,P_T)$, defined in equation (103). Δt_o, in equation (13b), is in minutes, and a conversion to years must be

made. Substituting the vaues for P_T, pO_2, A_t, and $\mathfrak{T}_{.350,av}(\lambda, P_T)$ into Δt_o, dividing by $f(\lambda, P_T)$, and converting to years: $\Delta t_o(0,2) = 4.0 \times 10^4$ years, $\Delta t_o(\pm 30, 5) = 2.6 \times 10^5$ years, $\Delta t_o(0,5) = 1.5 \times 10^5$ years, $\Delta t_o(\pm 60,5) = 2.0 \times 10^6$ years, and $\Delta t_o(\pm 75,5) = 3.1 \times 10^6$ years. Hence, at the average 5 mb elevation level, the average $\Delta t_o(\lambda, 5)$ value, within the latitude range $-45^\circ < \lambda < 45^\circ$, is 10^5 years. From $\lambda = 45^\circ$ to 80° (and -45° to -80°), the average $\Delta t_o(\lambda, 5)$ value is around 10^6 years. Poleward of $\pm 80^\circ$, the oxidation rate can be assumed to be negligible. If it is assumed that all the magnetite was oxidized at the 5 mb level, the average thickness of a layer of all of the ferric oxide, accumulated over a period of 10^9 years, and distributed uniformly over the surface, would be .1 cm and 1 cm. From the experiment of Adams and McCord (1969), the average weight percent of ferric oxide in the basalts, which could account for the reflectance properties of the Martian surface, is approximately 3% (more in the brighter areas, and less in the darker regions). Then, the thickness of a uniform layer of oxidized basalt, covering the surface of Mars, composed of 3 weight percent ferric oxide, would be on the order of 2 cm to 20 cm.

This estimate neglects the fact that, on Mars, aeolean

erosion would remove the ferric oxide as rapidly as it is formed. Abrasion could even prevent the complete formation of the rapidly formed first stage protective oxide layer. As a result, the oxidation rate would be increased significantly.

On Mars, H_2O is adsorbed on the grain surfaces during a portion, $1 - \left[(a_{max} - a_{min}) / 2\pi \right]$, of every day. This is followed by desorption and oxidation of surface cations, including those leached from the grain interior by H_2O. In the laboratory experiment, the H_2O was adsorbed to the grain surfaces , and cations were brought to the surfaces from the interior, only at the onset of irradiation. As a result, there would be significantly more cations available for oxidation on the grain surfaces in the Martian environment, during the Δt_o interval, than there are on the laboratory grain surfaces, during the Δt_o interval.

In addition, the estimate assumes that the oxidation occurs at the 5 mb elevation level. From the Belton and Hunten study (1971), approximately 55 percent of the Mars surface regions are above the 5 mb elevation level. These high elevation regions have Δt_o values that average between one and two orders of magnitude smaller than the Δt_o values at and below the 5 mb elevation level.

Another factor which would also increase the estimated amount of ferric oxide produced in the Martian environment is the presence of photoelectron-producing cations other than iron. If these cations have lower work functions, the quantum yield (photoelectrons emitted per incident photon) would be increased at every wavelength, and additional wavelengths would be photoelectron-producers. For example, if ilmenite or Ülvospinel were present in the Martian surface materials, in addition to (or instead of) magnetite, the photoelectric work function would be reduced by between .2 eV and .8 eV (Eastman, 1970; Wilson, 1966; Burshtein and Shurmovskaya, 1964). The photoelectric yield would range from about 10^{-7}, at between 3.0 and 3.6 eV, depending on the work function, to around 10^{-3} to 10^{-2}, at 5.2 eV to 5.6 eV (Sommer and Spicer, 1965). This would result in a one to two order of magnitude increase in the steady state electron concentration at the surface of the crystal (see figure 16). Since the rate of the rate determining step, viz. electron attachment to adsorbed O, is proportional to the steady state electron concentration, the reaction rate , with ilmenite or Ülvospinel in the Martian surface materials, could be between one or two orders of magnitude more rapid.

The principal factors,which would decrease the amount of ferric oxide formed on the surface, are those which would limit the amount of available unoxidized material to the oxidizing environment. Such factors would include shadowing, and burial by oxidized sediments. However, impact gardening and aeolean transport would probably counteract a large portion of these effects (cf. Sagan et al., 1971).

Hence, the oxidation rate on Mars should be several orders of magnitude higher than the rate predicted by the kinetic rate equation. Instead of there being an equivalent layer of oxidized basalt on the order of only 10 cm thick, as predicted by the kinetic rate equation, the equivalent layer could be on the order of tens to hundreds of meters thick, or more. It is not the purpose of this work to determine the amount of ferric oxide on Mars, however. It is, rather, the purpose of this work to provide a mechanism which could oxidize basalts in the Martian environment. Such a mechanism has been provided, but the actual extent of oxidation on Mars can not be determined from this study alone.

Finally, it should be mentioned that the high frequency alternation between periods of H_2O adsorption and oxidation, during the Δt_o period on Mars, should not only drastically

decrease Δt_o on Mars, but it should also lead to the formation of goethite and limonite. Adsorption of H_2O to the hematite grain surfaces results in the formation of $Fe(O,OH)_6$ octahedra on the surfaces of the oxidation product. The rapid alteration between intervals of adsorption and oxidation, during the formation and accumulation of the oxidation product, could result in α-FeOOH, goethite. Similarly, if adsorbed H_2O molecules become trapped in the structure, during accumulation, limonite, α-$FeOOH \cdot nH_2O$, could result. The stabilization of goethite and limonite in the Martian environment is discussed by Fish (1966), Schmalz (1959), and O'Connor (1968a).

The UV-stimulated oxidation of minerals other than magnetite could lead to the formation of other hydrated oxidized minerals, such as boehmite, AlOOH, on Mars. The formation of hydrated minerals on Mars is still a spectulation, however. Further laboratory study is required, before any estimates of the surface mineralogy of Mars can be made.

VI. SUMMARY

It has been discovered that magnetite (Fe_3O_4) is rapidly oxidized to hematite (α-Fe_2O_3), upon illumination ($\lambda < .310\mu$) in an O_2-bearing atmosphere. A laboratory investigation has been carried out to determine the kinetics and mechanism of this rapid oxidation process. It has been found that the process consists of a series of reactions which are common to most oxidation mechanisms: (1) Atmospheric O_2 dissociates, on the surface, into two adsorbed O atoms, upon colliding with a pair of adjacent vacant adsorption sites; (2) This step is followed by the oxidation of Fe(II) cations to Fe(III) cations, simultaneously with the electron attachment to the adsorbed O atoms, to form adsorbed O^-; (3) Step (2) is followed by the rapid attachment of a second electron to the adsorbed O^-, to form chemisorbed O^{2-}; (4) Finally, the chemisorbed O^{2-} ions are incorporated into the Magnetite surface layer, forming hematite scales.

This process leads to the formation of a surface coating on the magnetite grains, which protects the magnetite from further oxidation. The presence of adsorbed H_2O at the onset of the exposure interval, however, disrupts the protective properties of this first-stage oxide layer, and the oxidation process proceeds. The

H_2O leaches cations from the magnetite substrate and brings them to the surface of the previously formed ferric oxide layer, where they can be oxidized and incorporated into the formation of a hematite crystallite in the magnetite surface layer. Since the hematite has a different spatial configuration than the magnetite layer within which it has been formed, the atoms at the hematite / magnetite interface are displaced from their normal positions. These displacements disrupt the protective properties of the protective oxide layer at the interface, and the oxidation process can proceed, in the absence of adsorbed H_2O. This "nucleation-disruption" of the protective properties of the first-stage oxide layer at the interface of the hematite nucleus and the surrounding magnetite allows the crystallite to grow radially away from the center of disruption. The atomic displacements increase with increased distance from the center of the nucleus until the displacement equals the interatomic distance of the magnetite. At this point a rupture in the continuity of the surface layer occurs, and hematite scales are formed. The leaching of cations during the formation of the hematite nuclei could lead to the formation of vacancy-disordered maghemite.

The factor which allows this oxidation process to

proceed in a low-temperature, low-O_2 partial pressure, water-free, otherwise nonoxidizing environment, is the presence of ultraviolet light. The UV illumination gives rise to photoemission, which increases the rates of Fe(II) oxidation, and the attachment of the electrons to the adsorbed oxygen. The slowest step in the oxidation mechanism, and therefore the rate determining step, is the attachment of an electron to adsorbed O.

Finally, it has been demonstrated that this oxidation mechanism could occur in the present-day Martian surface environment. It would occur at a rate which is sufficiently fast to account for the extent of oxidation of the Martian surface that has been proposed in the oxidized basalt model of Adams and McCord (1969). The actual rate of ferric oxide formation on Mars has not been determined, however, because many of the parameters which would affect the rate in the Martian environment, were not investigated in this experiment. Among the problems which much be solved before any estimates of the rate of ferric oxide formation on Mars can be made, include the effects of the rapid alternations between H_2O adsorption and oxidation intervals, the effects of aeolean abrasion, and the ferric oxide formation rates of other Fe(II)-bearing minerals. In addition,

the formation of goethite and limonite, as well as some of the clay minerals, need to be investigated in Martian-like environments. Oxidation of minerals, which contain cations in oxidation states that are not at their most oxidized natural state, is also likely, upon illumination in an O_2-bearing atmosphere. The kinetics and mechanisms of the photo-stimulated oxidation of these minerals must also be investigated.

Since the Earth's surface environment contains the necessary constituents for the photo-stimulated oxidation of magnetite, and probably other Fe(II)-bearing minerals, a series of investigations into the role of this process in "desert weathering", weathering during the early history of the Earth, and present-day ecological problems, would also prove interesting.

REFERENCES

Adamcik, J.A., "The Water Vapor Content of the Martian Atmosphere as a Problem of Chemical Equilibrium," Planet. Space Sci., 11, 355-358, 1963.

Adams, J.B., "Lunar and Martian Surfaces: Petrologic Significance of Absorption Bands in the Near-Infrared," Science, 159, 1453-1455, 1968.

Adams, J.B., and T.B. McCord, "Mars: Interpretation of Spectral Reflectivity of Light and Dark Regions," J. Geophys. Res., 74, 4851-4856, 1969.

Ahanori, A., E.H. Frei, and M. Schieber, "Some Properties of γ-Fe_2O_3 Obtained by Hydrogen Reduction of α-Fe_2O_3," J. Phys. Chem. Solids, 23, 545, 1962.

Allen, C.W., Astrophysical Quantities, Anthlone Press, London, 172, 1955.

Arkharov, V.I., "Mechanism of the Nucleation of Crystals of New Phases Resulting from Chemical Reactions in Solids, in Surface Interactions Between Metals and Gases, Edited by V.I. Arkharov and K.M. Gorbanova, Consultants Bureau, N.Y., 81-83, 1966.

Baily, P.C., "Absorption and Reflectivity Measurements On Some Rare Earth Iron Garnets and α-Fe_2O_3," J. Appl. Phys., 31, 39S-40S, 1960.

Balberg, I., and J.I. Pankove, "Optical Measurements On Magnetite Single Crystals," Phys. Rev. Letters, 27, 596-599, 1971a.

Balberg, I., and J.I. Pankove, "Cathodoluminescence of Magnetite," Phys. Rev. Letters, 27, 1371-1374, 1961.

Bando, Y., M. Kiyama, T. Takada, and S. Kachi, "The Effect of Particle Size of γ-Fe_2O_3 On the Transformation From γ-Form to α-Form," Japan J. Appl. Phys., 4, 240-241, 1965.

Bari, R.A., D. Adler, and R.V. Lange, "Electrical Conductivity in Narrow Energy Bands," Phys. Rev., B2, 2898-2905, 1970.

Barth, C.A., C.W. Hord, J.B. Pearce, K.K. Kelley, G.P. Anderson, and A.I. Stewart, "Mariner 6 and 7 Ultraviolet Spectrometer Experiment: Upper Atmosphere Data," J. Geophys. Res., 76, 2213-2227, 1971.

Barth, C.A., C.W. Hord, and A.I. Stewart, and A.L. Lane, "Mariner 9 Ultraviolet Spectrometer Experiment:

Initial Results," Science, 175, 309-312, 1972.

Basolo, F., and R.G. Pearson, Mechanisms of Inorganic Reactions, J. Wiley and Sons, N.Y., 1958.

Bauminger, R., S.G. Cohen, A. Marinov, S. Ofer, and E. Segal, "Study of the Low-Temperature Transition in Magnetite and the Internal Fields Acting on Iron Nuclei in Some Spinel Ferrites, Using Mössbauer Absorption," Phys. Rev., 122, 1447-1450, 1961.

Belton, M.J.S., and D.M. Hunten, "The Abundance and Temperature of CO_2 in the Martian Atmosphere," Astrophys. J., 145, 454, 1966.

Belton, M.J.S., A.L. Broadfoot, and D.M. Hunten, "Abundance and Temperature of CO_2 on Mars During the 1967 Opposition," J. Geophys. Res., 73, 4795-4806, 1968.

Belton, M.J.S., and D.M. Hunten, "The Distribution of CO_2 on Mars: A Spectroscopic Determination of Surface Topography," Icarus, 15, 204-232, 1971.

Binder, A.B., and D.P. Cruikshank, "Comparison of the Infrared Spectrum of Mars With the Spectra of Selected Terrestrial Rocks and Minerals," Comm. Lunar Plan. Lab. Univ. Arizona, 2, 193-196, 1964.

Binder, A.B., and D.P. Cruikshank, "Lithological and Mineralogical Investigation of the Surface of Mars," Icarus, 5, 521-525, 1966.

Blyholder, G., and E.A. Richardson, "Infrared and Volumetric Data on the Adsorption of Ammonia, Water, and Other Gases on Activated Iron (III) Oxide," J. Phys. Chem., 66,2597-2602, 1962.

Blyholder, G., and E.A. Richardson, "Infrared Spectral Observation of Surface States," J. Phys. Chem., 68, 3882-3884, 1964.

Bonnelle, C., "Contribution a l'Étude des Métaux de Transition du Premier Groupe, du Cuivre et de Leurs Oxydes par Spectroscopie X dans le Domaine de 13 à 22Å," Ann. Phys., I, 439-481, 1966.

Branscomb, L.M., "A Review of Photodetachment and Related Negative Ion Processes Relevant to Aeronomy," Ann. de Geophysique, 20, 88-105, 1964.

Braun, A., "A Superstructure in Spinels," Nature, 170, 1123, 1952.

Brunauer, S., "The Use of Low Temperature van der Walls Adsorption Isotherms in Determining the Surface Area of Synthetic Iron Ammonia Catalysts," J. Amer. Chem. Soc., 59, 1553-1564, 1937.

Brunauer, S., The Adsorption of Gases and Vapors, Vol. 1, Physical Adsorption, Princeton Univ. Press, N.J., 320, 1945.

Burch, D.S., and R. Geballe, "Ionic Drift Velocities and Electron Attachment Coefficients in Oxygen," Phys. Rev., 106, 183-187, 1957.

Burch, D.S., and R. Geballe, "Clustering of Negative Ions in Oxygen," Phys. Rev., 106, 188-190, 1957.

Burns, R.G., "Origin of Optical Pleochroism in Orthopyroxenes," Mineral. Mag., 35, 715-719, 1966.

Burns, R.G., Mineralogical Applications of Crystal Field Theory, Cambridge Univ. Press, London, 1970.

Burshtein, R.Kh., L.A. Larin, and S.I. Sergeev, "Effect of Oxygen and Water Vapor on the Surface Properties of Germanium and Silicon," in Surface Properties of Semiconductors, Edited by A.N. Frumkin, Consultants Bureau, N.Y., 20-33, 1964.

Burshtein, R.Kh., and N.A. Shurmovoskaya, "The Effect of Electro-Negative Gases on the Work Function of a Metal," Surface Science, 2, 210-216, 1964.

Chanin, L.M., A.V. Phelps, and M.A. Biondi, "Measurement of the Attachment of Slow Electrons in Oxygen," Phys. Rev. Letters, 2, 344-346, 1959.

Collins, F.C., and T. Nakayama, "Transport Processes in the Thermal Growth of Metal and Semiconductor Oxide Films," J. Electrochem. Soc., 114, 167-171, 1967.

Colombo, U., F.Gazzarrini, G. Lanzavecchia, and G. Sironi, "Magnetite Oxidation: A Proposed Mechanism," Science, 147, 1033, 1965.

Daniels, J.M., and A. Rosencwaig, "Mossbauer Spectroscopy of Stoichiometric and Nonstoichiometric Magnetite," J. Phys. Chem. Solids, 30, 1561-1571, 1969.

David, I., and A.J.E. Welch, "The Oxidation of Magnetite and Related Spinels. Constitution of Gamma Ferric Oxide," Trans. Faraday Soc., 52, 1642-1650, 1956.

Ditchburn, R.W., and P.A. Young, "The Absorption of Molecular Oxygen Between 1850 and 2580 Å," J. Atmos. Terr. Phys., 24, 127, 1962.

Dollfus, A.,"Etude des Planetes par la Polarisation de Leur Lumiere," Ann. Astrophys., Suppl. 4, 1957.

Dollfus, A., "Polarization Studies of Planets, in Planets and Satellites, Edited by G.P. Kuiper and B.M. Middlehurst, Univ. of Chicago Press, Ill., 1961.

Draper, A.L., J.A. Adamcik, and E.K. Gibson, "Comparison of the Spectra of Mars and a Goethite-Hematite Mixture in the 1 to 2 Micron Region," Icarus, 3, 63-65, 1964.

Dushman, S.,and J.M. Lafferty, Scientific Foundations of Vacuum Technique, J. Wiley and Sons, N.Y., 422, 1966.

Eastman, D.E., "Photoelectric Work Function of Transition, Rare-Earth, and Noble Metals," Phys. Rev., B2, 1-2, 1970.

Elder, T., "Particle Size Effect in Oxidation of Natural Magnetite," J. Appl. Phys., 36, 1012-1013, 1965.

Evans, U.R., "The Mechanism of Oxidation and Tarnishing," Trans. Electrochem. Soc., 91, 547-572, 1947.

Fanale, F.P., and W.A. Cannon, "Adsorption on the Martian Regolith," Nature, 230, 502-504, 1971.

Faye, G.H., P.G. Manning, and E.H. Nickel, "The Polarized Optical Absorption Spectra of Tourmaline, Cordierite, Chloritoid, and Vivianite: Ferrous-Ferric Electronic Interaction as a Source of Pleochroism," Amer. Min., 53, 1174-1201, 1968.

Feitknecht, W., "Oxidation of Small Particles of Iron and Fe_3O_4," in Processus de Nucleation dans les Reactions des Gaz sur les Metaux et Problemes Connexes, Paris, 121-126, 1966.

Fish, F.F., " The Stability of Goethite on Mars," J. Geophys. Res., 71, 3063-3068, 1966.

Fjeldbo, G., and Von R. Eshleman, "The Atmosphere of Mars Analyzed by Integral Inversion of the Mariner IV Occultation Data," Planet. Space Sci., 16, 1035-1059, 1968.

Fjeldbo, G., A.J. Kliore, and B.L. Seidel, "The Martian 1969 Occultation Measurements of the Upper Atmosphere of Mars," Radio Science, 5, 381, 1970.

Francombe, M.H., and H.P. Rooksby, "Structure Transformation Effected by the Dehydration of Diaspore, Goethite, and Delta Ferric Oxide," Clay Min. Bull., 4, 1-14, 1959.

Freier, S., M. Greenshpan, P. Hillman, and H. Shechter, "The Antiferromagnetic Curie Point in α-Fe_2O_3," Phys. Letters, 2, 191-192, 1962.

Fromhold, A.T., "Kinetics of Oxide Film Growth on Metal Crystals - I. Formulation and Numerical Solutions," J. Phys. Chem. Solids, 24, 1081-1092, 1963a.

Fromhold, A.T., "Kinetics of Oxide Film Growth on Metal Crystals - II. Homogeneous Field Approximations," J. Phys. Chem. Solids, 24, 1309-1323, 1963b.

Gallagher, P.K., J.B. MacChesney, and D.W. Buchanan, "Mössbauer Effect in the System $SrFeO_{2.5-3.0}$," J. Chem. Phys., 41, 2429-2434, 1964.

Gardner, R.F.G., F. Sweett, and D.W. Tanner, "The Electrical Properties of Alpha Ferric Oxide - II. Ferric Oxide of High Purity," J. Phys. Chem. Solids, 24, 1183-1196, 1963.

Goodenough, J.B., "Metallic Oxides, " Prog. in Solid State Chem., 5, 145-399, 1971.

Grimley, T.B., and B.M.W. Trapnell, "The Gas/Oxide Interface and the Oxidation of Metals," Proc. Roy. Soc., A234, 405-418, 1956.

Gulbransen, E.A., and W.S. Wysong, "Thin Oxide Films on Aluminum," J. Phys. Chem., 51, 1087-1103, 1947.

Hanel, R.A., B.J. Conrath, W.A. Hovis, V.G. Kunde, P.D. Lowman, J.C. Pearl, C. Prabhakara, B. Schlachman, and G.V. Levin, "Infrared Spectroscopy Experiment on the Mariner 9 Mission: Preliminary Results," Science, 175, 305-309, 1972.

Heikes, R.R., and W.D. Johnston, "Mechanism of Conduction in Li-Substituted Transition Metal Oxides," J. Chem. Phys., 26, 582-587, 1957.

Henry, R.J.W., P.G. Burke, and A.L. Sinfailam, "Scattering of Electrons by C, N, O, N^+, O^+, and O^{++}," Phys. Rev., 178, 218-225, 1969.

Inn, E.C.Y., and Y. Tanaka, "Ozone Absorption Coefficients in the Visible and Ultraviolet Regions," in Ozone Chemistry and Technology, Advances in Chemistry Series, 21, American Chemical Society, Washington, D.C., 263, 1959.

Johnson, H.P., and R.T. Merrill, "Magnetic and Mineralogical Changes Associated With Low-Temperature Oxidation of Magnetite," J. Geophys. Res., 77, 334-341, 1972.

Kachi, S., K. Momiyama, and S. Shimizu, "An Electron Diffraction Study and a Theory of the Transformation from γ-Fe_2O_3 to α-Fe_2O_3," J. Phys. Soc. Japan, 18, 106-116, 1963.

Kaplan, L.D., G. Münch, and H. Spinrad, "An Analysis of the Spectrum of Mars," Astrophys. J., 139, 1-15, 1964.

Kaufman, F., "Reactions of Oxygen Atoms," in Progress in Reaction Kinetics, Edited by G. Porter, Pergamon Press, N.Y., 1961.

Kaufman, F., "Neutral Reactions," in DASA Reaction Rate Handbook, Defence Atomic Support Agency, Washington, 1967.

Khare, B., M. Khare, and C. Sagan, "Laboratory Studies of Carbon Suboxide: Possible Planetary Significance," Paper Given at 2nd Ann. Meeting of Amer. Astron. Soc., Div. Plan. Sci., 20 March - 24 March, Kona, Hawaii, 1972.

Kliore, A.J., D.L. Cain, G. Fjeldbo, B.L. Seidel, and S.I. Rasool, "Mariner 9 S-Band Martian Occultation Experiment: Initial Results on the Atmosphere and Topography of Mars," Science, 175, 313-317, 1972.

Langmuir, I. "The Adsorption of Gases on Plane Surfaces of Glass, Mica, and Platinum," J. Amer. Chem. Soc., 40, 1361-1403, 1918.

Lendle, A., "Adsorption von Sauerstoff an Kohle. Calorimetric und Kinetik der Langsamen Adsorption," Z. Physik. Chem., A172, 77-94, 1935.

Lielmezs, J., and A.C.D. Chaklader, "Reversible Thermal Effect in α-Fe_2O_3 at $690 \pm 5^{\circ}C$," J. Appl. Phys., 36, 866, 1965.

McCafferty, E. V. Pravdie, and A.C. Zettlemoyer, "Dielectric Behavior of Adsorbed Water Films on the $-Fe_2O_3$ Surface," Trans. Faraday Soc., 66, 1720-1731, 1970.

McCord, T.B., "Comparison of the Reflectivity and Color of Bright and Dark Regions on the Surface of Mars," Astrophys. J., 156, 79-86, 1969.

McCord, T.B., and J.B. Adams, "Spectral Reflectivity of Mars," Science, 163, 1058-1060, 1969.

McCord, T.B., J.H. Elias, and J.A. Westphal, "Mars: The Spectral Albedo (0.3 - 2.5u) of Small Bright and Dark Regions," Icarus, 14, 245-251, 1971.

McCord, T.B., and J.A. Westphal, "Mars: Narrowband Photometry, From 0.3 to 2.5 Microns, of Surface Regions During the 1969 Apparition," Astrophys. J., 168, 141-153, 1971.

Meyer, W., and H. Neldel, "Uber die Beziehungen Zwischen der Energiekonstanten und der Mengenkonstanten a in der Leitwerts-Temperaturformed bei Oxydischen Halbleitern," Z. Tech. Physik, 18, 588-593, 1937.

Miles, P.A., W.B. Westphal, and A. von Hippel,"Dielectric Spectroscopy of Ferromagnetic Semiconductors," Reviews of Modern Physics, 39, 279-307, 1957.

Morin, F.J., "Electrical Properties of α-Fe_2O_3, and α-Fe_2O_3 Containing Titanium," Phys. Rev.,83, 1005-1010, 1951.

Moroz, V.I.,"The Infrared Spectrum of Mars (1.1-4.1μ)," Astron. Zh. (USSR), 41, 350-361, 1964.

Morrison, D., C. Sagan, and J.B. Pollack, "Martian Tempera-.tures and Thermal Properties," Icarus,11, 36-45, 1969.

Mott, N.F., "Theory of the Formation of Protective Oxide Films on Metals, II," Trans. Faraday Soc., 36, 472-483, 1940.

Mott, N.F., "Theory of the Formation of Protective Oxide Films on Metals, III.," Trans. Faraday Soc., 43, 429-434, 1947.

Nagata, T., Rock Magnetism, Maruzen Company, Tokyo, Japan, 1961.

Neel, L., "Proprietes Magnetiques des Ferrites; Ferrimagnetisme et Antiferromagnetisme," Ann. Phys., 3, 137, 1948.

O'Connor, J.T., "Mineral Stability at the Martian Surface," J. Geophys. Res., 73, 5301-5311, 1968a.

O'Connor, J.T., "Fossil Martian Weathering," Icarus, 8, 513-517, 1968b.

O'Leary, B.T., and D.G.Rae, "The Opposition Effect of Mars and its Applications," Icarus, 9, 238-240, 1968.

Ono, K., Y. Ishikawa, A. Ito, and E. Hirahara, "A Study of the Low Temperature Transition in Magnetite," J. Phys. Soc. Japan, 18, 1465-1473, 1963.

Owen, T., "The Composition and Surface Pressure of the Martian Atmosphere: Results from the 1965 Opposition," Astrophys. J., 146, 257-270, 1966.

Perls, T.A., "Carbon Suboxide on Mars: A Working Hypothesis," Icarus, 14, 252-264, 1969.

Phelps, A.V., and J.L. Pack, "Collisional Detachment in Molecular Oxygen," Phys. Rev. Letters, 6, 111-113, 1961.

Pignocco, A.J., and G.E. Pellisier, "LEED Studies of Oxygen Adsorption and Oxide Formation on an (0111) Iron Surface," Surface Science, 7, 261-278, 1967.

Plummer, W.T., and R.K. Carson, "Mars-Is the Surface Covered by Carbon Suboxide?" Science, 166, 1141-1142, 1969.

Prasad, A.N., and J.D. Craggs, "Measurement of Townsend's Ionization Coefficients and Attachment Coefficients in Oxygen," Proc. Phys. Soc., 77, 285-398, 1961.

Renshaw, G.D., and C. Roscoe, "Thermal Stability of -Ferric Oxide," Nature,224, 263-264, 1969.

Ritchie, I.M., and G.L. Hunt, "The Kinetic Rate and Pressure Dependence of Surface Controlled Metal Oxidation Reactions," Surface Science, 15, 524-534, 1969.

Rowe, H., "On the Adsorption of Gases by Activated Charcoal at Very Low Pressures - I. At Air Temperature," Phil. Mag., 1, 109-131, 1926.

Rowe, H., "On the Adsorption of Gases by Activated Charcoal at Very Low Pressures - II. At -183°C," Phil. Mag., 1, 1042-1064, 1926.

Sagan, C., J.P. Phaneuf, and M. Ihnat, "Total Reflection Spectrophotometry and Thermogravimetric Analysis of Simulated Martian Surface Materials," Icarus, 4, 43-61, 1965.

Sagan, C., "Mariner IV Observations and the Possibility of Iron Oxides on the Martian Surface," Icarus, 5, 102-103, 1966.

Sagan, C., and J. Veverka, "The Microwave Spectrum of Mars: An Analysis," Icarus, 14, 222-234, 1971.

Sagan, C., J. Veverka, and P. Gierasch, "Observational Consequences of Martian Wind Regimes," Icarus, 15, 253-278, 1971.

Salisbury, J.W., "The Light and Dark Areas of Mars," Icarus, 5, 291-298, 1966.

Salisbury, J.W., and G.R. Hunt, "Martian Surface Materials-Effect of Particle Size on Spectral Behavior," Science, 161, 365-366, 1968.

Salisbury, J.W., and G.R. Hunt, "Compositional Implications of the Spectral Behavior of the Martian Surface," Nature, 222, 132-136, 1969.

Samokhvalov, A.A., N.M. Tutikov, and G.P. Skornyakov, "Optical Properties Associated With the Conduction Mechanism of Ferrites," Soviet Physics-Solid State, 10, 2172-2176, 1969.

Samorjai, G.A., "Effect of Light on the Evaporation and Oxidation of CdS Single Crystals," Surface Science, 2, 298-306, 1964.

Schmalz, R.F.,"A Note on the System Fe_2O_3-H_2O," J. Geophys. Res., 64, 575-579, 1959.

Schorn, R.A., H. Spinrad, R.C. Moore, H.J. Smith, and L.P. Giver, "High Dispersion Spectroscopic Observations of Mars. II. The Water Vapor Variations," Astrophys. J., 147, 743-752, 1966.

Sharonov, V.V., "A Lithological Interpretation of the Photometric and Colorimetric Studies of Mars," Soviet Astron.-AJ, 5, 199-202, 1961.

Sinton, W., and J. Strong,"Observations of the Infrared Emission of Planets and Determination of their Temperatures," ONR Contr. Rept., No. 248(01), 1960.

Sinton, W.M.,"On the Composition of Martian Surface Materials," Icarus, 6, 222-228, 1967.

Sommer, A.H., and W.E. Spicer,"Photoelectric Emission," in Photoelectronic Materials and Devices, Edited by S. Larach, D. Van Nostrand Co., Inc., Princeton, N.J., 1965.

Spinrad, H., G. Münch, and L.D. Kaplan, "The Detection of Water Vapor on Mars," Astrophys. J., 137, 1319-1321, 1963.

Spinrad, H.R.A., R. Schorn, R. Moore, L.P. Giver, and H.J. Smith, "High Dispersion Spectroscopic Observations of Mars. I. The CO_2 Content and Surface Pressure," Astrophys. J., 146, 331-338, 1966.

Takei, H., and S. Chiba, "Vacancy Ordering in Epitaxially-Grown Single Crystals of γ-Fe_2O_3," J. Phys. Soc. of Japan, 21, 1255-1263, 1966.

Tallman, R.L., and E.A. Gulbransen, "Dislocation and Grain Boundary Diffusion in the Growth of α-Fe_2O_3 Whiskers and Twinned Platelets Peculiar to Gaseous Oxidation," Nature, 218, 1046-1047, 1968a.

Tallman, R.L., and E.A. Gulbransen, "Selected Area Electron Diffraction Study of Twinned α-Fe_2O_3 Bladelike Platelet Growths on Iron," J. Electrochem. Soc., 115, 770-775, 1968b.

Tannhauser, D.S., "Conductivity in Iron Oxides," J. Phys. Chem. Solids, 23, 25-34, 1962.

Thompson, B.A., P. Harteck, and R.R. Reeves, Jr., "Ultraviolet Absorption Coefficients of CO_2, CO, O_2, H_2O, N_2O, NH_3, NO, SO_2, and CH_4 Between 1850 and 4000 Å," J. Geophys. Res., 68, 6431-6436, 1963.

Tombaugh, C.W., "A Survey of Long-Term Observational Behaviour of Various Martian Features that Affect Some Recently Proposed Interpretations," Icarus, 8, 227-258, 1968.

Traub, W.A., and N.P. Carleton, "Observations of O_2 on Mars and Venus," paper presented at the 2nd Ann. Meeting of the Amer. Astron. Soc., Div. Plan. Sci., Kona, Hawaii, 20 March - 24 March, 1972.

Tull, R.G., "The Reflectivity Spectrum of Mars in the Near Infrared," Icarus, 5, 505-514, 1966.

Van Tassel, R.A., and J.W. Salisbury, "The Composition of the Martian Surface," Icarus, 3, 264, 1964.

Verwey, E.J.W., and P.W. Haayman, "Electronic Conductivity and Transition Point of Magnetite," Physica, 8, 979-987, 1941.

Waldron, R.D., "Infrared Spectra of Ferrites," Phys. Rev., 99, 1727-1735, 1955.

Weast, R.C., ed., Handbook of Physics and Chemistry, 49th. Ed., Chem. Rubber Co., Cleveland, Ohio, D-108, 1969.

Wickersheim, K.A., and R.A. Lefever, "Absorption Spectra of Ferric Iron Containing Oxides," J. Chem. Phys., 36, 844-850, 1962.

Wildt, R., "Ozon und Sauerstoff in den Planeten-Atmosphären," Veröffentli Univ. - Sternwarte Gottingen, No. 38, 1934.

Yosida, K., and M. Tachiki, "On the Origin of the Magnetic Anisotropy Energy of Ferrites," Prog. Theo. Phys., 17, 331-360, 1957.

Younkin, R.L., "A Search for Limonite Near-Infrared Spectral Features on Mars," Astrophys. J., 144, 809-818, 1966.